Bacteriophage Susceptibility and Genomic Analyses of Rapidly Growing and Slowly Growing Clinically Isolated Non-Tuberculous Mycobacteria

by

Elizabeth D. Amarh

Bachelor of Science, Eastern Illinois University, 2013

Submitted to the Graduate Faculty of the

Dietrich School of Arts and Sciences in partial fulfillment

of the requirements for the degree of

Doctor of Philosophy

University of Pittsburgh

2024

UNIVERSITY OF PITTSBURGH

DIETRICH SCHOOL OF ARTS AND SCIENCES

This dissertation was presented

by

Elizabeth D. Amarh

It was defended on

April 26, 2024

and approved by

Karen M. Arndt, PhD, Professor, Dept. of Biological Sciences

Craig L. Peebles, PhD, Professor Emeritus, Dept. of Biological Sciences

James M. Pipas, PhD, Professor, Dept. of Biological Sciences

N. Luisa Hiller, PhD, Professor, Dept. of Biological Sciences (Carnegie Mellon University)

Dissertation Director: Graham F. Hatfull, PhD, Professor, Dept. of Biological Sciences

Bacteriophage susceptibility and genomic analyses of rapidly growing and slowly growing clinically isolated non-tuberculous mycobacteria

Elizabeth D. Amarh, PhD

University of Pittsburgh, 2024

Non-tuberculous mycobacteria (NTM) cause pulmonary and disseminated infections that are difficult to treat with antibiotics. A renewed interest in phage therapy has yielded positive results in treating antibiotic resistant bacterial infections, including in NTM infections. Mycobacteriophage therapy has been well-documented, with over twenty published cases and zero adverse reactions to treatment. The number of phages that can be applied therapeutically is < 10, and this may be influenced by the host used to isolate most of the over 13,000 mycobacteriophages in the inventory. Most phages are temperate, with the ability to form a prophage in the genome of a susceptible host. The genomes of clinically isolated NTM species are replete with intact prophage sequences. These prophages can be induced to excise from the host genome, re-circularizing the phage genome, and producing phage particles (lytically propagated spontaneously induced prophages (LPSIPs)). We hypothesize these LPSIPs may demonstrate a host range more inclusive of clinically isolated NTM species, as their presence in the NTM genomes suggests they are able to temperately infect clinically isolated NTM successfully. The goal of this research is to increase the repertoire of therapeutically useful phage, by propagating LPSIPs from clinically isolated NTM strains, and generating a lytic mutant of the temperate LPSIP. So far, no LPSIPs isolated from pathogenic NTM infect the non-pathogenic *M. smegmatis* mc^2155. Because usual methods of phage engineering, BRED and CRISPY-BRED, are not available in NTM other than *M. smegmatis* mc^2155, CRISPR-Cas9

instead was implemented. Through characterizing clinically isolated NTM strains phenotypically, assessing the genomes for prophage content, isolating the prophage in LPSIP form, and using CRISPR-Cas9 to engineer a LPSIP lytic mutant, this work expands the repertoire of therapeutically useful mycobacteriophages.

Table of Contents

List of Tables

List of Figures

Preface

The last seven years has held challenges and triumphs, and completing this PhD would not have been possible without the support of so many people along the way. I want to thank my dissertation advisor, Dr. Graham Hatfull, for allowing me to learn and grow in this lab, and contribute my work to the pantheon that is phage research. I am incredibly grateful for his exceptionally inspiring example, encouragement, and the guidance he has provided during this process. The inquisitive and good-humored environment in the Hatfull lab is inspiring, and I am grateful to have had an advisor that fosters such an environment for learning. I am grateful for my dissertation committee, Drs. Karen Arndt, Luisa Hiller, Jim Pipas, and Craig Peebles, whose guidance helped me to stay focused and reduce overwhelm with this research project.

I have had the absolute pleasure of researching alongside similarly inspiring lab mates, who have supported and encouraged me over the years. I want to thank Dr. Krista Freeman, whose invaluable mentorship continues to inform my decisions and inspires a sense of confidence in my capabilities as a scientist. I am grateful for Dr. Katherine Sheehan-Wetzel, whose positivity and energy are absolutely contagious, and whose driven nature encourages the same in others. I am grateful to Dr. Ching-Chung Ko, who readily shares his deep knowledge of molecular and phage biology, and availed himself for countless random science questions and pointed discussions. Dr. Carlos Guerrero-Bustamante and Dr. Christian Gauthier have been exceedingly helpful through the years, particularly as I have neared my dissertation defe nse, and I am unbelievably grateful for their guidance and encouragement.

The inquisitive and good-humored environment of the Hatfull lab is maintained by the tens of scientists in the lab, in the forms of research technicians, undergraduate researchers, and

post-doctoral researchers, and I could not have asked for better lab mates. Even when feeling low or distempered, I knew if I could just get into the lab, I would be surrounded by some of the most inspiring and fun people I have ever met, and I am so grateful for the Hatfull lab members past and present.

Completing this work would not have been possible without my family, both genetic and chosen. I am grateful for my mother, Zoraida Irizarry, who encouraged a love of learning in me from a young age. I have never doubted that I am loved and supported, and I am grateful for the many pep-talks over the years. I am grateful for my father, Jacob Archibald Amarh, for the countless discussions about life and learning, and whose prayers and love have given me the strength to continue. I would not have been able to complete the last two years of this journey without the incredible and selfless support of my Tía, Iris Margarita Irizarry-Velez. I am grateful for my sister, Agnes Margarita Amarh, as so much of what I am has been shaped by her, and truly, I do not know how I could have continued without her boundless love, support, and all the cackles. Thank you to Jahree Sosa, with whom I entered the Hot Metal Bridge Program, and for whose friendship and support I am forever grateful. Finally, I want to thank my cats, Marley and Merlin, who have been my companions for the past five years, and have supported me on this journey in their own ways. Genuinely, there are not enough words to give everyone their due gratitude, but I can start with saying: thank you.

1.0 Introduction

Non-tuberculous mycobacteria (NTM) are gram-positive, acid-fast, actinobacteria (Kazda, Pavlik et al. 2009). They are grouped into complexes based on relatedness, and are either rapidly growing or slowly growing (Johansen, Herrmann et al. 2020). Species belonging to NTM include the non-pathogenic laboratory strain *M. smegmatis* mc^2155, and pathogenic strains (Kazda, Pavlik et al. 2009). Pathogenic NTM are not only found in the natural environment, but their resilience to most water treatments means they are found in civil plumbing and cause nosocomial infections (Lee, Sheng et al. 2015, Schreiber, Kuster et al. 2016). Infections caused by NTM are resilient against most first- and second-line antibiotic treatments (Kim, Oh et al. 2023). A significant contributor to the robust nature of NTM is the mycobacterial envelope, which is more complex than most gram-positive cell membranes (Rajagopal and Walker 2017, Luthra, Rominski et al. 2018). In recent years, there has been a consistent increase in multi-drug resistant (MDR) NTM infections (Ratnatunga CN 2019, Johansen, Herrmann et al. 2020).

Entering the post-antibiotic era has spurred interests in returning to a pre-antibiotic approach to managing bacterial infections – bacteriophage therapy. Bacteriophages, viruses that infect bacteria, consistently have been applied therapeutically in French and Eastern European medicine. Recent collaborations between researchers and physicians produced three seminal publications that are a solid foundation for a return to phage therapy in the West, and there are multiple publications of mycobacteriophage therapy for MDR NTM infections. While the cases are generally successful, one challenge faced is a lack of phages that can be applied therapeutically (fewer than 10 phages). One possible reason for so few therapeutically useful phages is the clinically isolated strains of NTM have been screened with phages isolated on the

non-pathogenic *M. smegmatis* mc^{2}155, relying on finding *M. smegmatis* phages that have an expanded host range, one inclusive of pathogenic, clinically isolated strains belonging to different species and subspecies. In this research, we aimed to expand the repertoire of therapeutically useful phages by engineering spontaneously induced prophages, from clinically isolated NTM strains, to be obligately lytic, rendering them therapeutically useful.

In Chapter 1 I introduce two complexes of pathogenic NTM, mycobacteriophages, and describe applications of mycobacteriophages as therapy. The chapter ends with an introduction to the clinically isolated strains and mycobacteriophages specific to this research. Chapter 2 describes the methods and results of prophage content analyses on rapidly growing NTM. In Chapter 3 I present the results of phage infection susceptibility screens performed in both rapidly and slowly growing NTM. In Chapter 4, I describe isolating the spontaneously induced phage forms of two prophages described in Chapter 2, and generating an obligately lytic mutant of one of the phage forms. Chapter 4 ends with the results of challenging a rapidly growing, clinically isolated NTM strain with the mutant phage form and comparing the effective killing of the NTM to that of the parental phage. In Chapter 5, I discuss the results of this research, and thoughts on future experiments with these mycobacteriophages and clinically isolated NTM.

1.1 Mycobacteria: An Introduction

Mycobacteria comprise a group of actinobacteria most notably recognized for the members that demonstrate obligate pathogenesis – *Mycobacterium tuberculosis* and *M. leprae* (Santacroce, Del Prete et al. 2021, Koleske, Jacobs et al. 2023). However, this group includes non-tuberculous mycobacteria (NTM) as well. These NTM can exist saprophytically, as is seen

with the non-pathogenic *M. smegmatis* mc^2155 (Kazda, Pavlik et al. 2009) and pathogenically, as is seen with mycobacteria belonging to the *M. abscessus* (MAB), and the *M. avium-chelonae* (MAC) complexes (Pavlik, Ulmann et al. 2022).

1.2 Non-tuberculous mycobacterial phylogeny

Early methods for differentiating known species of mycobacteria relied heavily on the use of experimental animals for differences in infection phenotypes (Kazda, Pavlik et al. 2009); modern methods allow for genomic differentiation of the various NTM (Griffith, Brown-Elliott et al. 2015). In fact, the MAB complex of mycobacteria has been repeatedly genomically differentiated over the years, as laboratory methods have advanced and researchers have discovered more nuance in the genomics of mycobacteria (Gupta, Lo et al. 2018, Tortoli, Brown-Elliott et al. 2019, Tortoli, Meehan et al. 2019). Generally, the most useful descriptions of mycobacterial species are based on factors that are valuable in both laboratory and clinical settings - factors such as sequence identities of housekeeping genes and susceptibilities to antibiotics used in treatment of NTM mycobacteriosis (Griffith, Aksamit et al. 2007, Griffith, Brown-Elliott et al. 2015). Extensive analyses of Average Nucleotide Identity (ANI) across whole genome sequences (WGS) of strains suggest species belonging to the rapid growing mycobacteria are the more ancestral species (*M. abscessus-chelonae*) and slow growers are the most derived species (*M. avium*) (*Hoyosella altamirensis* as mycobacteriaceae outgroup; Mtb Complex as one species) (Tortoli, Fedrizzi et al. 2017). Through the years of species and subspecies reassignments, the separation of rapidly and slowly growing species of mycobacteria has been maintained, as *16S rRNA* sequencing consistently demonstrates that slow growing

NTM have a 12-14 nucleotide insertion in helix 18, that is lacking in the *16S rRNA* of rapidly growing NTM (Mignard and Flandrois 2008, Tortoli, Fedrizzi et al. 2017, Zhang, Wang et al. 2023). Further differentiation among the rapidly growing mycobacteria based on *16S rRNA* sequencing is obfuscated by the unusually high sequence identity (94 – 100%), but the same is not seen for the slowly growing mycobacteria (Tortoli, Fedrizzi et al. 2017).

1.2.1 MAB complex – rapidly growing NTM

Mycobacterium abscessus complex (MAB complex) bacteria are rapidly growing species of mycobacteria (RGM). The complex is divided into subspecies (subsp.), including *M. abscessus* subsp. *abscessus* (*M. abscessus*), *M. abscessus* subsp. *massiliense* (*M. massiliense*), *M. abscessus* subsp. *bolletii* (*M. bolletii*) (Griffith, Brown-Elliott et al. 2015). The highly conserved *16S rRNA* sequence of species belonging to the MAB complex necessitates multilocus sequence analysis (MLSA) for subspecies identification (Mendum, Chilima et al. 2000, Mignard and Flandrois 2008). There are three additional canonical loci that can be sequenced to identify RGM at the subspecies level – *erm*(41), *hsp65*, and *rpoβ* (Mignard and Flandrois 2008). The erythromycin resistance gene *erm*(41) varies between *M. bolletii* and *M. massiliense*, in that *M. massiliense* has a truncated *erm*(41), rendering it susceptible to macrolides. *M. abscessus* and *M. bolletii* do not have this truncation, and demonstrate macrolide resistance (Griffith, Brown-Elliott et al. 2015). Analysis of the *rpoβ* among members of MAB complex yields sequences unique to the three subspecies, and the same can be said for WGS (Griffith, Brown-Elliott et al. 2015).

Species in the MAB complex demonstrate two classes of colony morphotypes, based on the presence or absence of glycopeptidolipids (GPLs) on the cell surface – smooth and rough morphotypes, respectively. A more detailed discussion of the mycobacterial membrane is

covered in a later section (1.4). The smooth colony morphotype forms colonies that reflect more light, appearing shiny and moist, with clearly defined and symmetrical edges, and a creamy texture (Brambilla, Llorens-Fons et al. 2016). Some MAB smooth colonies appear to have a lighter or darker spot in their center while others do not. When viewed under magnification, smooth colony cells exist planktonically and demonstrate motility by sliding across top agar (Brambilla, Llorens-Fons et al. 2016).

In contrast to the smooth phenotype, rough colonies appear matte, with irregular edges. Extended incubation times show the colonies will form wrinkles (Brambilla, Llorens-Fons et al. 2016). Under magnification, cells are clumped, appearing to stick together and forming long cords. The smooth colony morphotype is able to form biofilms, while the rough colonies are not (Brambilla, Llorens-Fons et al. 2016).

1.2.2 MAC Complex – slowly growing NTM

The MAC complex is comprised of 12 species, including *M. avium*, *M. intracellulare*, *M. chimaera*, and *M. columbiense* (van Ingen, Turenne et al. 2018). MAC species grow in smooth and rough morphotypes with different opacities (Wright, Zywno-van Ginkel et al. 1996). Species in the MAC complex grow as smooth-opaque colonies (SmO) or smooth-transparent (SmT) colonies (Wright, Zywno-van Ginkel et al. 1996). The SmO colonies are circular, light reflective, and resemble the smooth morphotype demonstrated by MAB species. The SmT colonies, as the designation suggests, form circular, transparent colonies that are better viewed at an angle, rather than directly perpendicularly. MAC strains with rough morphology (Rg) form irregular colonies that are matte, similar to the rough colonies observed in MAB species, and rough strains can be transparent (RgT) (Kansal, Gomez-Flores et al. 1998) (Torrelles, Chatterjee et al. 2000). As in

the MAB species, MAC morphotype is determined by the presence or absence of GPLs on the cell surface (1.4).

As is used in MAB complex species differentiation, MLSA differentiates among species belonging to the MAC complex, with genes *rpoB* and *hsp65* (van Ingen, Turenne et al. 2018). The ANI between a MAC strain in question and the American Type Culture Collection (ATCC) type strains at these housekeeping genes can be used to classify a strain as belonging to the MAC complex (ATCC25291 *M. avium* or ATCC13950 – 16S rRNA, 99.5%; *hsp65*, 97%; *rpoB*, 94%-97%; ANI >85%) (van Ingen, Turenne et al. 2018). Genomic elements other than housekeeping genes, such as Insertion Sequences (IS) are used to differentiate among MAC species (van Ingen, Turenne et al. 2018). Sequences for *IS1245* and *IS1311* are unique to *M. avium*; *IS900* is unique to *M. avium* subsp. *paratuberculosis* (*M. paratuberculosis*); and *IS901* is specific to *M. avium* subsp. *avium* (Turenne, Wallace et al. 2007, Harman-McKenna and De Buck 2023).

1.3 Non-tuberculous mycobacteria ecology – Natural and Nosocomial

1.3.1 Natural Habitats of NTM

NTM exist saprophytically, with the ability to survive and multiply on both abiotic material and within a biotic host, such as a human (Hubalek 2003), and as such, NTM are found in environmental samples (soil and water) (Kazda, Pavlik et al. 2009). Saprophytic mycobacteria were first isolated from timothy prairie grass in the late 19th century, and since this report, mycobacteria have been found living in soils across varying climates (excepting deserts), with peat-rich sphagnum bogs consistently demonstrating a suitable habitat for NTM (Moeller,

1898)(Falkinham 2015). It has been suggested that NTM make their way to reservoirs of surface water from soil run-off (Falkinham 2021).

1.3.2 Civil Habitats of NTM

Once in the surface water, NTM make their way to civil water reservoirs through their resilience to the chemical treatments in water treatment centers (Hilborn, Covert et al. 2006). Civil water reservoirs, such as domestic plumbing, points of use like water fountains, faucets, shower heads, and anywhere water can remain still and within NTM habitable temperatures (Tzou, Dirac et al. 2020). Another of the reservoirs that we are able to find in the home is the water heater, necessitating temperatures as high as 130F to prevent biofilm formation (Honda, Virdi et al. 2018). In a study evaluating the presence of NTM in the homes of patients diagnosed with MAC mycobacteriosis, shower heads were identified as a significant source of exposure to opportunistic infection by NTM (Tzou, Dirac et al. 2020). On pig farms, NTM can be found in the water troughs and the nozzles of spray-misters used to keep the pigs comfortable during warmer months (Kazda, Pavlik et al. 2009). Though more sterile than a pig farm, hospitals have reported finding NTM in heater-cooler units necessary during open heart surgeries, unfortunately leading to soft tissue infections in patients during recovery (Baker, Lewis et al. 2017, Honda, Virdi et al. 2018, van Tonder, Ellis et al. 2023). The waxy mycobacterial membrane gives mycobacteria a hydrophobic characteristic that increases its resistance to harsh environments and chlorine treatment (Hilborn, Covert et al. 2006).

1.4 Mycomembrane and Morphotype

The resilient nature of NTM bacteria largely is due to the formidable mycobacterial cell membrane (Hilborn, Covert et al. 2006). Bacteria are separated into two groups based on key characteristics of their membranes – gram-negative and gram-positive (Silhavy, Kahne et al. 2010). The description is based on the phenotype observed after gram staining (Bartholomew and Mittwer 1952), during which a primary stain (crystal violet dye) is applied to a sample, followed by application of a decolorizer (alcohol or acetone), and finally a secondary stain (fuchsin). Gram-negative bacteria will take up the color of the secondary stain (pink or red) while gram-positive bacteria will retain the color of the primary stain (purple or blue). The gram-negative bacterial membrane is considered complex when compared to most gram-positive bacteria (Silhavy, Kahne et al. 2010). The gram-negative membrane consists of a phospholipid bilayer that is the plasma membrane, the periplasmic space, a thin layer of peptidoglycan, and an outer membrane, largely composed of lippopolysacharides (Silhavy, Kahne et al. 2010). The gram-positive bacterial membrane usually is considered less complex in comparison, the plasma membrane is followed by a periplasmic groove, and surrounded by a thick layer of peptidoglycan (Silhavy, Kahne et al. 2010). Bacteria belonging to the gram-negative and gram-positive groups may have additional acids on their surfaces such as teichoic acids (Silhavy, Kahne et al. 2010), but the above describes the simplified characteristics of these membranes. The mycobacterial membrane is unique in that it can be three-fold less permeable to some antibiotics than the gram-negative membrane (Jarlier and Nikaido 1990), and this can be attributed to the mycobacterial envelope (Rath, Saurel et al. 2013).

1.4.1 The Gram-Positive NTM and the NTM Cell Envelope

Like other gram-positive bacteria, the mycobacterial envelope is constituted by the plasma membrane, periplasmic groove, and a thick peptidoglycan layer, but the mycobacterial cell wall has two additional layers – an arabinogalactan layer and finally a layer of mycolic acid (Mamadou Daffé 2019). The mycolic acid layer is termed the mycomembrane, and it has a significant role in the robust nature of the mycobacterial cell wall. Mycolic acids, or mycolates, are long chain fatty acids that give the mycobacterial cell wall a waxy characteristic, making it hydrophobic in nature and particularly impermeable to acid-alcohol treatment, as demonstrated by acid-fast staining (Nataraj, Varela et al. 2015).

The mycobacterial cytoplasmic membrane consists of the typical bilayer of glycophospholipids, but also, it has phosphatidylinositol mannosides (PIMs), lipomannans (LMs) and lipoarabinomannans (LAMs), with the latter two of these components being derivatives of PIMs (Bansal-Mutalik and Nikaido 2014, Chiaradia, Lefebvre et al. 2017). In infectious conditions, PIMs evoke a cytokine response in the host that aids in establishing granulomas (Nigou, Vasselon et al. 2008). The LMs also evoke a cytokine response from the host, however both LMs and LAMs are expressed at low levels during logarithmic growth and the levels increase substantially to higher levels during stationary phase (Guerin, Kordulakova et al. 2010, Bacon, Alderwick et al. 2014). All three of these components, PIMs, LMs, and LAMs, inhibit Toll-like receptor 2 (TLR2) signaling in the host, leading to a downregulation in MHC class II antigen presentation, allowing the mycobacteria to survive inside macrophages and dendritic cells, without the infected antigen presenting cells presenting antigens that indicate infection, and avoid T-cell killing of the infected antigen presenting cells (Nigou, Vasselon et al. 2008, Harding

and Boom 2010). The ability of these bacteria to find refuge in antigen presenting cells is key in establishing latent infections.

The thick peptidoglycan layer is made of the alternating linear sugar strands *N*-acetylmuramic acid and *N*-acetylglucosamine. These sugar strands are crosslinked by peptides, thought to have a structure that resembles a honeycomb (Meroueh, Bencze et al. 2006). Peptidoglycan metabolism is regulated by the serine-threonine protein kinase (STPK) protein kinase B (PknB) (Kaur, Rausch et al. 2019). The peptidoglycan precursor, lipid II, regulates the kinase activity of PknB, which indirectly activates MurA, a dedicated enzyme in the synthesis of peptidoglycan precursors. The direct activator of MurA, CwlM, activates MurA when it is phosphorylated by PknB, and when CwlM is unphosphorylated, the unphosphorylated CwlM associates with the lipid II flippase MurJ, and it has been suggested this aids in ensuring there is steady synthesis of peptidoglycan precursors during active growth (Nigou, Vasselon et al. 2008, Boutte, Baer et al. 2016) . During stasis, *pknB* is downregulated, suggesting that cell wall synthesis is inactive when the cell is in stasis, in which the less active cell wall is less permeable, making the cell more resistant to penetration by antibiotic molecules (Sarathy, Dartois et al. 2013). The peptidoglycan layer is surrounded by arabinogalactan sugars that make up the arabinogalactan layer, and these sugars rely on the linker disaccharide rhamnose-GlcNAc. During stasis the assembly genes for the galactan and linker rmlB, rmlC, cpsA2, and glfT2 are downregulated (Betts, Lukey et al. 2002).

The mycomembrane, the outermost layer of the mycobacterial envelope, is composed of an outer leaflet and an inner leaflet. The outer leaflet is mostly mycolic acids which can exist with a trehalose sugar as trehalose monomycolates (TMMs) or as phagosome-lysosome fusion blocking trehalose dimycolate (TDM) (Marrakchi, Laneelle et al. 2014, Patin, Geffken et al.

2017). The mycolic acids are made up of 2-alykl, 3-hydroxy long-chain fatty acids (Nataraj, Varela et al. 2015). The fatty acid chains are synthesized by fatty acid synthase I (FAS-I) and elongated by FAS-II enzymes (Nataraj, Varela et al. 2015). Loss of acid-fastness after *KasB* phosphorylation suggests KasB inhibition increases cell wall permeability (Vilcheze, Molle et al. 2014). When *KasB* is active, its action reduces tumor necrosis factor (TNF) stimulation in the host. In stasis or latent infection conditions, the presence of TDM and TMM on the membrane decreases, and trehalose is repurposed in the cytoplasm (Vilcheze, Molle et al. 2014).

Surface lipids on the mycomembrane are important for establishing infection in the host. The lipid phthiocerol dimycocerosate (PDIM) protects NTM from the immune system by shielding the pathogen-associated molecular patterns recognized by the host immune system. PDIM also has been implicated in phagosome rupture, a necessary step in reactivation of a latent infection (Barczak, Avraham et al. 2017).

Biosynthesis of glycopeptidolipids (GPLs) is specific to non-tuberculous species, and aberrations in the production or transport of GPL to the mycomembrane surface contribute to a distinct change in colony morphology, with the lack of GPLs on the membrane surface yielding a rough colony morphotype, and the presence of GPLs on the membrane surface yielding a smooth colony morphotype (Schorey and Sweet 2008).

These surface lipids are differentiated by alkali stability, a measure of whether the protein folding is maintained in basic environments. Alkali stable GPLs, termed c-mycosides, are found in *M. smegmatis*, *M. abscessus*, *M. avium*, and other NTM (Schorey and Sweet 2008). The most common form of c-type GPLs is the apolar c-type GPL. Apolar c-type GPLs are considered non-specific (nsGPLs); polar c-type GPLs are serospecific and they are noted as ssGPLs. These ssGPLs differ from nsGPLs in that they have additional sugar subunits on their 6-deoxyatalosyl

residue. Particularly within *M. avium* subspecies, subtle changes in the GPL oligosacharide chain cause serological variation between strains (Schorey and Sweet 2008).

The c-type GPLs can be considered the Schaefer typing antigens that were once used in NTM typing, and usually presents a smooth colony morphotype that demonstrates Ruthenium Red membrane staining (Reznikov and Leggo 1972, Schorey and Sweet 2008). Overall, in the MAC complex, there are roughly 28 total ssGPLs (Brennan, Heifets et al. 1982, Tsang, Denner et al. 1992, Naka, Nakata et al. 2011). A strain with ssGPLs has unique sugars, with glucaronic acid and glucaronic acid variants, and acetaminophen-dideoxy-hexosyl residues. Investigation of mycolic acid composition in MAC species through High Performance Liquid Chromatography (HPLC) reveals MAC species yield similar peak clustering patterns, excepting *M. chimaera*, which is missing one of the three consistent peak clusters (van Ingen, Turenne et al. 2018). In infectious conditions *M. avium* will increase production of GPLs, which are known to accumulate in the host macrophage (Schorey and Sweet 2008).

Surface proteins are transported to the membrane surface by Mycobacterial membrane proteins large/small (MmpL/MmpS) and accessory proteins such as GPL-addressing proteins (GAPs) (Parmar and Tocheva 2023). Aberrations in GPL sequence or transport gives the rough colony morphotype, deletion of the *mmpL4a* or *mmpL4b* gives a smooth to rough conversion (Parmar and Tocheva 2023). The mycobacterial envelope surface proteins are immunogenic and significant contributors to the survival and proliferation of NTM in infectious conditions.

1.5 NTM as Pathogens

Pathogenically, NTM are a significant causative agent of mycobacteriosis in pulmonary and soft tissue infections (Pavlik, Ulmann et al. 2022). These opportunistic infections frequently are found in cases of cystic fibrosis (CF), chronic obstructive pulmonary disorder (COPD), and in cases of bronchiectasis (Torrens, Dawkins et al. 1998, Daley, Iaccarino et al. 2020, Pavlik, Ulmann et al. 2022, Baird and Bell 2023). In cases of CF, dysfunctional CF transmembrane conductance regulator (CFTR) affects airway epithelial cells in such a way the water content of the mucus is low, yielding a thick mucus that is inefficiently cleared by the airway cilia, and creating a favorable environment for bacteria, including NTM (Parmar and Tocheva 2023). Patients with NTM mycobacteriosis can experience symptoms for years before receiving a diagnosis; many times, these individuals experience a misdiagnosis, owed to the non-specific nature of mycobacteriosis symptoms (e.g.: sputum production, hemoptysis, and tissue lesions) (Maiga, Siddiqui et al. 2012, Sun, Zhang et al. 2022).

Many of the antibiotics currently in use are active against the same cellular processes as their predecessors, natural and synthetic (Aminov 2010). The overuse of antibiotics and dearth of novel antimicrobials have led to an inevitable rise of antibiotic resistance, as bacteria continue evolving to evade antibiotic mechanisms (Luthra, Rominski et al. 2018). Infections caused by NTM that are resistant to first-line antibiotics are termed multi-drug resistant (MDR) infections, and infections caused by NTM that are resistant to second-line antibiotics are termed extremely drug resistant (XDR) infections (Consortium, the et al. 2018). Mycobacterial secretion systems identified in tuberculosis have been implicated in infectious conditions by secreting virulence factors (substrates) that support intracellular proliferation and evade bactericidal efforts by the host cell (Bar-Oz, Meir et al. 2022). Mycobacteria have three types of secretion systems: the

Twin-Arginine translocation (TAT) pathway, the Sec pathway, and the Type VII secretion systems (T7SS). Of these secretion systems, the T7SS are a major mycobacterial secretion system, and it is composed of five subtypes – ESX-1 – ESX-5 (Abdallah, Bestebroer et al. 2011).

1.5.1 *M. avium* pathogenesis

MAC species can cause gastrointestinal, skin, and soft tissue infections. MAC strains can also be fibrous-cavernous (pulmonary as in MAC-PD) or nodular (disseminated soft tissue) (Kaczmarkowska, Didkowska et al. 2022). Pulmonary disease caused by MAC strains has been given the name: Lady Windermere syndrome, meant to inspire visions of an exceptionally fastidious Victorian woman, the kind of woman who would perform voluntary cough suppression (Reich and Johnson 1992). There have been no extensive studies to support that voluntary cough suppression is a factor in MAC infections (Schorey and Sweet 2008). Pulmonary infections caused by MAC complex species are most commonly seen in Caucasian, post-menopausal women, who have low body weight (Reich and Johnson 1992). Recurrence of MAC infections has been rated at 32% - 48% after successful treatment with one year of negative cultures (Kaczmarkowska, Didkowska et al. 2022). The T7SS subtype ESX-5 has been found to be specific to slowly growing mycobacteria, and has been implicated in nutrient uptake by NTM and macrophage immunomodulation (Parmar and Tocheva 2023).

1.5.2 *M. abscessus* pathogenesis

M. abscessus sensu lato continues to be a persistent pathogen in patients with respiratory disorders and compromised immune systems, including those with CF, COPD, and

bronchiectasis (Nessar, Cambau et al. 2012). To date, there is one documented case of person-to-person transmission of a MAB mycobacteriosis, though it appears to be rare (Ruis, Bryant et al. 2021). During infectious conditions, *M. abscessus* will modify the cell envelope and increase the lipid components (GPLs, TDM, TMM, TPP, and PIM) of the mycomembrane. Upregulation in GPLs on the cell surface decreases surface hydrophobicity, and this allows macrophages to engulf the planktonic cells (Parmar and Tocheva 2023). Cells without GPL on the surface are more difficult for the macrophages to engulf because the cells clump and form chords that make infection containment more difficult for the macrophage (Parmar and Tocheva 2023). When engulfed by the macrophage, rough strains are able to proliferate inside the macrophage. Rough morphotype cells are less likely to infect epithelial cells and are a major contributor to establishment of latent infections, while smooth morphotype cells are more likely to infect epithelial cells and are a major contributor to establishing an infection (Parmar and Tocheva 2023). In these ways, modification of the mycobacterial envelope is necessary for infection progression, with smooth morphotype cells initiating infection through epithelial surface attachment, and rough morphotype cells establishing latent infections by way of intracellular proliferation.

Of the five T7SS subtypes, *M. abscessus* has only ESX-3 and ESX-4. The ESX-3 system primarily has been implicated in zinc and iron uptake by the cell, and macrophage immune modulation (Kim, Yang et al. 2017). In *M. tuberculosis*, high levels of zinc and iron lead to a reduction in *esx-3* expression. The ESX-3 substrates EsxG and EsxH have been shown to interfere with lysosomal trafficking and phagosome maturation (Parmar and Tocheva 2023). In *M. abscessus*, the ESX-3 system has been shown to induce cytokines TNF-α, interleukin-6 (IL-

6), IL-1β, and IL-12P40, inducing a pro-inflammatory response in human macrophages (Kim, Yang et al. 2017).

A closer look at the ESX-4 substrates EsxU and EsxT shows the two substrates form a heterodimer that is involved in macrophage phagosome membrane damage (Parmar and Tocheva 2023), while downregulation of EsxU/T has been shown to induce granuloma formation in the zebrafish model (Johansen, Spaink et al. 2023, Parmar and Tocheva 2023). The ESX-4 secretion system has been shown to cause phagosome damage and promote NTM intracellular survival by reducing phagosome acidification (Laencina, Dubois et al. 2018). The complexity of the mycobacterial envelope is a formidable challenge to mammalian immune systems and antibiotics treatments; over billions of years, the natural antagonists of mycobacteria, mycobacteriophages, have evolved ways to meet and overcome this challenge (Hatfull 2012).

1.6 Mycobacteriophages

1.6.1 Mycobacteriophage morphotypes

Mycobacteriophages are double stranded DNA (dsDNA), tailed phages belonging to the *Caudovirales* order (Ackermann 1998). Two families of *Caudovirales*, *Siphoviridae* and *Myoviridae*, represent two morphotypes (Ackermann 1998). Siphoviral phages have relatively long, flexible, noncontractile tails, and exhibit variation in tail length (~100 – ~300 nm in length) and capsid morphology. Siphoviral capsids can be isometric, icosahedral in shape or elongated, prolate. Prolate capsids have a range of lengths, while isometric capsids tend to be roughly the same size (~50 – ~85 nm in diameter) (Hatfull, Jacobs-Sera et al. 2010). Myoviral phages have

contractile tails and less morphological variation . No mycobacteriophages isolated so far belong to the *Podovirales* family, which demonstrates the stubby-tailed podoviral morphotype, and no mycobacteriophages use ribonucleic acid (RNA) as genetic material (Hatfull 2018).

1.6.2 Mycobacteriophage Life Cycles

Mycobacteriophages demonstrate two lifestyles, lytic and temperate. Lytic phages are capable of one life cycle – the lytic life cycle. The lytic life cycle results in propagation of phage particles, degradation of the host membrane, and finally death of the host by lysis. Temperate phages are capable of two life cycles, the lytic life cycle and the lysogenic life cycle. Lysogeny does not end in cell lysis and instead results in phage genome propagation with the host genome, either as an extrachromosomal replicon that is inherited by the daughter cells (Wetzel, Guerrero-Bustamante et al. 2021), or as a prophage integrated into the host chromosome (Dedrick, Aull et al. 2021). The prophage is formed through site specific recombination between the phage attachment site, *attP*, and the bacterial attachment site *attB*. Integration is catalyzed by the phage encoded integrase (*int*) that can be grouped into one of two families, serine or tyrosine, based on the amino acid residue that covalently binds to DNA (Grindley, Whiteson et al. 2006). The integrase recognizes 35-40 base pairs of homology between the *attP* and the *attB* that is the common core sequence (Broussard, Oldfield et al. 2013, Lunt and Hatfull 2016).

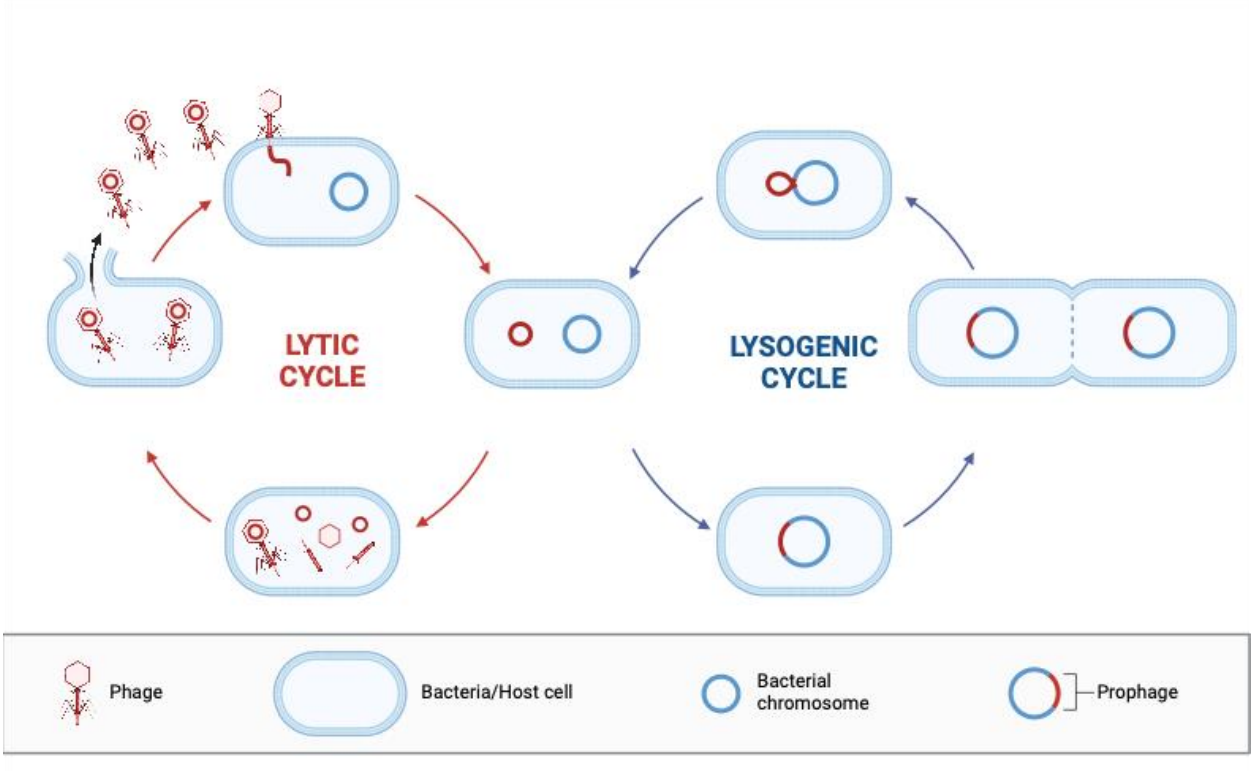

Figure 1 Bacteriophage Life Cycles.

On the left is a depiction of the lytic life cycle, the only life cycle lytic phages are able to undergo. Beginning at the top cell and continuing clockwise, the phage adsorbs to the cell membrane and injects its DNA into the host. The phage DNA circularizes, and utilizes host cell machinery to transcribe the DNA and produce phage particles, eventually lysing the cell. This results in cell death, phage particle propagation and subsequent infections of nearby cells by progeny phage. On the right, is a depiction of the lysogenic life cycle. Beginning at the center cell and continuing counterclockwise, the circularized phage DNA integrates into the host chromosome through site-specific recombination, resulting in a prophage and survival of the host cell. The prophage is inherited by daughter cells, and can be induced to excise from the host chromosome, recircularize, and continue through the lytic life cycle.

1.6.3 Phage Clustering and Phams

Since sequencing of the first mycobacteriophage L5 in 1993, over 2,000 mycobacteriophages have been isolated and sequenced. These sequences, along with those of

other Actinobacteriophages and *Bacillus* phages, are hosted on the Actinobacteriophage database – Phagesdb (Russell and Hatfull 2017). This sizable and centralized repository of phage data hosts details on phages isolated by novice and beginner scientists from the Phage Hunters Integrating Research Education (PHIRE) program, which was subsequently broadened to the Science Education Alliance-Phage Hunters Advancing Genomics and Evolutionary Science (SEA-PHAGES) program (Jordan, Burnett et al. 2014, Hanauer, Graham et al. 2017). The international scope of the SEA-PHAGES program and the advent of Next-Generation Sequencing (NGS) led to a boom in phage and comparative genomics, necessitating organization of the wealth of information that continues to grow.

Initial efforts to understand the taxonomic nature of phages added to Phagesdb assembled groups ("clusters" and "subclusters") based on average nucleotide identity (ANI). However, phage genomes, like bacterial genomes, are the product of both vertical and horizontal genetic exchange (Hendrix, Smith et al. 1999, Pedulla, Ford et al. 2003), constructing genomes that are exceptionally mosaic (Pedulla, Ford et al. 2003). This mosaicism is heavily influenced by the lifestyle of the phage and phage host (Mavrich and Hatfull 2017). The scope of mosaicism has only increased as more phages are isolated and sequenced, leading to increased heterogeneity within clusters and subclusters formed with a basis on ANI (Hatfull, Jacobs-Sera et al. 2010). Further, identification of prophage sequences in *M. abscessus* genomes necessitates a dependable method for including sequences that are generally only distantly related to *M. smegmatis* phages (Dedrick, Aull et al. 2021, Gauthier, Abad et al. 2022).

An updated method for gaining an understanding of inter-genomic relatedness and taxonomy, inclusive of phages and prophages, is based on homologous protein grouping into phamilies (phams) with PhaMMseqs (Gauthier, Cresawn et al. 2022). PhaMMseqs constructs

genome-pham-translation mapping that can be analyzed with PhamClust (Gauthier and Hatfull 2023). PhamClust conducts pairwise comparisons and calculates the protein equivalence quotient (PEQ) for each pair of phages (default settings) (Gauthier and Hatfull 2023). The PEQ of a pair of phages is based on the amino acid sequence identity of shared genes (Gauthier and Hatfull 2023). PhamClust groupings mostly parallel extant clusters, with a few exceptions (Abad, Gauthier et al. 2023). The extant Cluster A Supercluster includes Subcluster A1, and manual clustering recognizes the distant intra-relatedness between Subcluster A1 and other subclusters in Supercluster A (Grose and Casjens 2014). As such PhamClust calculates a PEQ < 25% between Subcluster A1 and other Cluster A genomes, but substantial historical precedent of previously recorded analyses supports inclusion of Subcluster A1 in the supercluster Cluster A (Gauthier and Hatfull 2023). A similar case is seen with Subcluster F2 and other members of the Supercluster Cluster F (Gauthier and Hatfull 2023). Clusters do not demonstrate uniform PEQ indices, and comparing two clusters with the same number of genomes can have distinct PEQ values. The lack of uniformity translates to a lack of a universal threshold for subclustering. Further intra-cluster grouping into subcluster can be achieved with a PEQ threshold ranging from 50% to 70% (Gauthier and Hatfull 2023). Phage genomes that do not meet the PEQ threshold for clustering are termed “singletons”. Pairwise comparisons of phage genome sequences can be visualized in the comparative genomics tool Phamerator (Cresawn, Bogel et al. 2011) (Phamerator Database under100contigmycos v12).

1.6.4 A Genetic Switch – L5 to Lambda

The *Escherichia coli* phage Lambda served as one of the first model systems in which DNA and genes could be studied (Casjens and Hendrix 2015). As such, key components of the

molecular mechanisms involved in the lysis-lysogeny decision of Lambda when infecting *E. coli* have been thoroughly described, and analogs can be found in the model mycobacteriophage L5 (Ptashne, Jeffrey et al. 1980, Sanger, Coulson et al. 1982, Hatfull and Sarkis 1993, Casjens and Hendrix 2015). Originally isolated on *M. smegmatis*, L5 has G+C content of about 63%, and the genome is divided into two halves, the left and the right (Hatfull and Sarkis 1993). The left half is transcribed rightward and has three tRNAs clustered between the minor tail subunit (gene *6*) and the lysin A (gene *10*) (Hatfull and Sarkis 1993). The genomes is divided by the *attP* site, and there is a *cos* site at the ends of the genome. In the left arm of the genome are structural genes and in the right half are the genes necessary for lysogeny, including a tyrosine integrase (Int-Y) (Hatfull and Sarkis 1993).

Integration of the L5 genome into the host chromosome relies on dual DNA-binding by the integrase (Int-L5), with N-terminal binding to arm-type sites and C-terminal binding to the core and catalytic residues (Lewis and Hatfull 2003). The Int-L5 dual DNA-binding activity is similar to that seen in Int-Lambda integration, and in both cases, host derived factors are necessary for binding – mycobacterial integration host factor (mIHF) and IHF respectively (Pedulla, Lee et al. 1996, Lewis and Hatfull 2003). The L5 lysogenic state is maintained by the repressor (gp71) which differs from the cI Lambda repressor in that the L5 repressor does not rely on an activator (as cI relies on cII) (Ptashne, Jeffrey et al. 1980, Lewis and Hatfull 2003). Further, the L5 repressor has multiple binding sites throughout the L5 genome, allowing lysogenic maintenance through lytic transcription silencing (Brown, Sarkis et al. 1997). The L5 switch from lysogenic to lytic relies on the recombination directionality factor (RDF) excise (Xis-L5; gp36) (Lewis and Hatfull 2003). The Xis-L5 binds to the *attL* forming an intermediate intasome-L that readily recombines with the intasome-R intermediate formed by Int-L5 and *attR*.

Integrative recombination by Int-L5 is indirectly inhibited by DNA-bending resulting from Xis-L5 binding. Recombination of intasome-L and intasome-R produces the resultant *attP* and *attB* sites in the phage and bacterial genomes respectively (Lewis and Hatfull 2003).

1.6.5 Integration-Dependent Superinfection Immunity

The unique arrangement of *attP*, including the common core sequence, positioned within the repressor gene has a two-fold effect in that the *attP* has to act as a recognition site for the integrase, and it has to code an active repressor upon integration. Integration-dependent superinfection immunity can be found in phages and prophages that encode a tyrosine integrase (Broussard, Oldfield et al. 2013). There are three key characteristics of an integration-dependent superinfection immunity system, the first of which is the common core sequence of the phage encoded *attP* is located in the coding sequence of the phage repressor. The second is that upon site-specific recombination, the repressor is split across the attachment sites, with most of the repressor at the *attL* end, and third is the 3' remnant of the repressor, including the ssrA-like degradation tag with two alanine residues (- -AA), is at the *attR* (Broussard, Oldfield et al. 2013). A stop codon introduced by the bacterial chromosome near the *attL* junction means the prophage encoded repressor is truncated compared to the repressor encoded by the phage form, and the prophage encoded repressor does not have the ssrA-like degradation tag, making it more stable, active, able to maintain the lysogenic state in the host, and confer superinfection immunity to the host. The phage encoded repressor is larger, and the ssrA-like tag promotes degradation by the host protease ClpXP system (Broussard, Oldfield et al. 2013). Integration dependent immunity was first described in the phages BPs, Brujita, and Charlie (Broussard, Oldfield et al. 2013, Lunt

and Hatfull 2016). Each of these phages produces turbid plaques, indicative of some lysogeny (Broussard, Oldfield et al. 2013).

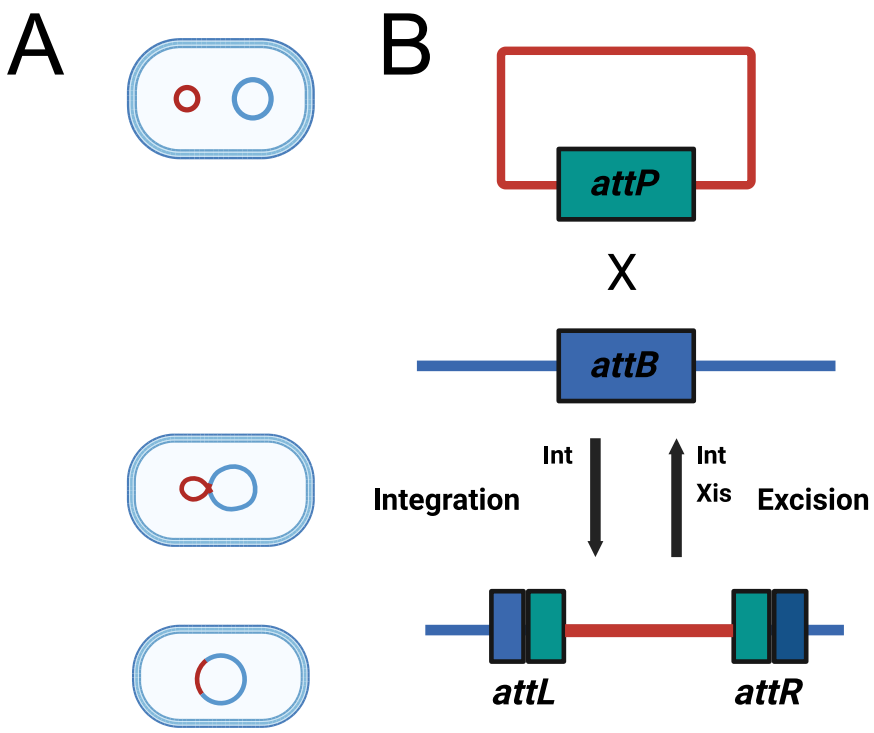

Figure 2 Integration and excision by site-specific recombination

A. Cells depicting the status of the phage DNA and the host chromosome. At the top, the circularized phage DNA is in red and the host chromosome is in blue. The center cell shows the status of the respective DNA during integration or during excision. The last cell shows the integrated prophage combined with the host chromosome. B. The circularized phage DNA is shown in red with the attP represented in teal. Site-specific recombination between the *attP* and the *attB* on the host chromosome (shown in blue), is catalyzed by integrase enzyme, forming an integrated prophage (shown at the bottom). The prophage is flanked by the *attL* and the *attR*, which are constituted by the recombined *attP* and *attB* sites. When induced, excision is catalyzed by integrase in the presence of the recombination directionality factor (RDF) excise, forming the circularized phage genome, and the recombined host chromosome.

When a lysogen is formed with these phages, the chromosomal *attB* site, with which the *attP* undergoes site-specific recombination, is located in a host encoded tRNA (tRNA-Arg

(Msmeg_6349), tRNA-Thr (Msmeg_6152), and tRNA-Lys (Msmeg_5758) for BPs, Brujita, and Charlie respectively). Western-blot analysis shows that the BPs repressor binds to the intergenic region between the repressor (gene *33*) and Cro (gene *34*) (Broussard, Oldfield et al. 2013). This DNA binding by the repressor suggests the repressor actively inhibits Cro from being synthesized, thus inhibiting lytic growth (Broussard, Oldfield et al. 2013).

Phages BPs, Brujita, and Charlie all have tyrosine integrases that are less complex than the Lambda integrase in that they do not require arm-binding (Broussard and Hatfull 2013, Broussard, Oldfield et al. 2013, Landy 2015). These Int-Y have an ssrA-like tag on their C-terminus, and this is similar to the tag seen in the Lambda integrase (Broussard, Oldfield et al. 2013). Integrase degradation by host factors results in the low levels of lysogeny. The fate of the cell after infection by phages with integration-dependent immunity cassettes is determined by the amount of integrase that is present, this differs from the genetic switches seen in Lambda and L5 that require the Recombination Directionality Factor (RDF) excise. In fact, all the components necessary for the lytic-lysogenic genetic switch is within the ~2kb region that is the immunity cassette. The simplicity of this genetic switch compared to the complex Lambda genetic switch supports that the integration-dependent superinfection immunity cassette is an evolutionary ancestor of the Lambda genetic switch (Broussard and Hatfull 2013, Broussard, Oldfield et al. 2013).

1.7 Phage Therapy

1.7.1 History of phage therapy

Before the antibiotic Golden Age in the 1940s (Aminov 2010) there was widespread interest in phage therapy as an antimicrobial treatment. The efficiency of antibiotics and broad application across genera of bacteria led to a decrease in interest in Western Europe and the United States; interests were maintained in Eastern Europe (Georgia, Poland, and Russia) (Kutter, Kuhl et al. 2015) and France (Abedon, Kuhl et al. 2011). Though interests persisted in these regions, most of the reports are incomplete, anecdotal, and a far cry from clinical trials (Kutter, De Vos et al. 2010). Detailed knowledge on phage therapy primarily comes from the Republic of Georgia, where Giorgi (George) Eliava, and Felix d'Hérelle, converted Eliava's Microbiology Institute to the world center for phage research and phage therapy – the G. Eliava Institute of Bacteriophages, Microbiology and Virology. In the 1930's, d'Hérelle brought two major phage cocktails from France to Georgia, *pyophage* and *intestiphage*, and both still can be found in contemporary Georgian and Russian pharmacies (Kutter, De Vos et al. 2010). The names for these cocktails are generic and do not describe cocktails of specific phages. As such, variations in host range across batches of respective cocktails, including batches from a single producer, are to be expected. Local laws require that licensed phage cocktails are tested for efficacy against problematic bacterial strains every six months, and cocktails are "upgraded" for efficacy as needed (Kutter, De Vos et al. 2010). The *pyophage* cocktail is active against *Staphylococcus aureus*, *E. coli*, *Pseudomonas aeruginosa* (*P. aeruginosa*), two species of *Proteus*, and several species of *Streptococcus*; the *intestiphage* cocktail, is active against over 20 different enteric bacteria, and gut-derived strains of *S. aureus* and *P. aeruginosa*. The cocktails

are administered as treatment for an active infection or as a prophylactic measure, and they are primarily available in the form of purified lysate in an ampoule or powdered in a tablet (Kutter, De Vos et al. 2010).

1.7.2 Renewed interests in phage therapy in western medicine

Contemporary phage therapy in western medicine is applied in two forms, through compassionate use or randomized clinical trials. The three seminal cases published between 2017 and 2019 describe compassionate use applications of phage therapy, allowed by the United States Food and Drug Administration (USFDA) as an emergency Investigational New Drug (eIND). The first in this series described phage therapy in a male with a disseminated, multi-drug-resistant *Acinetobacter baumannii* infection (Schooley, Biswas et al. 2017). Phages from Texas A&M University, AmpliPhi Corporation, CA, and the Biological Defense Research Directorate (BDRD) of the Naval Medical Research Center (NMRC) were screened on the *A. baumannii* isolated from the patient, which was given the designation TP1. In the first month of treatment, two additional isolates from the patient were screened, designated TP2 and TP3 (Schooley, Biswas et al. 2017). The initial phage cocktail was administered as an intracavitary wash through percutaneous catheters draining intra-abdominal cavities, and the patient demonstrated minor improvements. The patient's renal and hepatic functions improved from failure states only after the phage cocktail was administered intravenously, highlighting the importance of administration methods in treatment considerations. The susceptibility profile of TP2 was found to have reduced susceptibility to the first phage cocktail, suggesting the *A. baumannii* evolved mechanisms of phage infection resistance when challenged with the cocktail (Schooley, Biswas et al. 2017). Of the nine phages in the three respective cocktails, one phage

was effective against all three isolates from the patient. Serum analyses performed *in vitro* showed a decrease in circulating phage concentrations, suggesting the patient immune system could account for decreases in phage titers in circulation. Interestingly, isolates collected after the first phage cocktail application were susceptible to the antibiotic minocycline, which was subsequently added to the patient treatment regimen. The patient continued to improve and eventually returned to his regular lifestyle (Schooley, Biswas et al. 2017). This case underscores the dynamic nature of phage-host interactions, in that application of phage can induce the bacterial host to evolve resistance to the applied phage, a response that was exploited in a single emergency case of an MDR *P. aeruginosa* infection the following year (Chan, Turner et al. 2018).

Researchers at Yale University isolated 42 *P. aeruginosa* phages from environmental samples (lakes, rivers sewage, streams, and compost) (Chan, Sistrom et al. 2016). A collection of transposon mutants with knockouts for the outer membrane porin M (OprM) of the MexAB and MexXY efflux systems were screened against the isolated phages. One phage, OMKO1 (outer-membrane porin M knockout dependent phage #1), was determined to require OprM for infection (Chan, Sistrom et al. 2016). Phage OMKO1 subsequently was screened against environmentally and clinically isolated strains of *P. aeruginosa* and their corresponding Δ*oprm* variants. Further, the Δ*oprm* variants were investigated for minimum inhibitory concentrations (MIC) of four antibiotics of differing drug classes with varying capacities of efflux by the MexAB and/or MexXY-OprM systems. The *P. aeruginosa* Δ*oprm* strains demonstrated resistance to infection by OMKO1 and increased sensitivities to antibiotics to which the Mex systems provide primary (tetracycline and erythromycin) or moderate (ceftazidime) resistance (Chan, Sistrom et al. 2016). Resistance to OMKO1 infection coincided with increased

sensitivities to antibiotics that use the efflux systems as primary to two antibiotics known to primarily utilize these efflux systems in *P. aeruginosa*, tetracycline and erythromycin, and one that uses the efflux pumps and inducible resistance, ceftazidime (Chan, Sistrom et al. 2016).

This work preceded application of OMKO1 in a case of a prosthetic vascular graft infection (PVGI) caused by MDR *P. aeruginosa* (Chan, Turner et al. 2018). An initial attempt to administer a mixture of OMKO1 and ceftazidime through the patient chest wall was impeded by scar tissue caused by the persistent infection, and so the mixture was applied to the patient's mediastinal fistula, followed by continued treatment with ceftazidime. Unrelated complications necessitated emergency exploratory surgery four weeks after the patient received the single dose of OMKO1 and ceftazidime mixture, and no *P. aeruginosa* was cultured from the aortic graft, leading to cessation of ceftazidime administration (Chan, Turner et al. 2018). After 18 months, the patient did not display symptoms of *P. aeruginosa* reinfection, even without sustained antibiotic treatment, suggesting application of OMKO1 may have exerted selection pressure *in vivo* as was observed *in vitro*.

1.7.3 Applications of Mycobacteriophage Therapy

The first documented application of mycobacteriophage as a therapeutic treatment was in a CF patient with a MDR *M. abscessus* subsp. *massiliense* infection (Dedrick, Guerrero-Bustamante et al. 2019). After a bilateral lung transplant, the infection spread to the surgical wounds and antibiotic treatment was not well tolerated by the patient. The NTM was isolated from patient sputum, given the designation GD01, and screened against phages from the SEA-PHAGES program, including a pool of unsequenced phages. Phages Muddy (AB1), BPs (G1), and ZoeJ (K2) were identified as therapeutic candidates. While Muddy's genome supports that it

is obligately lytic, lytic derivatives of BPs and ZoeJ were engineered by Bacteriophage Recombineering of Electroporated DNA (BRED (Marinelli, Piuri et al. 2008), 4.3.1). Infection by the engineered BPsΔ*33*HTH lytic derivative was not as effective at infecting GD01, therefore a host range mutant of the lytic derivative was instead used in the final cocktail – BPsΔ*33*HTH_HRM10 (portal protein, N270D mutation). Enrichments performed by combining GD01 culture with pooled lysate and environmental samples resulted in the isolation of phages Isca, Gabriela, and Itos; of which, Isca does not infect *M. smegmatis* mc^2155. Interestingly, when the three phage cocktail of Muddy, BPsΔ*33*HTH_HRM10, and ZoeJΔ*45* was applied to another *M. abscessus* subsp. *massiliense* clinical isolate, GD02, the cocktail was ineffective, demonstrating the exceptionally specific nature of phage-host interactions.

The three-phage cocktail was administered to the patient intravenously every 12 hours at a concentration of 10^9 PFU ml^{-1}, with the sternal surgical wound receiving a topical treatment of the phage cocktail as well. One month after the start of treatment the sternal wound had demonstrated vast improvement compared to the other lesions, and so a topical treatment was administered to the other skin lesions. After six months of treatment, the sternal wound and skin lesions had healed substantially, and the patient's liver function had improved. The patient demonstrated apparent sputum conversion quickly after the initiation of phage therapy. Patient serum analyses yielded phage persistence at administration titers through the first 24 hours of treatment, dropping below detectable titer after a week. Phage were also detected in one sputum sample at 10^{10} PFU ml^{-1} early in the course of treatment, and fecal samples also contained phage, supporting that the phage were continuing to propagate in the patient. The patient appeared to experience a mild immune response after treatment, with low cytokine responses detected, including interferon-γ (IFNγ), IL-6, IL-10, TNFα, with IL-6 persisting through the first 4 months

of treatment. Overall, the patient tolerated the phage therapy substantially better than the patient had tolerated the antibiotic approach, and the patient experienced objective improvement compared to patients with similar prognoses and no phage therapy.

The patient with the GD01 infection underwent phage therapy for 44 months, and throughout treatment, skin nodules tested positive for NTM inconsistently, patient sputum did not demonstrate a definite conversion. After two years of phage therapy, patient sera demonstrated phage neutralizing antibodies. The subsequent publication in 2022 further describes the course of treatment for the GD01 infection as well as 19 patients presenting with various symptoms and pathologies (Dedrick, Smith et al. 2023). While the patient from which GD01 was isolated had undergone a bilateral lung transplant and was experiencing several additional comorbidities, the other 19 patients in the 2022 publication included individuals with CF, bronchiectasis independent of CF, a patient with a genetic predisposition for NTM infection by Mendelian susceptibility to mycobacterial disease (MSMD), and patients with other coinfections and comorbidities (Dedrick, Smith et al. 2023).

Phages were found to infect strains of the 20 patients, with a majority of the patients battling *M. abscessus* (subsp. *abscessus* and subsp. *massiliense*) infections and CF simultaneously; an *M. chelonae* infection, an *M. avium* infection, and a BCG infection were included in the pathologies of the 20 patients. Favorable and partially favorable outcomes were achieved in 11 patients, with five of these patients demonstrating largely resolved infections, including the patient with an *M. avium* infection and the patient with an *M. chelonae* infection (Dedrick, Smith et al. 2023).

Five patients exhibited inconclusive outcomes, and it is possible could be attributed to neutralizing antibodies from the patient immune system. Unlike the patient from which GD01

was isolated, immunosuppressants were not an intrinsic part of the patient treatment. These patients all received intravenous (IV) application of phage or phage cocktails, with one patient being switched to aerosolized therapy later in treatment. After one month, sputum from these patients appeared to have substantially decreased CFU of NTM, the infection returned to untreated levels near the time serum samples were coming back with phage-neutralizing antibodies, suggesting the patient's macrophages were clearing the phage. Four patients (CF: *M. abscessus*; bronchiectasis: *M absscesus*) did not demonstrate improvement in symptoms or in serum samples or diagnostics, and the reason for this was not determined. Sera from this cohort suggested that 53% of patients have an immune system that will neutralize at least one phage (Dedrick, Smith et al. 2023).

1.7.4 Phage as an adjunctive therapy to antibiotic treatment

Phages were the first hope for antimicrobials since their discovery just over a century ago (Twort 1915, D'Hérelle 1917, Publications 2007), and while it is unlikely phage will be utilized as a monotherapy in MDR infections, the seminal cases described above demonstrate high potential for phage therapy as an adjunct to antibiotics in western medicine. The decades of reliance on antibiotics in the West necessitates complete, detailed, methodical research into the dynamics of phages and their hosts, particularly clinically isolated, MDR hosts.

1.8 An Introduction to the NTM Strains in this Research and the Phages Screened

This is a characterization of the NTM strains interrogated in this research. The MAB strains represent a set of clinical isolates received from the Eric J. Rubin lab at Harvard University. Strains were originally isolated from National Taiwan University in 2011 (T##) and Brigham and Women's Hospital (BWH) in 2017. The MAB strains received a more thorough interrogation; data collected for strains belonging to the MAC complex will also be included. The MAC strains were received from the Michael Strong and David Pride labs at National Jewish Health (8###) and the University of California San Diego (UCSD#), respectively. The majority of the data on the MAB complex strains has been published in previous publications (Amarh, Dedrick et al. 2021, Amarh, Gauthier et al. 2021, Amarh, Dedrick et al. 2023).

1.8.1 MAB Complex Strains in this Research

A group of 20 *M. abscessus* strains were analyzed for species designation and phylogenies, colony morphotype, prophage content, and phage susceptibility patterns. Whole genome sequencing of all the strains, including complete genome sequencing for strain T36, revealed 11 of the strains were subspecies *abscessus*, eight strains were subspecies *massiliense*, and one strain was subspecies *bolletii* (Figure 3). Of the 11 subsp. *abscessus* strains, three strains (T45, T46, and BWH-C) grouped into a major clade with the *M. abscessus* subsp. *abscessus* type strain ATCC19977. Strain T50 differs from the type strain ATCC19977 at 29,458 positions (0.6%), and is the most distantly related of these subsp. *abscessus* strains. Of the eight subsp. *massiliense* strains, five strains (T38, T48, T36, T44, and T52) are closely related to the same clade as the previously described GD44 and GD115 (Dedrick, Aull et al. 2021)(Figure 3).

The majority of these strains are smooth morphotype, and there are two strains demonstrating the rough morphotype – BWH-D, and T56R. The strains T56R and T56S are derived from the same clinical isolate, but their genomes differ at four positions, with one of these positions being a deletion in the *mps1* gene of T56R. The deletion in the T56R *mps1* is likely the cause of the T56R rough morphotype.

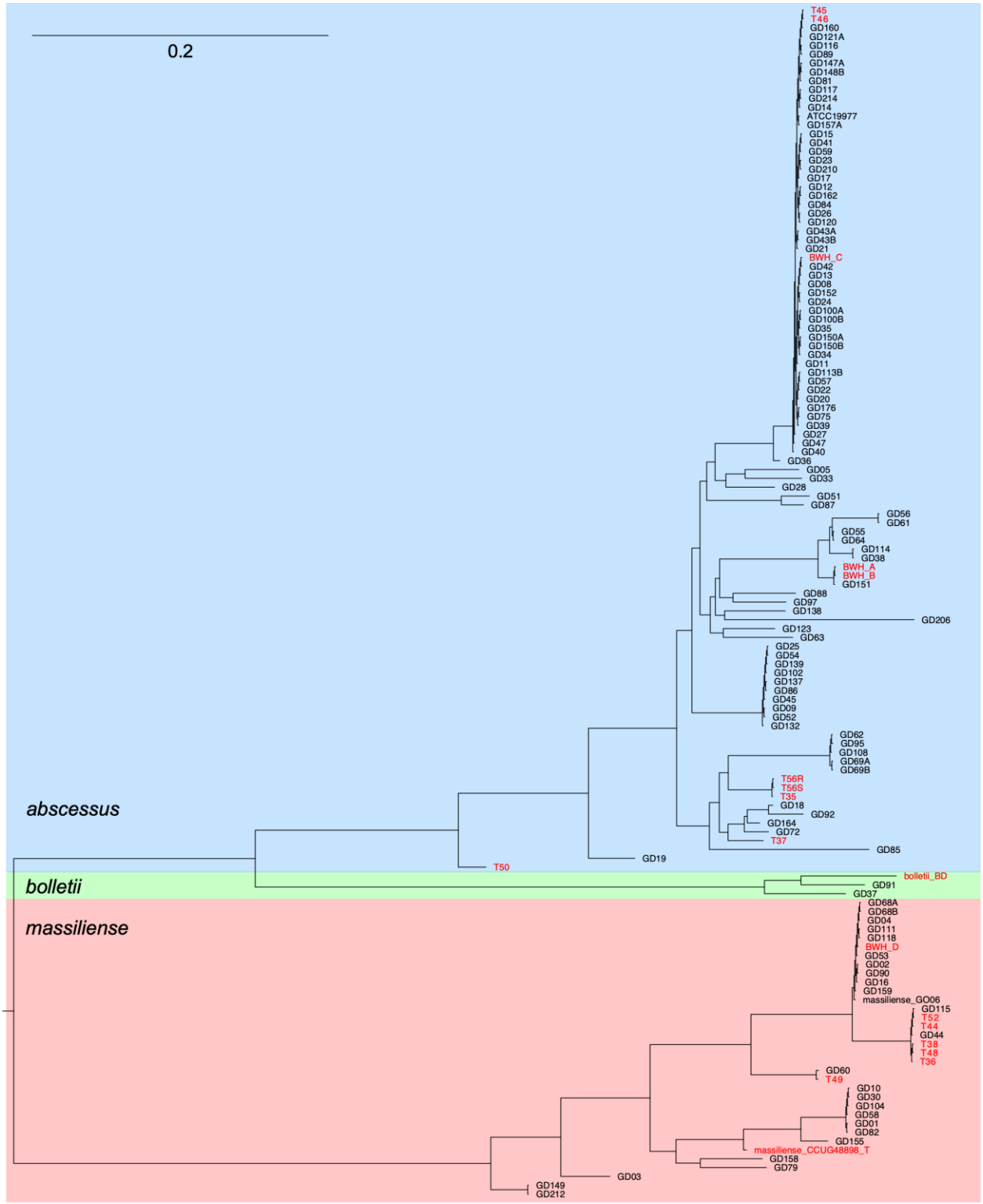

Figure 3. Phylogeny of *M. abscessus* strains.

Phylogenomic relationships of *M. abscessus* isolates based on 3,350,221 (65.8%) positions conserved in all strains. Subspecies are shaded blue, green, and salmon for *M. abscessus* subsp. *abscessus*, *M. abscessus* subsp. *bolletii*, and *M. abscessus* subsp. *massiliense*, respectively. Strain names in red are those described here. Other strains either were reported previously (Dedrick & Smith et al., 2021) or are unpublished data. Scale bar corresponds to 0.2 substitutions per position**.**

1.8.2 MAC Complex Strains in this Research

The MAC complex strains were given designations based on the information received from the collaborators. Strains given a four digit designation beginning with the number eight were taken from the serial numbers on the tubes received. Strain 8424 was sent as *M. intracellulare*, strain 8482 as *M. avium*, strain 8020 as *M. avium*, strain 8141 as *M. chimaera*. Most of the strains received from the Pride lab were not sent with species level details; strains UCSD1, UCSD3, UCSD4, UCSD11, UCSD13, UCSD19 and UCSD20 were sent as species *M. avium*. Strain UCSD6 was sent as *M. columbiense*, and the remaining strains were sent as MAIC complex.

1.8.3 Mycobacteriophages in this research

The mycobacteriophages in the screens described here largely represent phages isolated on *M. smegmatis* mc^2155; one group of phages was originally isolated on *M. avium*, and two phages spontaneously induced and propagated from filter sterilized culture supernatants. The *M. smegmatis* mc^2155 phages were chosen based on precious work which identified clusters with phages that demonstrated expanded host range (Jacobs-Sera, Marinelli et al. 2012). Phages with expanded host range belonged to subclusters of Cluster A (A1 and A2) and Cluster K. Cluster G

phages (BPs) demonstrated reduced infection phenotypes when spotted onto Mtb, and a host range mutant (HRM) able to infect at full efficiency was isolated.

1.9 Chapter 1 Summary

Non-tuberculous mycobacteria (NTM) are a causative agent of pulmonary and disseminated infections in patients with cystic fibrosis (CF) or bronchiectasis. Infections caused by NTM are difficult to treat with antibiotics, and treatments are difficult for the patient. A renewed interest in phage therapy has demonstrated success in antibiotic resistant bacterial infections, and more recently in NTM infections. The number of mycobacteriophages that can be applied therapeutically is relatively low, and this may be influenced by the isolation host for most phages in the mycobacteriophage repository (*M. smegmatis* mc^2155). Many phages are temperate, and capable of both lytic and lysogenic life cycles. The lysogenic life cycle results in the phage genome integrating into the host chromosome through integrase-mediated site-specific recombination between the *attP* site in the phage genome and the *attB* site in the bacterial genome. The prophage can be induced to re-circularize in the presence of excise, to produce virion particles, resulting in a temperate lytically propagated spontaneously induced prophage (LPSIP). Previous work suggests mycobacterial genomes are replete with intact prophage sequences, the result of a successful lysogenic life style of a phage that was able to infect the NTM. **The goal of this work is to expand the repertoire of phage that can be applied therapeutically, by mining clinically isolated NTM strains for LPSIPs.** This was completed by characterizing clinically isolated NTM phenotypically, assessing the strains for prophage

content, isolating the LPSIP phage form of the prophages, and engineering the LPSIP to be therapeutically useful.

2.0 Bioinformatic analyses of NTM

Analysis of prophage content in WGS of the 20 MAB strains identified 29 intact prophage sequences from 11 of the strains (Table 1). Similar to *M. smegmatis* phage genomes, the prophage sequences demonstrate broad mosaicism, with evidence of gene and cassette exchange between the prophages. One prophage appears to be a tandem prophage constituted by two unrelated prophages, and this prophage was identified in three closely related strains (T36, T38, T48).

2.1 Methods of Bioinformatic Prophage Extraction and DEPhT

Genomes were assessed for prophage content with a combination of manual prophage extraction supplemented with BLAST (Altschul, Gish et al. 1990),and PHASTER (Arndt, Marcu et al. 2019). Extracted sequences were annotated with DNA Master v3.02, GeneMarkS v4.30, and Glimmer v3.02 (Delcher, Bratke et al. 2007). Putative protein functions for genes were predicted using BLAST and HHpred (Soding, Biegert et al. 2005), and tRNA genes were identified using ARAGORN v1.2.41 (Laslett and Canback 2004).

2.1.1 Manual prophage extraction with PHASTER and BLAST

Initial efforts to identify prophages in the 20 MAB genome sequences used a combination of PHASTER (Arndt, Marcu et al. 2019) and manual inspection, as described

previously (Dedrick, Aull et al. 2021). The imprecision of PHASTER prophage and prophage-like element detection necessitates manual common core sequence mapping at prophage junctions *attL* and *attR*. Prophage detection with VirSorter2 (Guo, Bolduc et al. 2021) was attempted but did not prove to be significantly more precise than PHASTER. Prophage sequences were verified by the prophage discovery tool, DEPhT (Gauthier, Abad et al. 2022).

2.1.2 DEPhT Analysis

As the long form suggests, Discovery and Extraction of Phages Tool (DEPhT) is a multimodal tool trained to identify prophage regions in bacterial sequences (Gauthier, Abad et al. 2022). Largely trained on *Mycobacteria*, DEPhT identifies prophages with more precision than PHASTER, necessitating less manual inspection of the output. When the 20 genomes were run in DEPhT slow-mode, no new prophages were identified, suggesting all intact prophage regions had been identified with the combination of PHASTER and manual inspection. The tandem prophage identified in manual inspection was not detected by DEPhT, suggesting the tool cannot be applied to tandem prophages (Gauthier, Abad et al. 2022).

2.2 MAB prophage content summary

Prophages were extracted from 11 of the 20 MAB complex strains (Table 1), two of which were the type strains CCUG48898-T (subsp. *massiliense*) and CCUG50184-T (subsp. *bolletii*). The nature of WGS meant that two strains (BWH-C and T45) had prophages split across multiple contigs, one of which was isolated in its virion form (4.1). Five of the strains

(T35, T44, T52, T56R, and T56S) appear to be prophage free, with two of these strains being the T56 isolate derivatives. Some strains have more than one prophage (CCUG48898-T, T36, T38, T48, T49, T45), and strains T49 and T46 each have three prophages, the maximum number of prophages in this set of strains. All but one of the prophages had not been described previously; prophiBWHD-1 from strain BWH-D appeared to be identical to the previously described prophiGD04-1 (Dedrick, Aull et al. 2021). All the prophages extracted encode for a polymorphic toxin/immunity system, excepting the Cluster A prophages – prophiT46-3/prophiT45-2, prophiT49-3, prophiBWHA-1/prophiBWHB-1, which do not seem to have these systems. Three strains that are phylogenetically closely related, T36, T38, T48 have the same prophage content, including the identical prophage prophiT38-1, prophiT48-1, and prophiT36-1, although prophiT36-1 has a 45kbp insertion. These three strains encode for a tandemly inserted prophage, composed of an a-arm and a b-arm. Two other sets of prophages are identical to each other, but are integrated into different hosts, prophiT46-3 and prophiT45-2, and prophiBWHA-1 and prophiBWHB-1. Of the prophages identified, five of them encode tRNAs, and prophiT49-2 encodes 24 tRNAs and one tmRNA - the most tRNAs in this group. Eleven of the prophages have a tyrosine integrase (Y-Int) (Table 1), and they were found to use seven *attB* sites; five of the prophages have a serine integrase (S-Int), and they were found to use five *attB* sites among them (Table 1).

Table 1. *M. abscessus* strains and their prophages.

Strain	Source	R/S[1]	S[2]	Subsp[3]	Prophages	Coordinates[4]	Clust[5]	Other[6]
T35	Taiwan	S	W	a	None	N/A	N/A	None
T36	Taiwan	S	C	m	prophiT36-1	3482056-3592847	AD2	None
					prophiT36-2a	535142-613554	HN2	
					prophiT36-2b		HB3	
T37	Taiwan	S	W	a	prophiT37-1	C367 223812-300022	HK1	HC
T38	Taiwan	S	W	m	prophiT38-1	C1 448015-513273	AD2	None
					prophiT38-2a	C8 183836-262243	HN2	
					prophiT38-2b		HB3	
T44	Taiwan	S	W	a	None	N/A	N/A	None
T45	Taiwan	S	W	a	prophiT45-2	C393 19631-74641	A28	HA, HB, AD
T46	Taiwan	S	W	a	prophiT46-1	C3 260970-313843	HG1	HA, HB
					prophiT46-2	C2 346212-411463	AD2	
					prophiT46-3	C5 19238-74248	A28	
T48	Taiwan	S	W	m	prophiT48-1	C1 952938-1018196	AD2	None
					prophiT48-2a	C7 34327-	HN2	

						112734		
					prophiT48-2b		HB3	
T49	Taiwan	S	W	m	prophiT49-1	C1 832090-898129	AD2	None
					prophiT49-2	C1 1081832-1162060	M5	
					prophiT49-3	C3 393982-447365	A28	
T50	Taiwan	S	W	m	prophiT50-1	C387 35546-76736	HB1	Plasmid
T52	Taiwan	S	W	m	None	N/A	N/A	None
T56R	Taiwan	R	W	a	None	N/A	N/A	Plasmid
T56S	Taiwan	S	W	a	None	N/A	N/A	Plasmid
BWH-A	Boston	S	W	a	prophiBWHA-1	C10 143636-200007	A28	Plasmid
BWH-B	Boston	S	W	a	prophiBWHB-1	C10 143836-200208	A28	Plasmid
BWH-C	Boston	S	W	a	None	N/A	N/A	HA; Plasmid
BWH-D	Boston	R	W	m	prophiBHWD-1	C2 272234-332665	HE1	None
CCUG50184-T	CCUG	S	W	b	prophiCCUG50184T-1	C1 1340084-1405291	AD2	= bolletii BD
CCUG48898-T	CCUG	R	W	m	prophiCCUG48898T-1	C3 369722-419386	HC1	None
					prophiCCUG48898T-2	C7 228947-	HA5	

						290995		

[1]Colony morphotype. R, rough; S, smooth

[2]Genome sequencing. W, whole genome sequence; C, complete genome sequence

[3]Strain subspecies; a, subspecies *abscessus*; m, subsp. *massiliense*; b, subsp. *bolletii*

[4]Prophage coordinates within the strain genome; WGS data analyzed for all but T36, contig number indicated by C. Prophage orientation is that of the host; coordinates followed by an "r" indicate prophage is in reverse complement orientation.

[5]Cluster of each prophage, based on designation in (Abad, Gauthier et al. 2023).

[6]BLASTN searches indicate some strains contain additional prophages, but their sequences are split between two or more contigs and cannot be extracted as a single prophage sequence; their predicted cluster designations are shown. Some strains contain a plasmid, which is also noted.

2.2.1 Unusual tandemly integrated prophages in strains T36, T38, and T48

An unusual prophage constituted of two different prophages was identified in the three closely related strains T36, T38, and T48. The T36 strain and tandem prophage will be used as the description for this prophage, but the descriptions apply to the tandem prophage that is in strains T38, and T48 as well. The entire prophage region is denoted prophiT36-2, while the constituent arms are denoted prophiT36-2a and prophiT36-2b (Figure 4; panel A). The left, a-arm, prophiT36-2a shares nucleotide similarity with prophages belonging to Subcluster HN2; the right, b-arm, prophiT36-2b shares nucleotide similarity with prophages belonging to Subcluster HB3. Though each arm appears to be unrelated to the other, there is some nucleotide similarity between them (Figure 4; panels B and C). Genome comparisons suggest the tandem prophage came to be through superinfection of a lysogen, leading to integrase-mediated site-specific recombination between the superinfecting phage *attP* and the *attR* of the resident prophage (Figure 6).

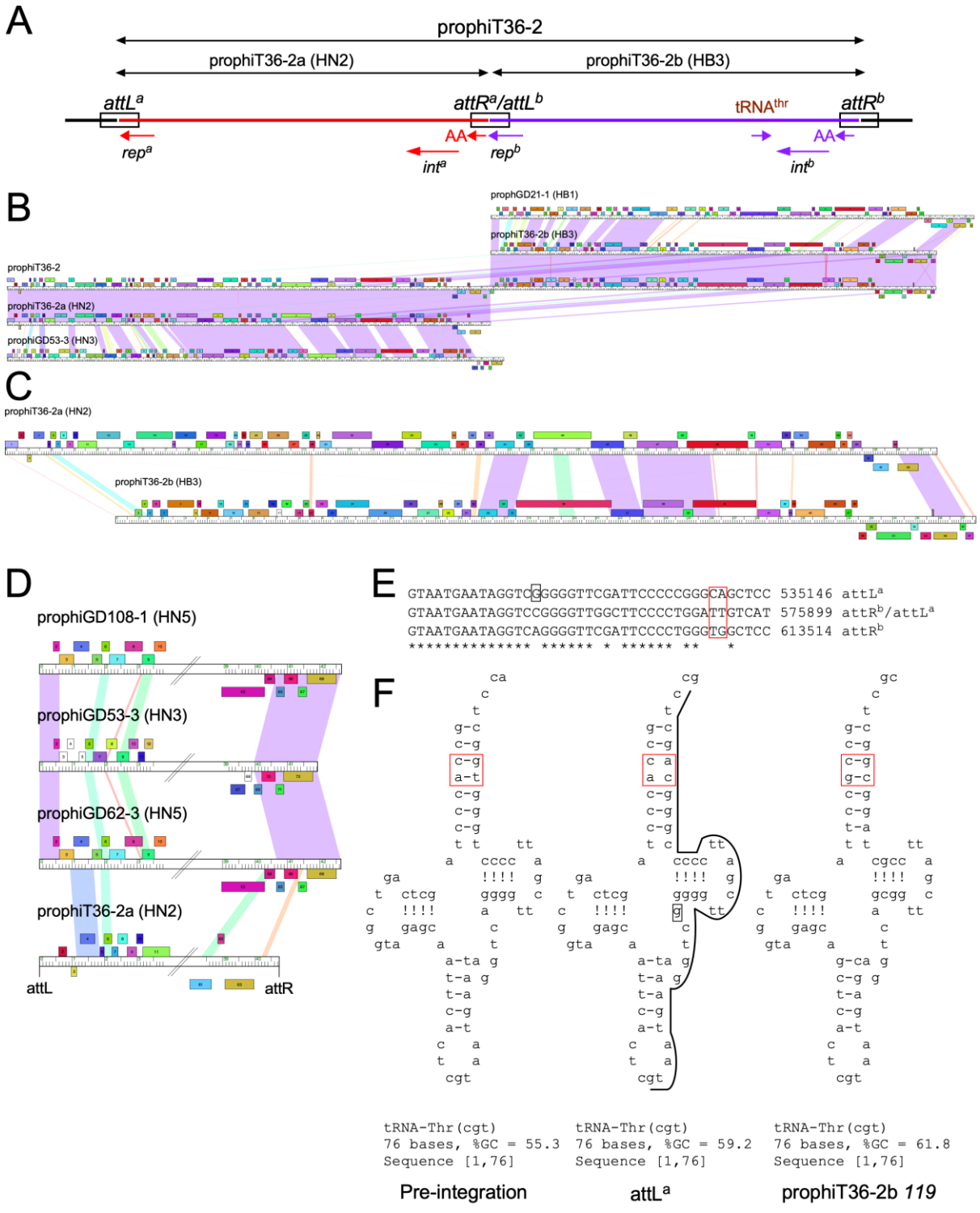

Figure 4. An unusual tandem prophage in *M. abscessus* T36.

A. An overview of the proposed tandem prophage insertion, prophiT36-2a and b, in strain M. abscessus T36. B. Alignment of prophage genomes in the form of phamerator genome maps. Panel C. Comparison of prophiT36-2a and prophiT36-2b genomes, showing regions of similarity. D. Genome alignment of the left ends of Cluster HN prophages. Panel E. Sequences of the common core at the att sites. Panel F. Predicted secondary structures of the pre-integration tRNA (equivalent to MAB_t5010) and the tRNA at attLa and the prophage tRNA gene (*119*).

Prophage prophiT36-2a clusters with Subcluster HN2 prophages, integrates at *attB-2* site, and demonstrates some differences from other Subcluster HN2 prophages (Figure 4). The portal (g*33*) and major capsid (g*35*) proteins are unrelated to those of other HN2 members, and the polymorphic toxin-immunity cassette is only distantly related. The extreme ends – $attL^a$ and $attR^b$ – of prophiT36-2 prophage have the expected 40 bp common core sequence, and in the "middle" of prophiT36-2 is the common core at the junction of the a- and b-arms – $attR^a$/$attL^b$. The three common cores are not identical and have several nucleotide substitutions among them (Figure 5). The $attL^a$ core sequence in particular deviates from the other att-site cores at the 3'-end, and it overlaps a host encoded $tRNA_{Thr}$ that corresponds to the ATCC19977 gene *t5010*. The deviations at the 3'-end of the $attL^a$ core lead to mismatches in the acceptor stem of the $tRNA_{Thr}$ (Figure 4; panel F) and it is likely that this change impairs or wholly inactivates the host encoded $tRNA_{Thr}$.

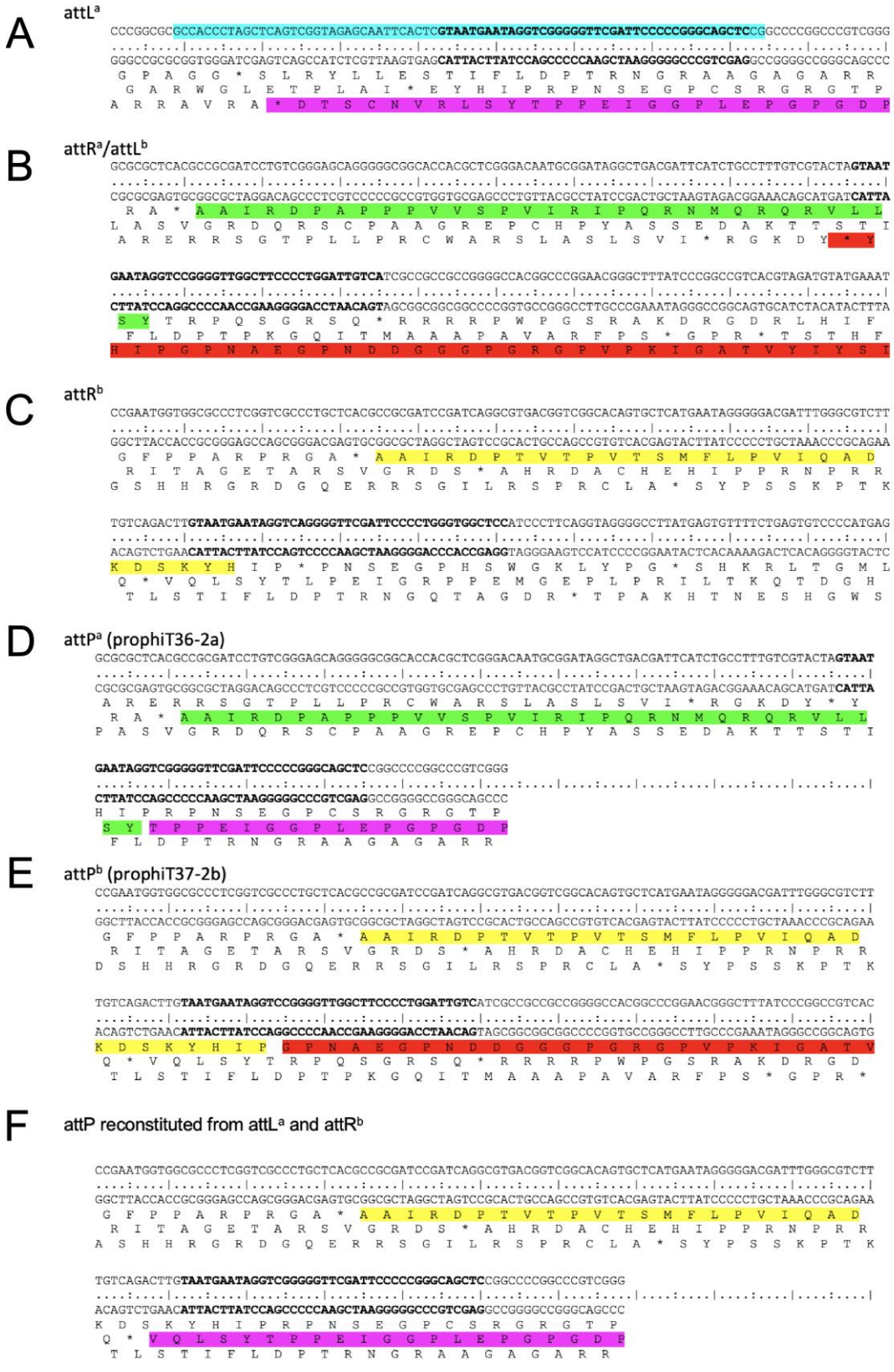

Figure 5. Sequences of *att* sites and repressors in prophiT36-2.

A-F. Strands of DNA sequence and the three translated reading frames that are transcribed leftwards.

The tandem prophage utilizes integration-dependent superinfection immunity (1.6.5). Identifying the putative 3' remnants of prophiT36-2a and prophiT36-2b at the $attR^a/attL^b$ and $attR^b$ sites, respectively, show the characteristic ssrA-like degradation tag, and the respective repressors are unrelated at the amino acid level. A closer look at the repressors reveals they are not encoded in the same reading frame. If this were not the case, and the prophiT36-2a repressor and prophiT36-2b repressor shared the same reading frame, this would result in the in-frame fusion of the prophiT36-2b 3' repressor remnant with the prophiT36-2a repressor 5', and since these repressors are not related, such a fusion would not yield a functional repressor protein. An attempt to reconstruct the putative *attP* between the $attL^a$ and $attR^b$ does not make a full phage repressor gene with an ssrA-like degradation tag. The only *att* site combinations yielding a functioning repressor with an ssrA-like degradation tag are the combinations: $attL^a$ x $attR^a/attL^b$ and $attR^a/attL^b$ x $attR^b$.

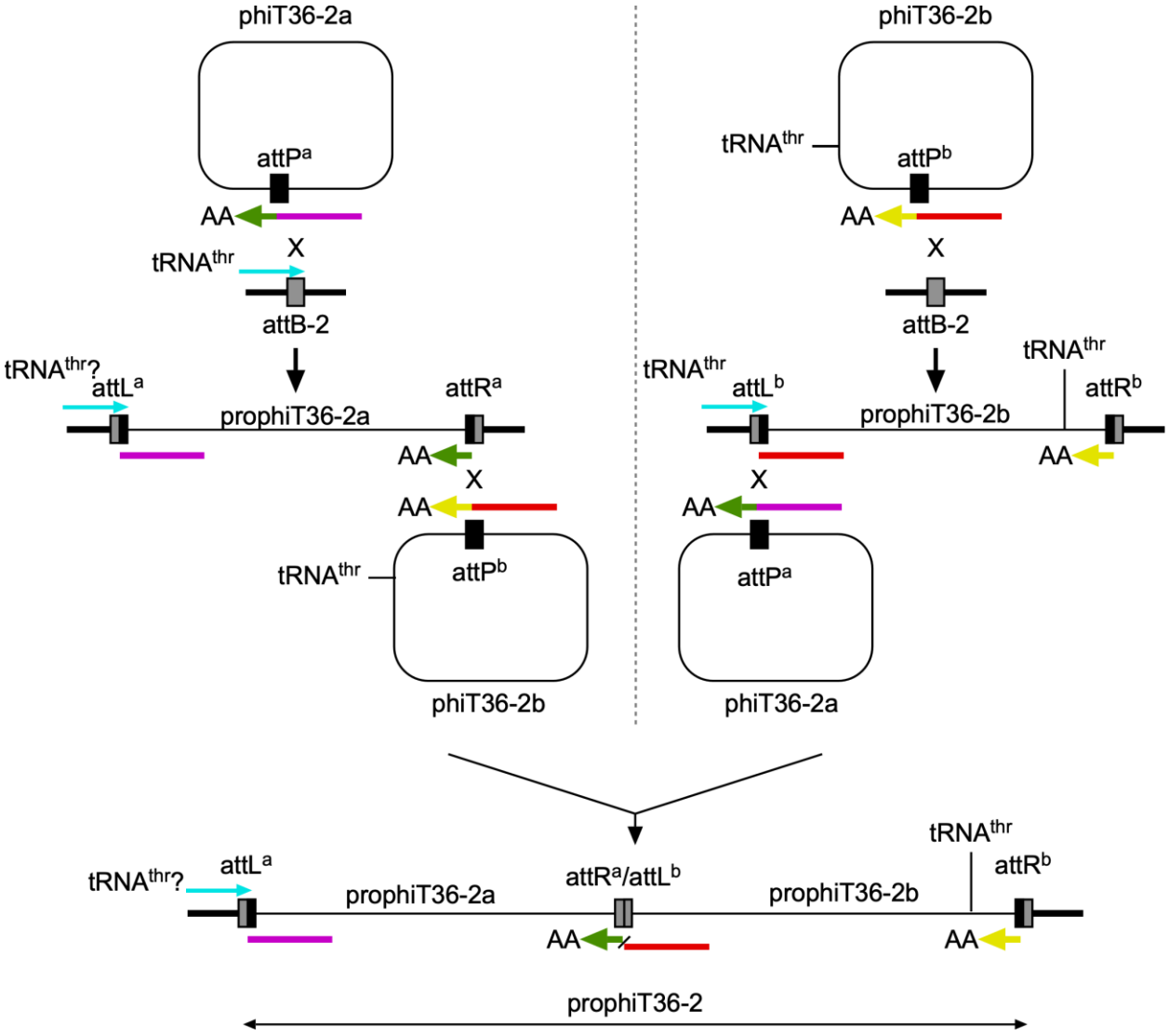

Figure 6. Pathways for formation of tandem prophages in T36.

The entire prophage prophiT36-2 (bottom) is constituted by prophiT36-2a (top left) and prophiT36-2b (top right).

The deviations in the 3' end of the common core sequence in the attL^{a} site suggests integration of phiT36-2a leads to impairment of the host encoded tRNA$_{Thr}$ that is overlapped by the attB-2 integration site. At the extreme end (~ 2 kbp upstream of the attR^{b}) of prophiT36-2b is a prophage encoded tRNA$_{Thr}$ (cgt), a characteristic shared with one other HB3 prophage, prophi1962118.130_2-1 (Phamerator Database under100contigMycos v12). The location of the

prophiT36-2b tRNA suggests that it is expressed lysogenically, supporting that the prophage encoded $tRNA_{Thr}$ complements any $tRNA_{Thr}$ function that is lost from integration of phiT36-2a.

It is likely that of the two phages, phiT36-2a and phiT36-2b, phiT36-2a was the first to integrate into the T36 host chromosome. Integration of phiT36-2a and inactivation of the host $tRNA_{Thr}$ at the $attL^a$ site when prophiT36-2a is formed is more likely to impose a selection requirement for a $tRNA_{Thr}$ in a temperate, superinfecting phage, allowing for T36 continue normal cellular growth as a double lysogen. The integration-dependent superinfection immunity systems in prophiT36-2a and prophiT36-2b necessitate that they do not share a reading frame, allowing for each repressor to be unperturbed by a fusion with the other.

Table 2. *M. abscessus* prophages.

Prophages	Clust	Length (bp)	ORFs	tRNA/tmRNA	attB	Int	Comment
prophiT46-3	A28	55011	82	2	attB-7	Y	
prophiT45-2							
prophiT49-3		53384	73	2	attB-21	S	
prophiBWHA-1		56372	91	2	attB-7	S	
prophiBWHB-1							
prophiT36-1	AD2	110792	129	0	attB-10	Y	
prophiT46-2		65252	95	0	attB-3	S	
prophiT48-1		65259	93	0	attB-10	Y	
prophiT38-1							
prophiT49-1		66040	92	0	attB-10	Y	
prophiCCUG50184T-1		65208	93	0	attB-10	Y	
prophiCCUG48898T-2	HA5	62049	89	0	attB-20	Y	
prophiT50-1	HB1	41191	59	0	attB-2	Y	
prophiT36-2b	HB3	37655	51	1	attB-2	Y	
prophiT38-2b							
prophiT48-2b							
prophiCCUG48898T-1	HC1	49665	68	0	attB-13	Y	
prophiBWHD-1	HE1	60432	80	0	attB-4	Y	
prophiT46-1	HG1	52874	79	0	attB-11	Y	
prophiT37-1	HK1	76211	110	0	attB-1	Y	
prophiT36-2a	HN2	40793	54	0	attB-2	Y	
prophiT38-2a							
prophiT48-2a							
prophiT49-2	M5	80229	161	24; tmRNA	attB-17	S	

[1]Prophages are designated as prophixxx, and identical prophages are listed indented. Identical prophage regions identified in strains T36, T38, and T48 were designated as prophiT36-2, prophiT38-2, and prophiT48-2, respectively, but each contains tandemly integrated prophages, designated as prophiT36-2a and prophiT36-2b.

[2]Cluster designations of prophages according to the system described in Abad et al., 2023.

[3]The *attB* site occupied by the prophage is according to the designations described in Dedrick & Aull et al., 2021.

[4]The prophage-encded integrase (Int) is indicated as either a tyrosine-integrase (Y) or a serine-integrase (S).

[5]Detailed genome maps are shown in figures indicated.

2.2.2 Variation among Subcluster AD2 prophages

Two of the five prophages that are closely related to Subcluster AD2 prophages are the identical prophages prophiT38-1 and prophiT48-1. The prophage prophiT36-1 is nearly identical to prophiT38-1 and prophiT48-1, but it has an insertion of about 45 kbp between the minor tail (gene *80*) and lysin A (gene *122*). The 45 kbp insertion actually is a duplication of a 22.5 kbp region which codes for 18 genes - 36 genes total. This insertion is found elsewhere in the T36 genome, between genes *T36_00429* and *T36_00464*, and related copies of this insertion can be found in some subsp. *massiliense* strains. Of the 36 genes in the duplication, one set (genes *82* and *102*) appears to be a functional tyrosine integrase. A second set of genes (genes *83* and *103*) are closely similar to tyrosine integrase, but they have a c-terminus that is extended. A third set of genes (genes *84* and *104*) have a small, integrase-like domain but are globally distinct from true integrases (Figure 7). Annotation of the other genes in this insertion include a DNA helicase (genes *86* and *106*), an AAA-ATPase (genes *92* and *110*), and an LqpN-like predicted lipoprotein (genes *99* and *118*). Genes *96* and *114* each have an RpoD-like sigma factor domain, and TnsA transposase related motif. It is very likely the 45 kbp insertion is too large to allow for the sequence to be packaged into a capsid as-is, and it is possible DNA packaging for the

prophiT36-1 phage form may involve a transposition event like the one seen between the prophage and phage form of GD20-1 (Dedrick, Aull et al. 2021).

2.2.3 Genetic exchange of polymorphic toxin-immunity cassettes

Polymorphic toxin-immunity cassettes have been described previously (Zhang, de Souza et al. 2012, Amarh, Dedrick et al. 2021, Amarh, Gauthier et al. 2021, Dedrick, Aull et al. 2021), they are rare in *M. smegmatis* phages outside of Subcluster K1 but can be found in prophages, including the prophages described here. Prophages belonging to Cluster A did not encode polymorphic toxin-immunity cassettes. Polymorphic toxin-immunity cassettes are constituted of three components: (1) a polymorphic toxin (2) an immunity gene whose protein protects from the toxicity of the polymorphic toxin (3) and a WXG-100. The N-terminal of the WXG-100 motif indicates that the proteins from this cassette are exported by a Type VII secretion system (T7SS) (1.5). Genome comparison of the prophages with polymorphic toxin-immunity cassettes suggests the mosaicism of these genomes includes, and conserves, these cassettes.

When looking at prophage prophiCCUG48898T-1, it appears to be closely related to the Subcluster HC1 prophages, which are generally dissimilar to the Subcluster HD1 prophages (Figure 8). The right arm of the genome contains a stretch of 2.3 kbp that is dissimilar to other Subcluster HC1 prophages and similar to the Subcluster HD1 prophage prophiGD17-1. The 2.3 kbp stretch includes genes *67 – 70* of prophiCCUG48898T-1, of which *68 – 70* share 97% nucleotide identity with the homologues in prophiGD17-1, while the 3’ half of gene *67* of prophiCCUG48898T-1 shares 77% nucleotide identity to the prophiGD17-1 homolog (gene *85*) Figure 8. While it is not clear how many events resulted in the exchange of this polymorphic toxin-immunity cassette, the similarity in this region of the Subcluster HC1

prophiCCUG48898T-1 and the HD1 prophiGD17-1 suggest this polymorphic toxin-immunity cassette was exchanged relatively recently in the evolutionary history of these two prophages.

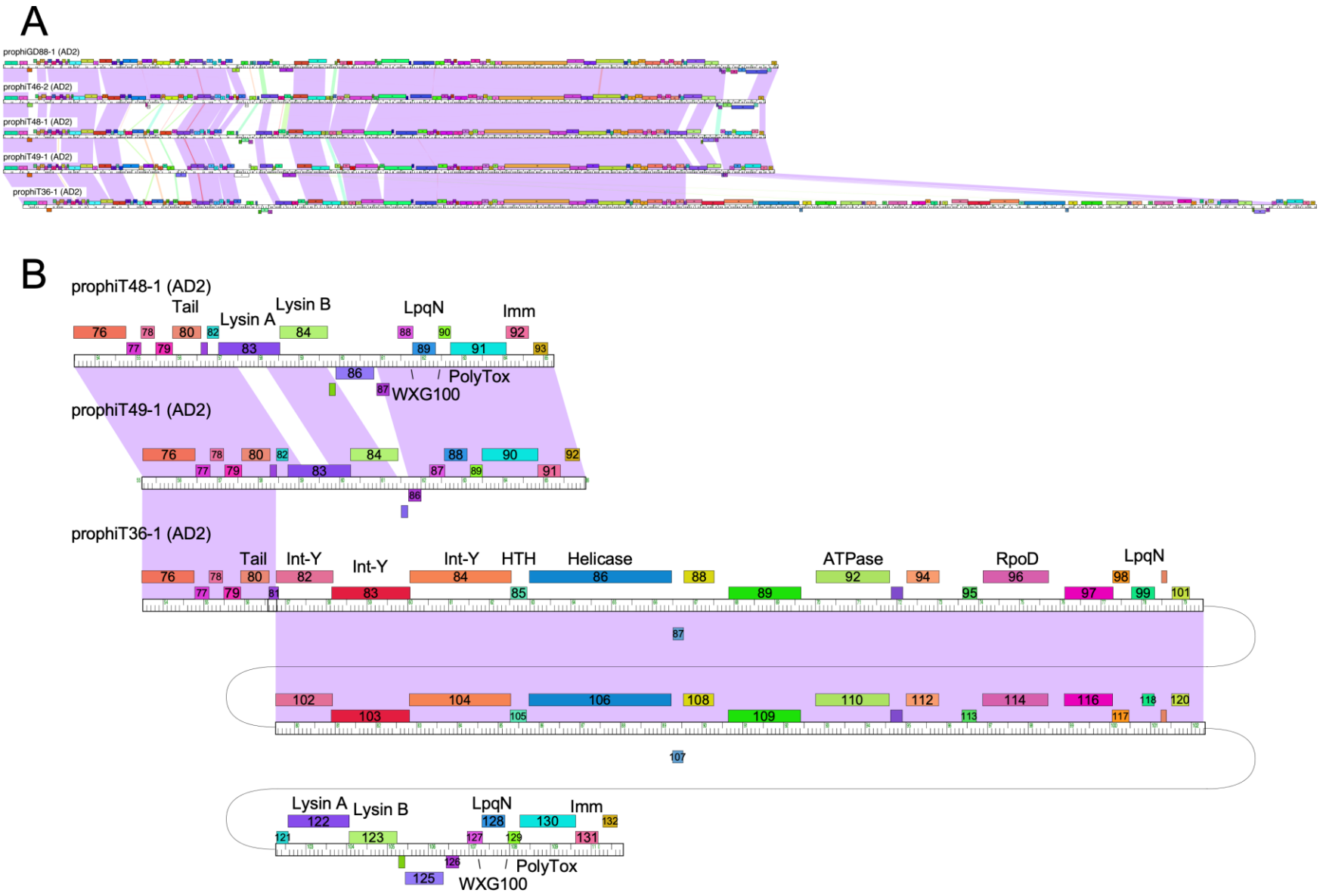

Figure 7. A large insertion in prophiT36-1.

Panel A. ProphiT36-1 is a member of Subcluster AD2 and is closely related with other cluster members. Five genomes (prophiGD88-1, prophiT46-2, prophiT48-1, prophiT49-1, and prophiT36-1). Panel B. The tandemly inserted 22.5 kbp DNA segment in prophiT36-1.

The polymorphic toxin-immunity (PT) cassette (genes *103 – 105*) in the Subcluster HK1 prophage prophiT37-1 is transcribed rightwards, a characteristic shared with tens of other members of Subcluster HK1 (Figure 9). The rightward transcription of this PT cassette is unique in these prophages in that they are usually transcribed leftwards, as seen in the PT-cassette in the Subcluster A28 prophage prophiGD43A-5 (genes *110 – 112*). Genes *103 – 105* of prophage prophiT37-1 are distantly related to genes *80 – 82* of the Cluster AQ prophage prophiGD79-1 with 54%, 38%, and 48% amino acid identities, respectively, suggesting this polymorphic toxin-immunity cassette was exchanged between these clusters. Interestingly, although the PT-cassette in prophiGD79-1 is transcribed rightwards, the Cluster HQ prophage prophiAJGF01-3 PT-cassette is transcribed rightwards, while genes on either side of the cassette are transcribed leftwards (Phamerator Database under100contigmycos v12).

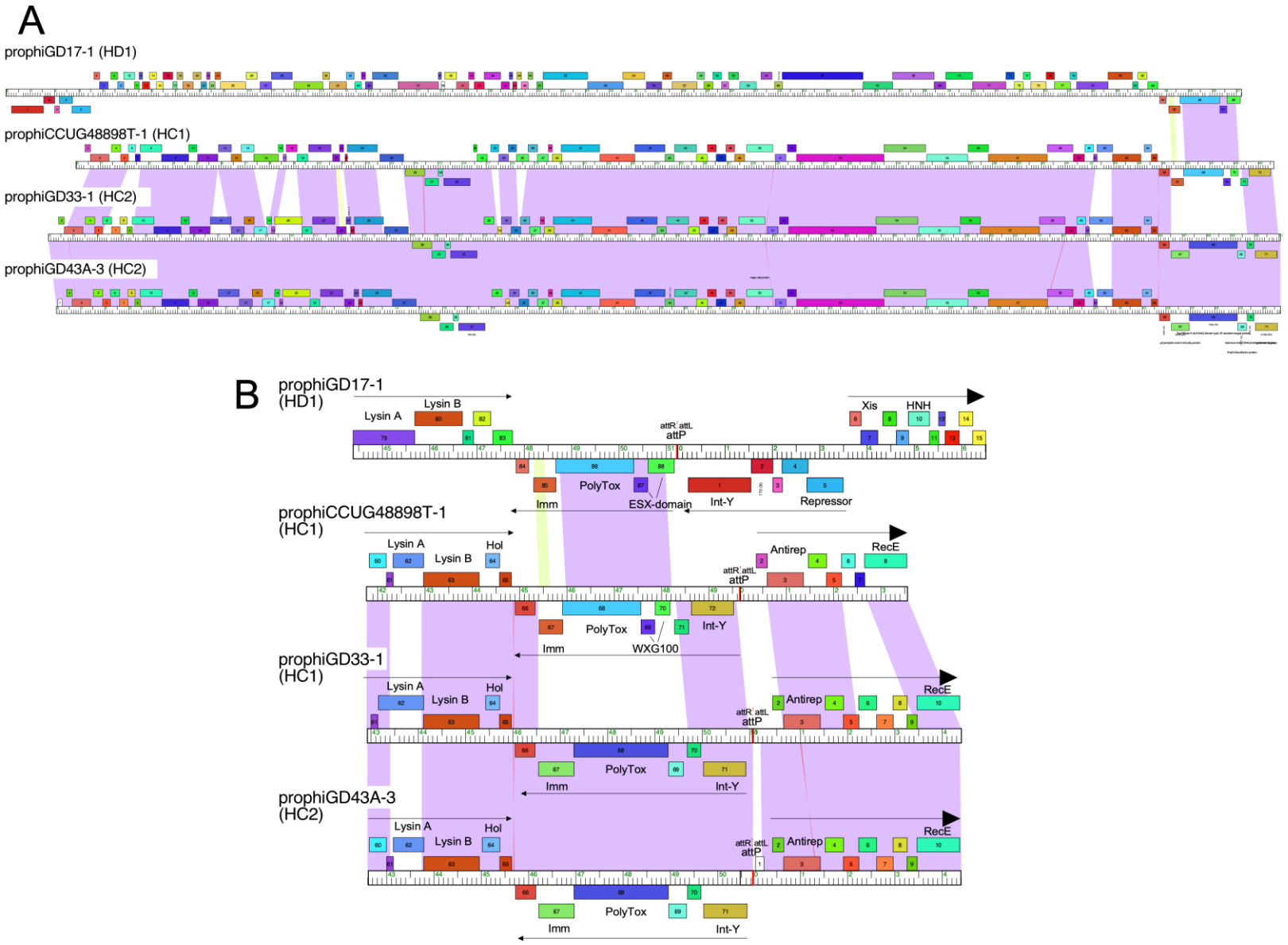

Figure 8. Polymorphic toxin-immunity systems swapping between HC and HD genomes.

Panel A. Phamerator genome maps for prophiGD17-1, prophiCCUG48898T-1, prophiGD33-1, and prophiGD43A-3 are displayed. Panel B. Exchange of the polymorphic toxin-immunity cassette between HD and HC prophages.

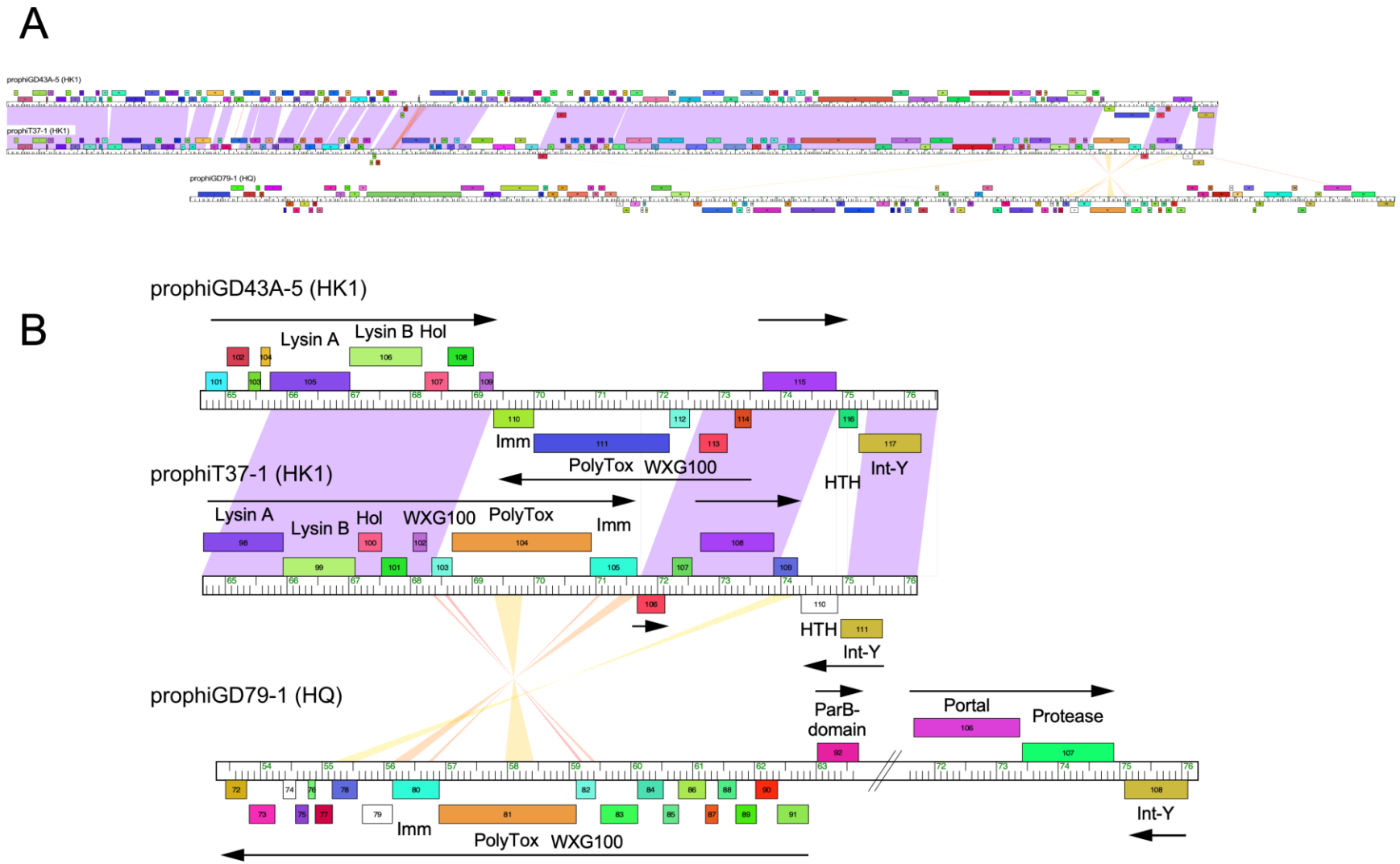

Figure 9. Polymorphic toxin-immunity system swapping between HK and HQ genomes

A. Phamerator genome maps of two Cluster HK prophages. B. Exchange of the polymorphic toxin-immunity cassettes between HK and HQ genomes.

2.2.4 A stoperator system similar to those observed in *M. smegmatis* phages in Cluster A

Prophages identified here belonging to Subcluster A28 display a characteristic similar to one seen in *M. smegmatis* phages belonging to Cluster A. Cluster A phages have an unusual repressor system involving multiple repressor binding sites across the phage genome (Brown, Sarkis et al. 1997, Mavrich and Hatfull 2019). The repressor is relatively small, and the repressor binding sites are asymmetrical, ~ 14 bp binding sites that are all transcribed in one direction. The binding sites are located in intergenic regions, with a higher density of the binding sites near the *cos* site (Brown, Sarkis et al. 1997, Dedrick, Mavrich et al. 2017). One of the repressor binding sites overlaps the strong early lytic promoter P_{left} (Brown, Sarkis et al. 1997). The other repressor binding sites are likely to act as repressor-dependent transcription termination sites. Genome comparisons of the A28 prophages described here suggest they use a similar stoperator system.

The prophiT49-3 repressor encoded by gene *41* has a 155 amino acid product. The prophiT49-3 repressor shares 40% amino acid identity with Subcluster A8 *M. smegmatis* phage repressors, such as the repressor used by phage Expelliarmus. Prophage prophiT49-3 has 14 identified stoperator sites (Figure 10), all with the same sequence 5’ – cTTgACATACGaCC. The twelfth stoperator site overlaps the prophiT49-3 P_{left} promoter, and so it is likely site 12 acts as a true operator site for the early lytic promoter(Figure 10). The other Subcluster A28 prophages in this collection have some sequence variation among the repressors, but it appears they recognize similar stoperators. These stoperator systems are diverse yet conserved between Subcluster A8 *M. smegmatis* phages and Subcluster A28 prophages.

A

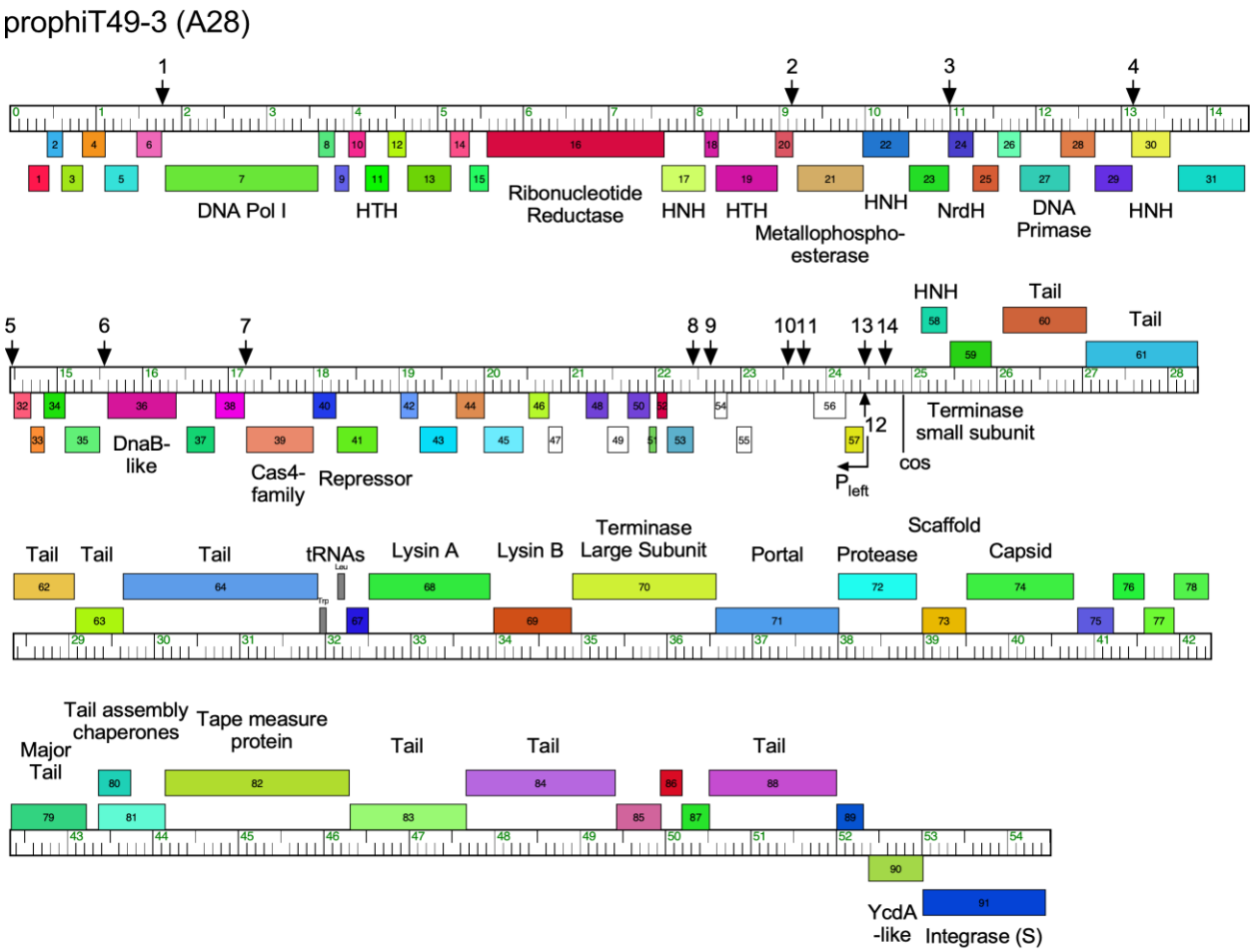

B

Site	Sequence	Orient^n	Coordinates
1	CTTGACATACAACC	-	1782. .1795
2	CTTGACATACGACC	-	9148. .9161
3	CTTGACATACGACC	-	10995. .11008
4	CTTGACATACGACC	-	13148. .13161
5	CTTGACATACGGCC	-	14581. .14594
6	CTTGACATACGACC	-	15525. .15538
7	CTTGACATACGACC	-	17206. .17219
8	CTTGATATACCACC	-	22465. .22478
9	CTTTACATACGACC	-	22646. .22659
10	CTTGACATACGGCC	-	23548. .23561
11	CTTGACATACGACC	-	23720. .23733
12	TTTGACATACGACC	+	24431. .24444
13	CTTGACATACGGCC	-	24460. .24473
14	CTTTACATACGACC	-	24696. .24709
	cTTgACATACGaCC	Consensus	

Figure 10. Repressor binding sites in A28 prophage prophiT49-3.

Panel A. Genome map of prophiT49-3. Panel B. Sequences of operator and stoperator sites, showing their genome coordinates, orientation, and consensus sequence.

2.2.5 Most prophages spontaneously induce to form phage particles

The prophages that have been bioinformatically identified appear to be fully intact and are not cryptic or decaying prophages. To detect if the prophages produce virion forms, we amplified the predicted *attP* for the prophages that have been fully sequenced, by running PCR with oligonucleotide primers that amplify the predicted *attP* sites on filter sterilized culture supernatants. Most of the predicted *attP* sites were amplified Figure 11.

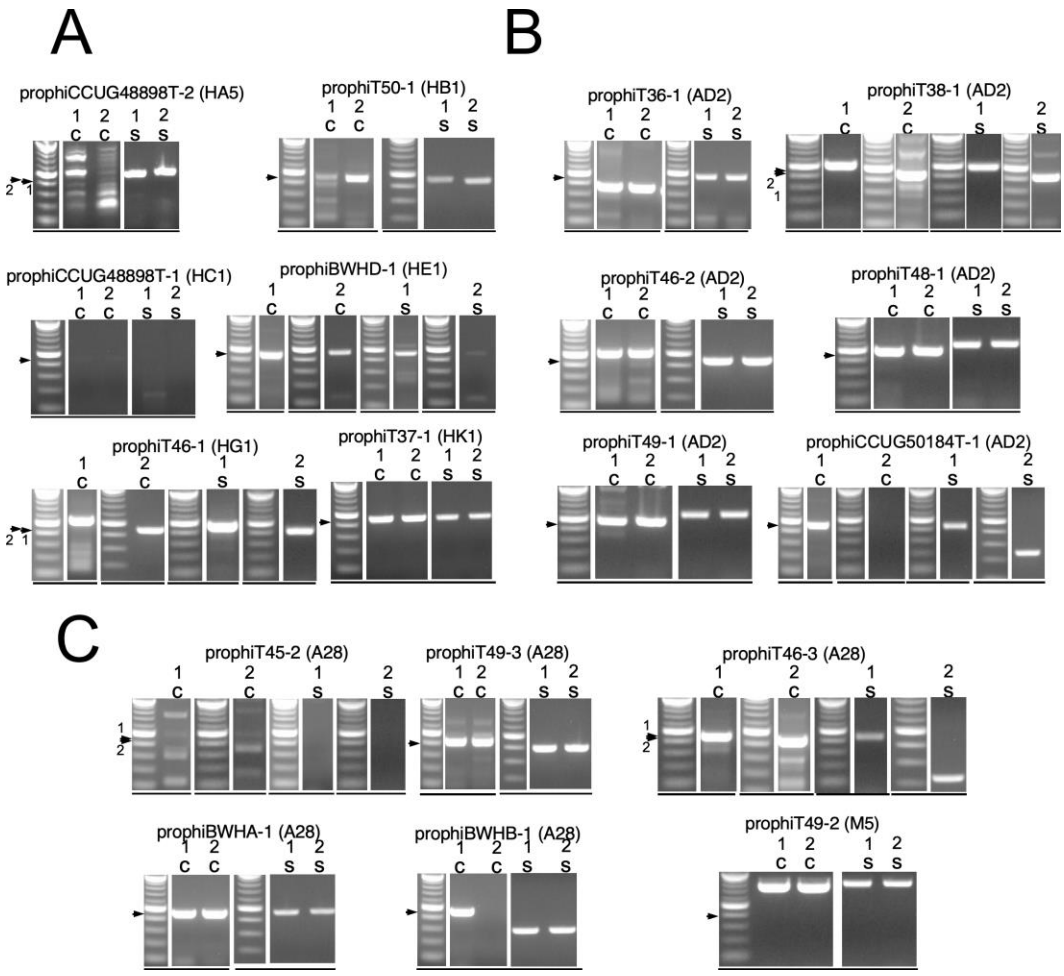

Figure 11 Detection of phage virions by PCR.

PCR products from primers flanking the predicted *attP* from prophage sequences. For many prophages, two primer sets were used, designated 1 (primer set 1) and 2 (primer set 2) above the lanes. The input for the reaction was either from bacterial culture (C) or culture supernatant (S) as indicated. A. Predicted Cluster H *attP* sites.

As hypothesized, the *attP* for the tandem prophage prophiT36-2 was not detected in culture supernatant (Figure 12). The virion forms of the constituent prophages, phiT36-2a and phiT36-2b have been detected by PCR, and this is consistent with the only successful *att* site combinations being between $attL^a$ and $attR^a/attL^b$ and $attR^a/attL^b$ and $attR^b$. Interestingly, the predicted *attP* was detected in the bacterial culture of T36, indicating the recombination event does occur but is not packaged in the virion particle form (Figure 12). The prophiT45-2 *attP* site is not detected in either the T45 filter sterilized culture supernatant or the T45 culture, however, the identical prophage prophiT46-3 is detected in both the culture and the supernatant of T46. Bacterial attachment sites for some strains were detected in filter sterilized supernatants, and it is possible this is an artifact of cell lysis from spontaneous prophage induction. Detection of predicted *attP* sites for most of the prophages suggests the phage forms can be isolated if a strain susceptible to infection by the phage form is available, and this is explored more in Chapter 4 (3.3).

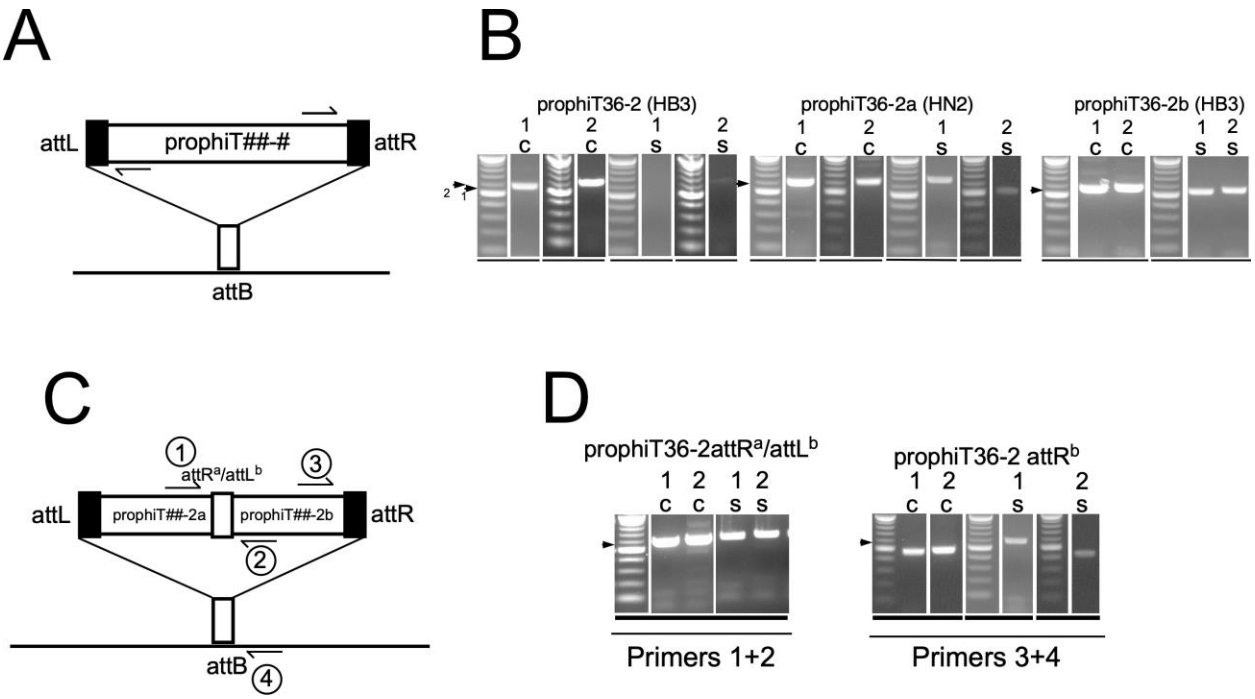

Figure 12. Detection of tandem prophage phage virions by PCR.

A. A schematic of the primer annealing locations, annotated with right and left facing half-headed arrows for the forward and reverse primers respecitvely. The line represents the host chromosome, with the *attB* site indicated. The rectangle indicates the integrated prophage, flanked by *attL* and *attR* sites. B. PCR products from primers flanking the predicted *attP* from the tandem prophage prophiT36-2. For many prophages, two primer sets were used, designated 1 (primer set 1) and 2 (primer set 2) above the lanes. The input for the reaction was either from bacterial culture (C) or culture supernatant (S) as indicated. C. A shematic of the primer annealing locations, annotated with half-headed arrows as in panel A, for the 2a-2b $attR^a/attL^b$ site and the *attR* site of prophiT36-2. Culture or supernatant input indicated as in panel B. Either primers 1 and 2, or 3 and 4 were used for PCR as shown in panel C. PCR products for identical prophages prophiT38-2 and prophiT48-2 can be found in the appendix.

Table 3. Presence of *attP* in cultures and culture supernatants.

Strain	**Prophages**	**Clust[1]**	**attP; culture[2]**		**attP; s/n[3]**	
			1	2	1	2
T36	prophiT36-1	AD2	+++	+++	+++	+++
	prophiT36-2	HB3	++	+++	-	-/+
	prophiT36-2a	HN2	++	++	+	++
	prophiT36-2b	HB3	+++	+++	++	++
T37	prophiT37-1	HK1	+++	+++	+++	+++
T38	prophiT38-1	AD2	+++	+++	+++	+++
	prophiT38-2	HB3	+	+++	-	-
	prophiT38-2a	HN2	+++	+++	++	++
	prophiT38-2b	HB3	+++	+++	++	++
T45	prophiT45-1	HH1	++	+++	++	++
	prophiT45-2	AD2	-	-	-	-
T46	prophiT46-1	HG1	+++	+++	+++	+++

	prophiT46-2	AD2	+++	+++	+++	+++
	prophiT46-3	A28	+++	+++	+++	++
T48	prophiT48-1	AD2	+++	+++	+++	+++
	prophiT48-2	HB3	+	+++	-	-
	prophiT48-2a	HN2	+++	+++	++	+++
	prophiT48-2b	HB3	+++	+++	++	++
T49	prophiT49-1	AD2	+++	+++	+	++
	prophiT49-2	M5	+++	+++	+++	+++
	prophiT49-3	A28	+++	+++	+++	+++
T50	prophiT50-1	HB1	-	+++	+++	+++
BWH-A	prophiBWHA-1	A28	+++	+++	+++	+++
BWH-B	prophiBWHB-1	A28	+++	-	+++	+++
BWH-D	prophiBWHD-1	HE1	+++	++	++	-/+
CCUG50184-T	prophiCCUG50184T-1	AD2	-	-	++	++
CCUG48898-T	prophiCCUG48898T-1	HC1	-	++	-/+	-/+
	prophiCCUG48898T-2	HA5	-	++	+++	+++

[1]Prophage cluster designation as described in Abad et al., 2023.

[2]Amplification of the *attP* site by PCR in cell cultures, product abundance denoted by – (absent), or with +, ++, or +++ reflecting increasing signal strength. Barely noticeable signals are indicated as -/+.

[3]Amplification of the *attP* site by PCR in filter sterilized culture supernatants is shown as described for results from cell cultures.

2.3 Chapter 2 Summary

MAB complex strains were sequenced to the level of WGS, one (T36) was sequenced to a complete, single contig, and analyzed for intact prophages through DEPhT. The 20 MAB strains analyzed included the three type strains: ATCC19977, CCUG48898-T, and CCUG50184-T, and 17 clinically isolated strains. A total of 29 intact prophage sequences were extracted, three which have been described previously (prophiATCC19977-1, prophibolletii-1 from the bolletii-BD strain of which CCUG50184-T is a re-sequenced assembly, and prophiBWHD-1, which is identical to prophiGD04-1 (Dedrick, Aull et al. 2021)). Two sets of prophages in this data set are identical to each other, prophiT45-2 and prophiT46-3, and prophiBWHA-1 and prophiBWHB-1. A set of three prophages, prophiT36-2, prophiT38-2 and prophiT48-2 were extracted from three closely related strains. One prophage spanning multiple contigs was identified in strain BWH-C (putative prophiBWHC-1) and one in strain T45 (prophiT45-1, the prophage form of phiT45-1 (4.1)), and these prophage sequences are incomplete. A total of 16 unique prophages were identified in this data set. Analysis of prophages belonging to Clusters HC and HD suggests the clusters have a history of exchanging polymorphic toxin-immunity cassettes, and the same can be said for prophages belonging to Clusters HK and HQ. Interestingly the unique stoperator system observed in phages that cluster to Cluster A appears to be shared by prophages that cluster to Cluster A. Of the MAC complex strains, one strain was sequenced and assessed for prophage content (UCSD2), and no prophages were detected.

3.0 Susceptibility of NTM to Bacteriophage Infection

Assessing strain susceptibility to phage infection necessitates differentiating cell lysis events that are from successful lytic life cycle completion from cell lysis that is caused by other events (e.g.: abortive infection, lysis from without). Spot titer

3.1 Mycobacterial Phage Susceptibility Analysis Methods

Determination of a strain's susceptibility to phage infection is assessed by the results of three assays, the lysate spot titer, phage killing, and strain survival assays. If a phage is to be applied therapeutically, it must be able to infect the strain of interest as efficiently as it infects a highly susceptible control strain. Of these phenotypes, the most useful for therapeutic purposes is the full infection phenotype. However, if a phage is to be applied therapeutically, it must also be able to kill the strain efficiently with no survivors. Most of the data presented in this section comes from lysate spot titer assays.

3.1.1 Mycobacteriophage Lysate Spot Titer Assay

Tenfold serial dilutions of phage lysate is spotted onto a top agar overlay of the control strain – either *M. smegmatis* mc^2155 or *M. abscessus* GD40, depending on phage host range – and on a top agar overlay of the strain of interest, and the efficiency of plaquing (EOP) is calculated based on the observed titers. An EOP equal to about 1.0 is considered a full infection

phenotype, and an EOP equal to about 10^{-3}-fold reduction in plaquing on the strain of interest compared to the control strain is considered a reduced infection phenotype. The reduced infection phenotype indicates it is possible a host range mutant that infects the strain at a higher EOP can be isolated with multiple purification steps/passages through the strain of interest (Jacobs-Sera, Marinelli et al. 2012). An EOP equal to 10^{-6} (about zero) is considered the no infection phenotype. Strain clearing at high concentrations of phage lysate, without individual plaques at lower concentrations, is considered the killing without plaquing (KWP) phenotype. The KWP phenotype is not one from which individual plaques can be propagated. There are a number of possibilities that could lead to this phenotype, one of which is lysis from without (LO), which can be virion-mediated (LO_v) or lysin-mediated (LO_L) (Abedon 2011).

3.1.2 Mycobacteriophage Killing Assays

This assay aims to measure phage killing efficiency in a strain of interest by incubating the strain and the phage(s) together, spotting the mixtures onto naked agar plates and counting the colonies that grow at high and low concentrations of phage lysate. A concentration of 10^8 CFU ml^{-1} is serially diluted tenfold and the cells are incubated with tenfold serial dilutions of 10^9 phage lysate, meaning the undiluted cells and lysate have a multiplicity of infection (MOI) equal to 10, and this decreases with the serial dilution. Ideally, the phage is able to efficiently kill the strain of interest at low MOI, as is seen with the Subcluster AB1 phage Muddy (Dedrick and Smith et al., 2021).

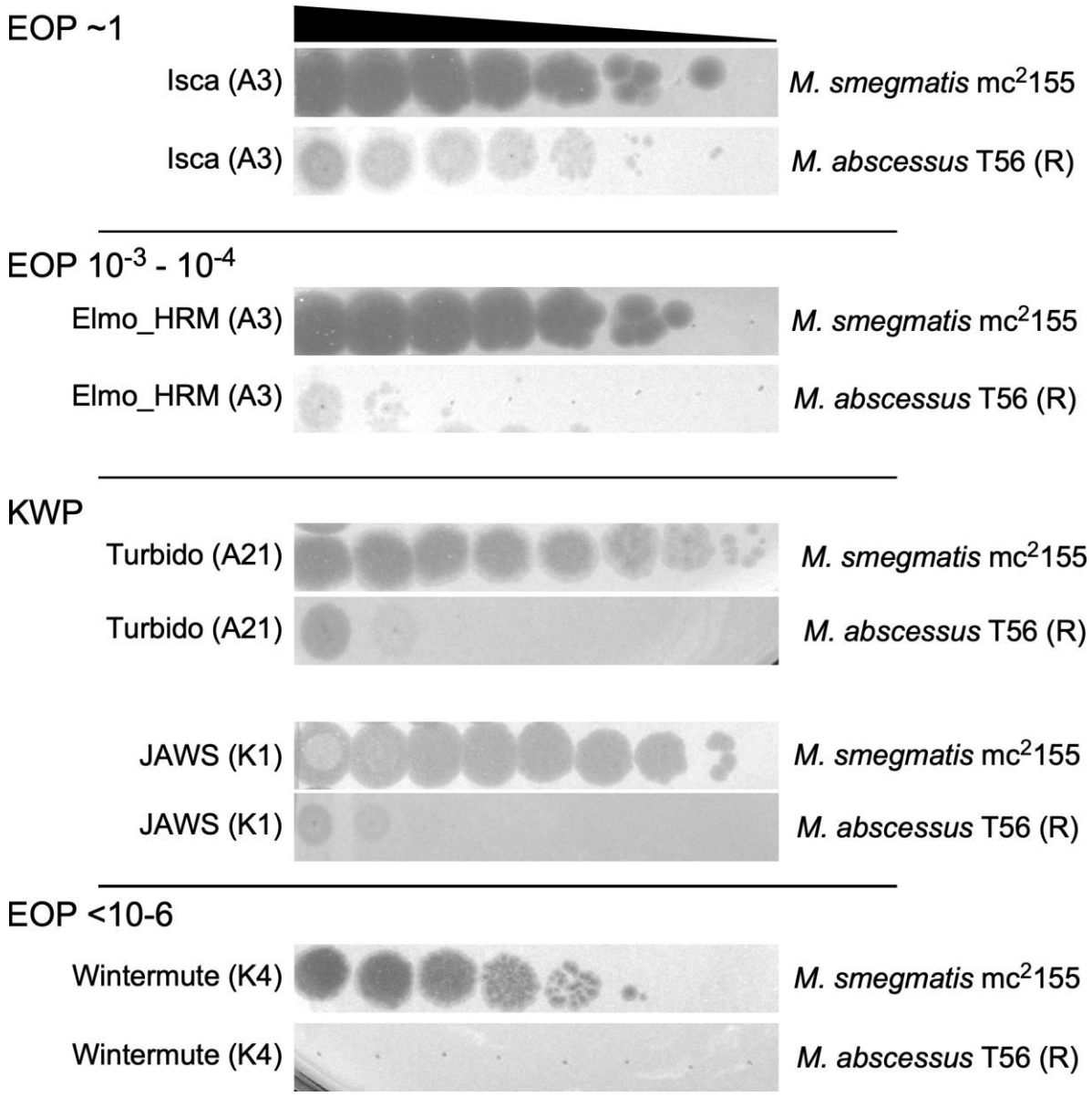

Figure 13. Spot titer assay infection phenotypes observed.

Examples of strain susceptibility phenotypes observed, and different categories of the efficiency of plaquing (EOP). Names of the phages are at the left and subcluster designations are shown in parenthesis. Ten-fold serially diluted phage lysates were spotted onto bacterial lawns (bacterial lawn strain shown at the right), with the lowest concentrations towards the right of each screen. Two examples of the Killing Without Plaquing (KWP) phenotype are shown, where individual plaques are not observed.

3.2 NTM Phage Infection Results

NTM demonstrate broad variation in susceptibility to infection within the complexes and generally (Dedrick, Smith et al. 2021). Hence, it is not atypical that the majority of the strains described here demonstrate insusceptibility to infection, with few strains demonstrating susceptibility to infection. Strain susceptibility to infection is described here as a function of efficiency of plaquing (EOP) calculated from plaquing assays in the form of lysate spot titration and top agar overlay infections.

3.2.1 MAB susceptibilities to phage infection

Sensitivity to phage infection was tested for each strain using 47 mycobacteriophages belonging to the Subclusters A2, A3, AB1, G1, G3, K1, K2, K3, K4, L2, and L3. The lytically propagated phiT45-1 and phiT46-1 were included in the screen, as well as the D302 mixed population. Strain CCUG50184-T is smooth but efficiently infected by Subcluster A3 phages Elmo_HRM^{mc2155}, Isca_cpm, the Subcluster AB1 phage Muddy, and the Subcluster G1 phage BPsΔ*33*HTH. The most common phenotypes observed were no detectable infection, and clearing at high titers/low dilutions of phage lysates without visible plaques, termed the Killing Without Plaquing (KWP) phenotype. There is substantial plaquing with reduced frequencies (EOP 10^{-3} ~ 10^{-4}), possibly from either a phenotypic escape from restriction or mutational escape from host- or prophage-mediated viral defense systems. Strain T56R is susceptible to infection by phages Muddy and Isca_cpm, and predictably the same is not seen for the smooth morphotype counterpart T56S. There is no obvious correlation between phage content of the strains and it is

likely numerous defense genes are determinants for phage susceptibility in addition to prophage content.

Lysogens of phiT45-1 were constructed in strains GD40, GD41, and GD245 (GD40_phiT45-1; GD41_phiT45-1; and GD245_phiT45-1). Lytically propagated phiT45-1 does not efficiently infect these strains, indicating there is a basal level of phage integrating into the strain chromosome in these sensitivity challenges. Lysogens were constructed and verified by PCR to be integrated at the attB-10 site in the hosts. The phiT45-1 lysogens demonstrate the expected phenotype of homoimmunity to superinfection by phiT45-1. The infection profiles of the lysogenic strains do not differ from the parental strains, suggesting either prophiT45-1 does not encode viral defense systems or the defense system is highly specific, and does not target the phages screened.

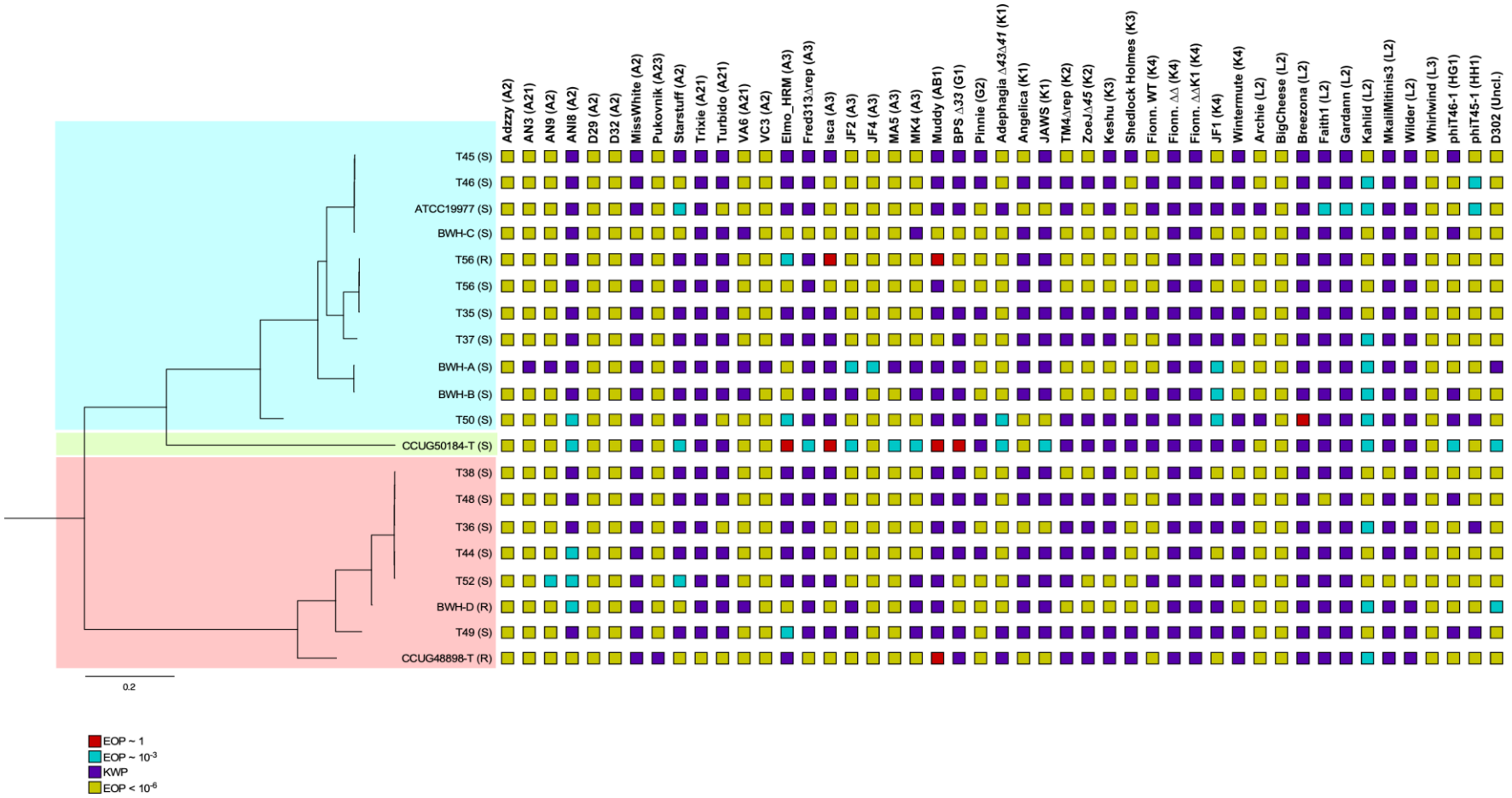

Figure 14. Phage susceptibility profiles of *M. abscessus* strains.

On the left, M. abscessus strains and their phylogenetic relationships, tigether with the infection profiles of a broad set of phages on the right.

3.2.2 MAC susceptibilities to phage infection

Similar to the infection phenotypes observed in MAB complex phage infection screens, the MAC complex strains demonstrated broad insusceptibility to infection with few (UCSD1, UCSD3, UCSD16, and 8424) exceptions. Strain UCSD1 is susceptible to Isca_cpm (A3), Muddy (AB1) and BPsΔ33HTH (G1), but insusceptible to most of the phages screened. Strain UCSD3 is susceptible to infection by Isca_cpm and Muddy. Strain 8424 is susceptible to infection by phage Breezona (L2). Interestingly, strain UCSD16 is susceptible to infection by 11 of the 31 phages screened, and is the only strain to demonstrate this phenotype. The phages UCSD16 is susceptible to phages isolated on *M. avium*, instead of *M. smegmatis* mc^2155, and so perhaps this is not exceptionally unexpected. The strain UCSD6 demonstrates reduced infection phenotype to more than half (57%) of the phages screened on these strains, and UCSD8 demonstrates a similar phenotype. Strain UCSD16 is the most susceptible in this group of MAC complex strains. Spotting filter sterilized supernatants of the MAC strains did not yield plaquing.

Phenotypes of interest from the MAC complex susceptibility screens are demonstrated by: UCSD1, UCSD3, UCSD16, UCSD20. In general it seems the MAC strains are even less susceptible than the MAB strains, which might have something to do with all the different colony morphologies we see in MAC complex strains compared to the ones we see in MAB complex strains.

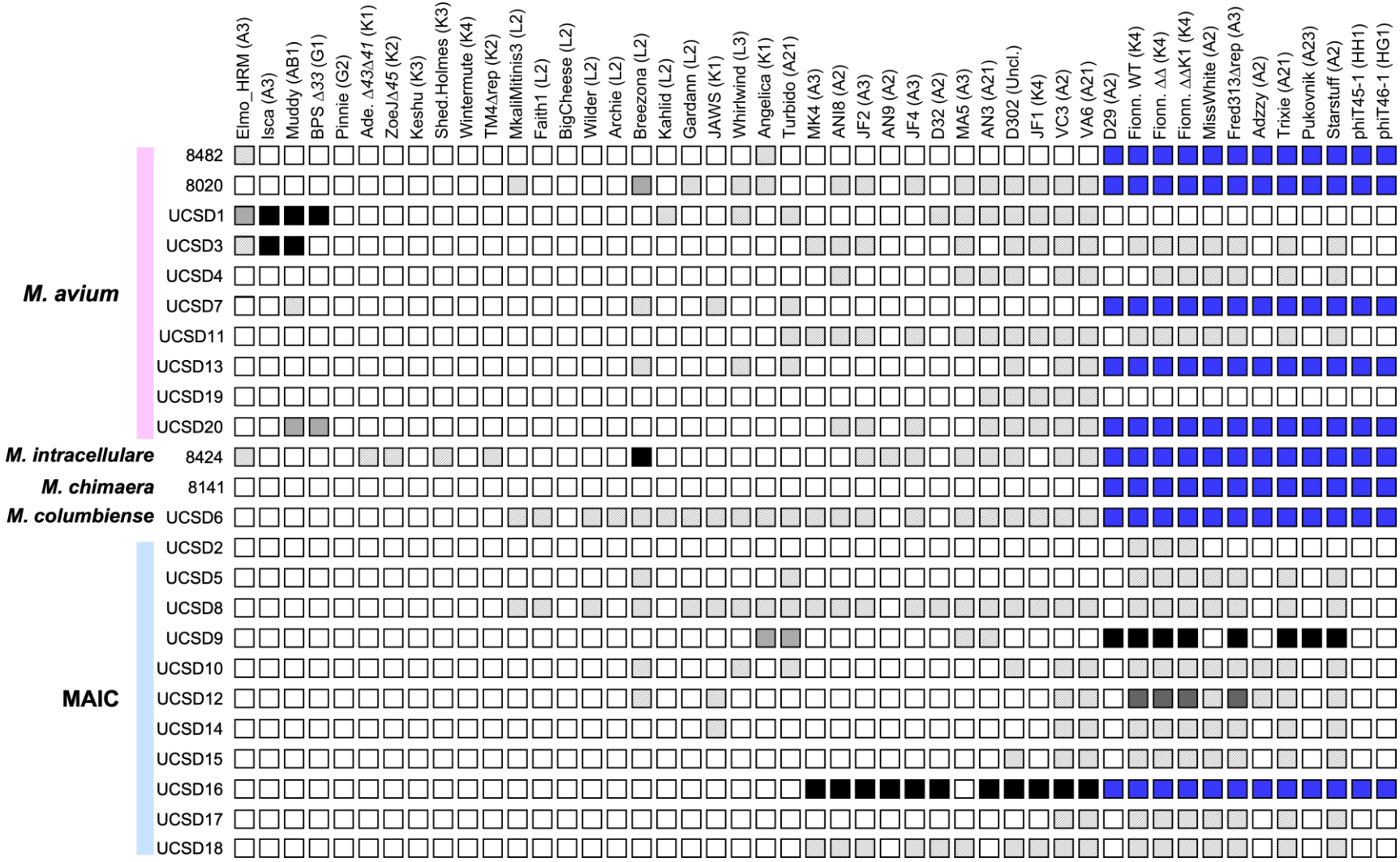

Figure 15. Phage susceptibility profiles of *M. avium* strains.

M. avium strains down the y-axis and phages screened along the x-axis. Black boxes indicate an EOP ~ 1.0; dark gray indicates a reduced EOP ~ 10^{-3} – 10^{-4}; light gray indicates the KWP phenotype; white indicates no detecable infection; and blue indicates strain-phage combinations that have not been assessed.

3.3 Chapter 3 Summary

Susceptibility screening in both complexes shows broad insusceptibilities to infection with few exceptions. The reduced infection phenotype (EOP ~ 10^{-3} – 10^{-4}) indicates a host range mutant (HRM) that infects the strain at an increased EOP could be isolated with subsequent screens. The reason for the KWP phenotype is unclear, and it is not an ideal phenotype when looking for a phage that can be therapeutically useful. Of the three MAB complex type strains, the *M. abscessus* subsp. *bolletii* strain CCUG50184-T was the most susceptible in this data set, demonstrating full susceptibility to four phages (Elmo_HRM (A3), Isca (A3), Muddy (AB1), BPsΔ*33* (G1)). Eleven phages demonstrated the reduced infection phenotype, and two of which are phages that were originally isolated on *M. avium* CDC-A1 and *M. avium* F2102 (ANI8 (A2) and MK4 (A3) respectively). The other nine phages (D302 (unclustered), MA5 (A3) , JF2 (A3), Starstuff (A2), Fred313Δ*71* (A3), Adephagia (K1), JAWS (K1), Kahlid (L2), phiT46-1 (HG1) and D302 (unclustered)) were isolated on *M. smegmatis*. The *M. abscessus* subsp. *massiliense* type strain CCUG48898-T was fully susceptible to Muddy, and the reduced infection phenotype observed when challenged with phage Kahlid (L2) suggests an HRM could be isolated on this strain.

Of the clinically isolated strains, the strain T56R is the most susceptible strain, demonstrating full susceptible to phages Isca (A3) and Muddy (AB1). The reduced infection

phenotype seen with Elmo_HRM challenges on T56R suggests a T56R HRM of Elmo_HRM could be isolated; the reduced infection phenotype is not observed on the T56S morphotype, and instead the smooth variant appears to be insusceptible to infection by Elmo_HRM. Including T56(R) there are eleven total MAB strains that appear to have potential phages for which HRMs could be isolated. The strain with the most potential for HRM isolation is the type strain CCUG50184-T, and the clinically isolated strain with the most potential for HRM isolation is T50. From this set of phages, the phage that demonstrated a reduced infection phenotype against the most strains is phage Kahlid. These putative HRM challenges are outlined in chart form 0.

In the set of MAC complex strains, there are no type strains described, and colony morphotyping suggests these strains more commonly have mixed morphotypes when streaked from frozen stocks (Figure 28, Figure 29). Similar to the MAB complex strains, most MAC complex strains demonstrated either no infection or the KWP phenotype when challenged with phages in this data set. The most susceptible strain was UCSD16, which was fully susceptible to 11 phages (MK4, ANI8, JF2, AN9, JF4, D32, AN3, D302, JF1, VC3, and VA6). Strain UCSD9 was second most susceptible of these strains, demonstrating full susceptibility to six phages (D29, Fionnbharth, Fred313Δ*71*, Trixie, Pukovnik, and Starstuff). Two phages, Angelina and Turbido appeared to have reduced efficiency of plaquing, and it is possible HRMs of these two phages could be isolated on UCSD9. Strains UCSD1 and UCSD3 were fully susceptible to phages Isca and Muddy, and the reduced infection phenotype observed when UCSD1 was challenged with Elmo_HRM suggests an HRM could be isolated. The Subcluster L2 phage Breezona was able to fully infect the strain 8424, which was sent with the speciation *M. intracellulare*.

4.0 Isolating phage forms of bioinformatically extracted prophages

Prophage induction was stumbled upon by Esther Lederberg after mixing UV treated *E. coli* K-12 cells with untreated *E. coli* cells (Lederberg 1950). The resulting plate had a cell lawn that appeared to have growth that was "nibbled and plaqued" (Lederberg 1950). The UV treatment had induced excision of the Lambda prophage and resulted in production of Lambda phage particles that subsequently lysed the untreated cells . At the time it was unknown that *E. coli* K-12 was lysogenic, and it was unknown that prophages can be spontaneously induced. Spontaneously induced prophages produce phage particles that can be separated from the cells by filter sterilizing culture supernatant. Mixing the supernatants with cells that are susceptible to the Lytically Propagated Spontaneously Induced Prophages (LPSIPs) allows the LPSIPs to be isolated and propagated.

The MAB and MAC strains described here were assessed for LPSIPs through supernatant spotting assays. Filter sterilized supernatants were spotted onto lawns of NTM and allowed to incubate for respective growth times. Any plaques that were observed were purified on the susceptible strain, and assessed for host range. When this was performed with MAC strains, no plaquing was observed, but the same was not seen for the MAB strains. Phage forms of two of the prophages identified bioinformatically, prophiT45-1 (incomplete) and prophiT46-1, were isolated with the supernatant spotting assay. Plaques were purified and assessed for host range, and a lytic form of phiT45-1 was engineered using CRISPR-Cas9 genome editing.

4.1 phiT45-1 Isolation and Genomic Analysis

Mycobacteriophage phiT45-1 is a spontaneously released, temperate phage (Figure 16). The prophage form of phiT45-1, prophiT45-1, is integrated in the chromosome of the *M. abscessus* subsp. *abscessus* strain Taiwan – 45 (T45). Phage phiT45-1 lytically infects *M. abscessus* strains BWH-C and type strain ATCC19977. phiT45-1 was isolated by spotting filter sterilized culture supernatant of T45 onto a top agar overlay of *M. abscessus* subsp. *abscessus* strain BWH-C. Plaques indicating infection of BWH-C by phiT45-1 are visible though considerably turbid, indicating a low level of lysogeny. Interestingly, the host range of phiT45-1 does not include the model mycobacterial strain *M. smegmatis* mc^2155. Areas of infection on the BWH-C top agar overlay were picked and plaque purified on BWH-C. Interestingly, phiT45-1 was able to form less turbid plaques on *M. abscessus* strain GD40, suggesting phiT45-1 more readily integrates into the BWH-C and ATCC19977 strains than the clinically isolated GD40 strain. DNA extraction performed with the Wizard DNA cleanup system (catalog no. A7280; Promega, Madison, WI) was followed by preparation of sequencing libraries and sequence read assembling. Genes predicted to code for proteins were identified and annotated, and putative functions were assigned. Further details on the sequencing methods are available in the Microbial Resource Announcement (MRA) (Amarh, Gauthier et al. 2021).

When compared to the genomes of phages isolated on *M. smegmatis*, phage phiT45-1 does not share overall sequence similarity, excluding its portal, capsid maturation protease, and capsid proteins, which share 70% amino acid identity with Cluster N mycobacteriophages. Perhaps expectedly, phiT45-1 demonstrates siphoviral morphology, alike to the Cluster N phages. A tyrosine integrase and immunity repressor are followed by a polymorphic toxin cassette. Within the cassette is an immunity protein, a polymorphic toxin with RipA-like and

WXG-100 domains and a WXG-100 motif. Based on the location of this polymorphic toxin cassette, it is likely these genes are expressed lysogenically, and exported by the Type VII secretion system. Lysogens of phiT45-1 isolated in the clinical strains GD40 and GD41 demonstrated the expected phenotype of phiT45-1 superinfection immunity (Amarh, Dedrick et al. 2023).

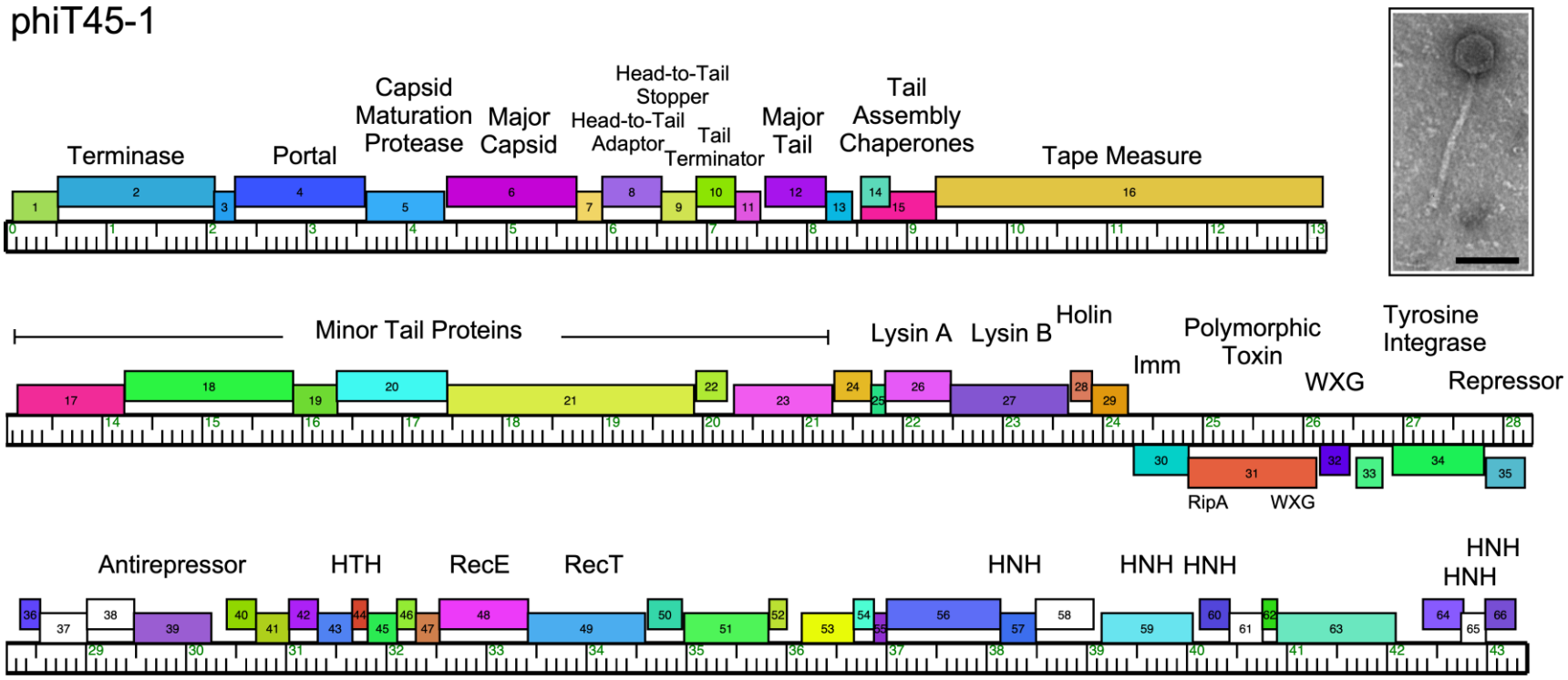

Figure 16. Organization of the phiT45-1 genome.

The genome for phage phiT45-1 represented as a horizontal bar with vertical markers for each kilobasepair. The colored boxes above and below the genome denote genes transcribed rightwards and leftwards, respectively. Genes with no close relatives, orphams, are shown in white boxes, and colors coordinate with the gene's phamily assignment, determined with Phamerator (Cresawn et al., 2011), with the database Abscessus_phage_and_prophage v3. Putative gene functions are annotated. The inset shows an electromicrograph of phiT45-1; scale bar is 100 nm.

4.2 phiT46-1 Isolation and Genomic Analysis

Mycobacteriophage phiT46-1 is a temperate phage that is spontaneously released from the *M. abscessus* subsp. *abscessus* host strain Taiwan-46 (T46) (Figure 17). Lytic phiT46-1 was isolated by spotting filter sterilized culture supernatant of strain T46 onto a top agar overlay of *M. abscessus* strain BWH-C. Dissimilar to phage phiT45-1, it is unable to infect the *M. abscessus* type strain ATCC19977, and similar to phiT45-1, it does not infect the model mycobacterial strain *M. smegmatis* mc^2155. Phage were picked from infected areas on the BWH-C top agar overlay, plaque purified, amplified on strain BWH-C, and DNA was extracted by phenol-chloroform-isoamyl alcohol extraction. The DNA was sequenced, and it was found that phiT46-1 does not have unique genome ends, indicating the genome is circularly permuted and undergoes head-full packaging, alike to the coliphage T4. As such, the genome was bioinformatically linearized and coordinate 1 was assigned to the first codon of the small-terminase subunit gene. Like phiT45-1, phiT46-1 is not closely related to phages isolated on *M. smegmatis* mc^2155. While phiT45-1 shares similarities to Cluster N phages, phiT46-1 shares similarities to Cluster Q minor tail proteins.

Further genomic analyses of the phiT46-1 genome identifies 78 protein-coding genes, of which 45% were assigned predicted gene functions. Further details of the methods used for genomic sequencing and annotation are detailed in the MRA (Amarh, Dedrick et al. 2021). Phage phiT46-1 does not have tRNA genes. Similar to phiT45-1, phiT46-1 has a tyrosine integrase, and the phage structure genes suggest that phiT46-1 exhibits siphoviral morphology. Other characteristics of the genome include HNH endonucleases, a phosphoadenosine

phosphosulfate (PAPS) reductase, an oxidoreductase, and a RecET-like recombination system. Like phiT45-1, the phiT46-1 genome houses a polymorphic toxin cassette, featuring a polymorphic toxin with a WXG motif and C-terminal domain with tuberculosis necrotizing toxin (TNT), immunity gene and an ESAT-6/WXG-like protein. Again, the position of this polymorphic toxin cassette is near the integrase and repressor, suggesting it is expressed lysogenically, with the gene products trafficked by the Type VII secretion system. The TNT motif is involved phagosome escape by tuberculosis infectious conditions, suggesting integration of the phiT46-1 into the T46 host chromosome aids in persistent infection by T46 in human cells.

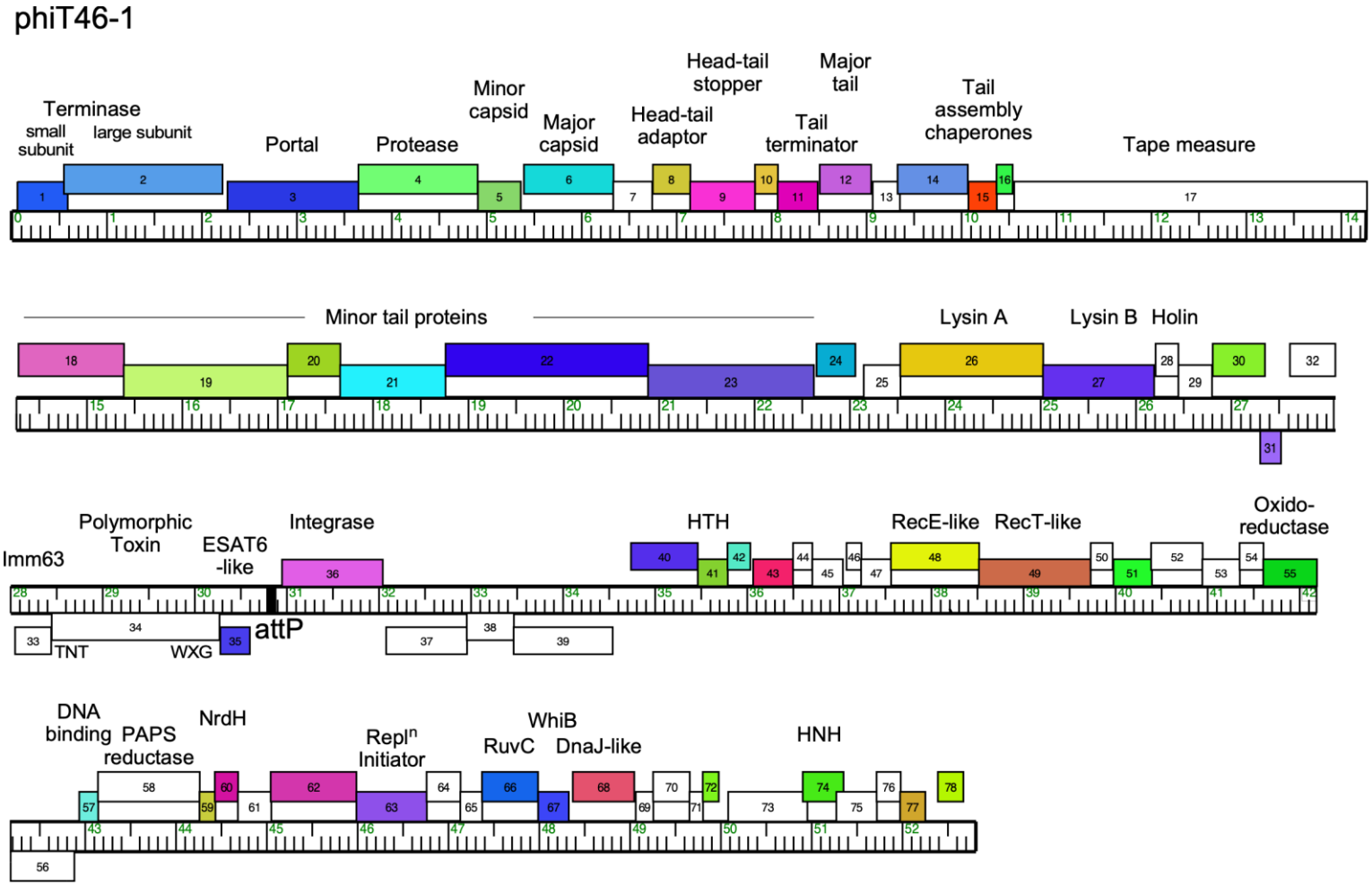

Figure 17. Organization of the phage phiT46-1 genome.

The phiT46-1 phage genome has been linearized for clarity. Genes are represented as in Figure 2 (4.1) Predicted gene functions are annotated.

4.3 Engineering a lytic mutant of phiT45-1

Genes coding for recombination proteins have been well described in the *E. coli* phage Lambda. These recombination systems have been utilized to allow increased levels of recombination events in the bacterial cell. In Lambda, the recombination system is termed the Lambda red (recombination deficient) system. The recombination genes of phage lambda are termed *exo* and *beta* and the proteins they transcribe, Exo and Beta, promote homologous recombination between linearized substrate DNA and the homologous targets on the bacterial chromosome. A similar system can be found in the *E. coli* prophage Rac, whose genome houses the sequences for a RecE and RecT (RecE/T) system (Cortes, Lin et al. 2021). Innately, these recombination systems allow for phages to undergo mutagenesis during integration of their genome into the host chromosome or during phage particle replication. In vitro, these recombination genes can be exploited and optimized to allow for various mutations in the phage genome, including and not limited to point mutations, insertions, and deletions (Marinelli, Piuri et al. 2008, da Silva, Piuri et al. 2013).

4.3.1 BRED, CRISPY-BRED, CRISPY-BRIP

Mycobacteriophage genomes also contain these recombination genes as seen in phage Che9c, whose genome encodes the RecE- and RecT-like recombination genes gene *60* and gene *61* (van Kessel, Marinelli et al. 2008). Since their first description, genes *60* and *61* were inserted into an anhydrotetracycline (ATc) inducible, kanamycin (Kan) marked plasmid, and transformed

into *M. smegmatis* mc^{2}155, generating the recombineering line of cells *M. smegmatis* mc^{2}155:pJV53 (van Kessel and Hatfull 2007).

The well established method of mycobacteriophage engineering that is predicated on the mc^{2}155:pJV53 cell line is termed Bacteriophage Recombineering of Electroporated DNA (BRED) (Marinelli, Piuri et al. 2008). The recombineering system results in increased levels of homologous recombination. Co-electroporation of phage DNA and a substrate that is bookended with 100-150bp of homology to the phage DNA into mc^{2}155:pJV53 allows for recovery of phages with the substrate inserted into the phage DNA at the region of homology when the transformed strain is plated on an acetamide agar. BRED is efficient for mycobacteriophage engineering, however, plaques with mixed populations of wild-type and recombinant phages, as well as a high background of unintended deletions and insertions, meant screening dozens of plaques by PCR and plaque purification were crucial to isolating a phage mutant of interest.

Combination of BRED with CRISPR-Cas9 (CRISPY-BRED) (Wetzel, Guerrero-Bustamante et al. 2021) increases rate of recombinant phage recovery up to 100%, without the need to screen dozens of plaques. In CRISPY-BRED, CRISPR-Cas9 is employed as a counter selector against non-recombinant phage. A plasmid is constructed containing the single guide RNA (sgRNA) sequence, a *Streptococcus thermophilus cas9* gene, a kanamycin resistance gene, an *E. coli* origin of replication, and an *attP-Int* cassette. The 20 bp sgRNA targeting the parental and non-recombinant phage is put under the control of an anhydrotetracycline (ATc)-inducible P_{tet} promoter. Phage DNA and synthetic DNA containing the mutation of interested are co-electroporated into the recombineering strain of *M. smegmatis* mc^{2}155:pJV138 and the cells are allowed to recover. After recovery the recombineering cells mixed with *M. smegmatis* cells containing the sgRNA plasmid, and the mixture is plated on kanamycin plates and kanamycin

plates with ATc. Plaques recovered from the ATc induced plate are subsequently PCR verified and plaque purified, containing the intended mutation.

Recombinant phage also can be recovered by Bacteriophage Recombineering with Infectious Particles (BRIP) (Wetzel, Guerrero-Bustamante et al. 2021), in which recombineering cells are electroporated with synthetic DNA, and the electroporated cells are infected with the parental phage after recovery, and before being plated on an ATc. Recovery of recombinant plaques by CRISPY-BRIP is at a lower frequency than CRISPY-BRED, but it can be particularly useful for engineering bacteriophages with larger genomes that tend to transfect poorly (Wetzel, Guerrero-Bustamante et al. 2021).

4.3.2 CRISPR-Cas9 targeting phiT45-1 gene *34* and gene *35*

One of the limitations of this approach is there is no control of the size of the deletion. With no control of the size of the deletion, it is possible the phenotype observed is from a deletion other than the one(s) intended, or polar effects of the deletion. However, with the dependence of BRED on the *M. smegmatis* strain mc^2155:pJV53 or mc^2155:pJV138, phages that do not infect *M. smegmatis* mc^2155 are not candidates for this method. To get around this limitation, I have employed the use of CRISPR-Cas9 with a sgRNA targeting the phiT45-1 integrase (gene *34*) and repressor (gene *35*).

A pIRL53 plasmid derivative was constructed with the integrase-targeting sgRNA fused to an anydrotetracycline (ATc)-inducible P_{tet} promoter. Similarly, a *Streptococcus thermophilus cas9* is fused to a P_{tet} promoter, and both are preceded with a kanamycin (Kan) resistance marker (Rock, Hopkins et al. 2017). The plasmid has an *E. coli OriE* origin of replication, as well as an L5 *attP-Int* cassette. The constructed plasmid (pEDA02) was electroporated into the phiT45-1

susceptible strain GD40 (Dedrick, Aull et al. 2021, Dedrick, Smith et al. 2021) to make the CRISPR-cas9 strain GD40:pEDA02. The CRISPR-cas9 strain was infected with parental phiT45-1 and plated as a top agar overlay on plates with ATc (500ng) and without. A reduction in EOP on the order of 10^{-3} indicates sgRNA induction (Wetzel, Guerrero-Bustamante et al. 2021). Plaques were picked from the induced ATc plate, purified, and verified by PCR.

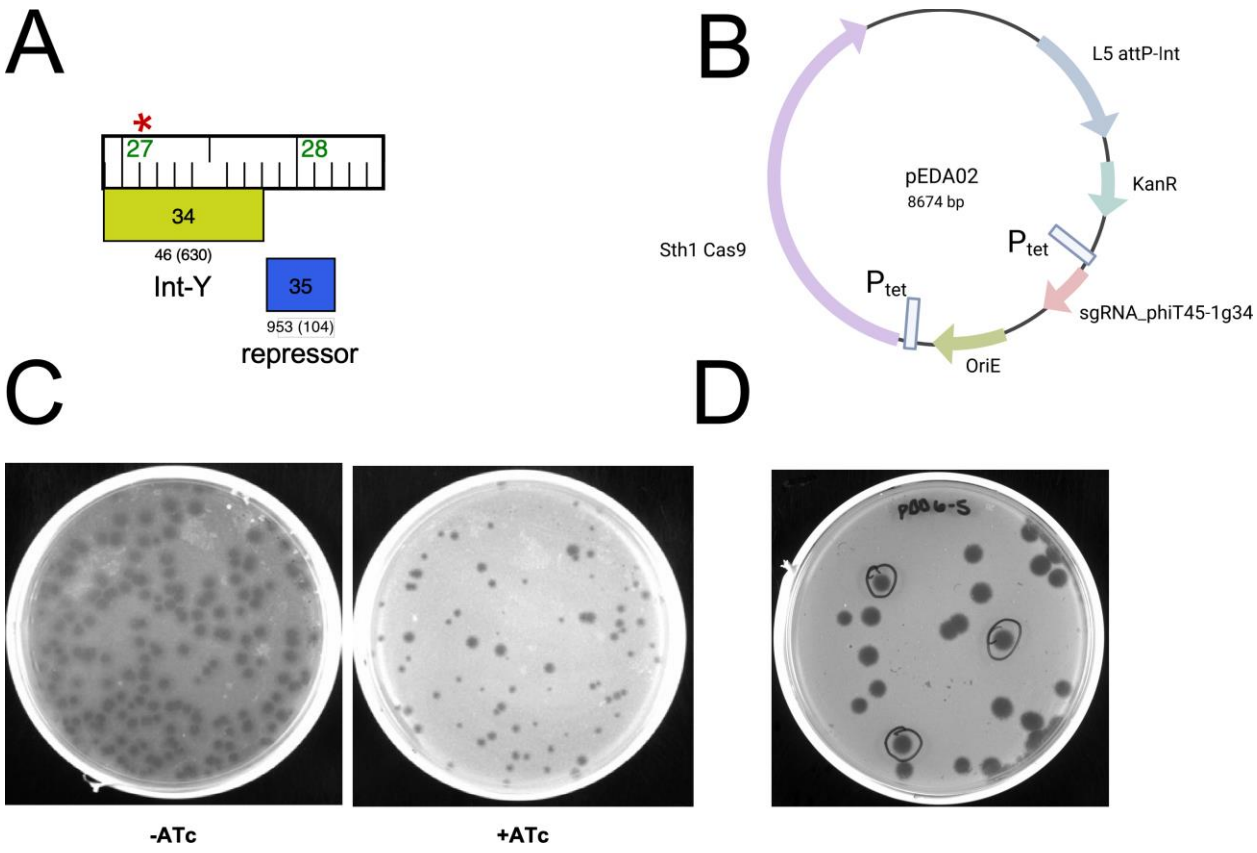

Figure 18 Isolating a phiT45-1 lytic mutant with CRISPR-Cas9

A. A map of genes *34* and *35* of phage phiT45-1, the tyrosine integrase (Int-Y) and repressor, respectively. The red asterisk indicates the sgRNA target, at basepair 27,125 at the 5' end of the integrase. The sgRNA utilizes the a protospacer adjacent motif (PAM) site AGAAC, and binds to the non-template strand. B. A schematic of the pIRL53 derived plasmid pEDA02. The plasmid has an L5 attP-Int cassette and an OriE. The Sth1 Cas9 and sgRNA are under tetracycline inducible promoters, and the plasmid has a kanamycin resistance (KanR) marker. C. Results of infecting GD41_pEDA02 without anhydroustetracycline (ATc) and with ATc. D. Purified plaques picked from the +ATc plate and twice passed through GD40.

4.3.3 phiT45-1ΔΔ Verification by PCR

Initial attempts to verify the deletion in the purified plaques were unsuccessful, suggesting the deletion generated from CRISPR-cas9 sgRNA targeting to extend beyond the integrase and possibly into the repressor. Primer pairs annealing to increasing distances upstream and downstream of the sgRNA target verified the deletion includes the 5' region of gene *35* (Figure 19).

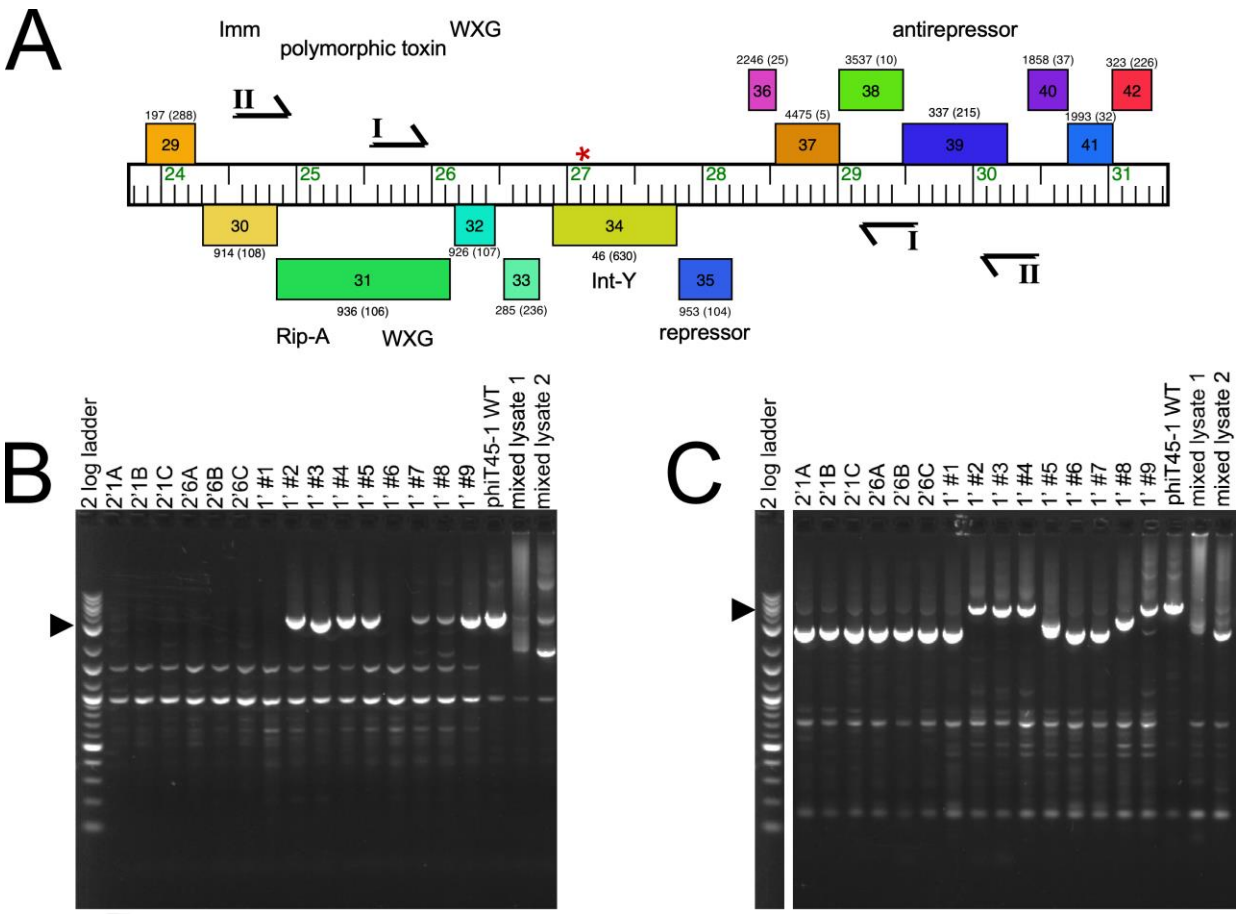

Figure 19 PCR verification of Δ*34* mutant.

A. Primer and sgRNA target mapping on phiT45-1 Phamerator genome map. The red asterisk indicates the sgRNA target at basepair 27125, sgRNA targets the non-template strand. Black arrows indicate primer binding sites, inner most arrows annotated "I" produce the 3.5 kbp product and the outermost primers amplify the 5.4 kbp product. B. Results of PCR with the inner set of primers annotated "I", amplifying the 3.5 kbp product. Lanes are labeled with

respective products, “2’1A” indicates secondary pick from secondary plating, plaque A; “1’#1” indicates primary pick number one from primary plating; “mixed lysate 1” indicates lysate with mixed population of phiT45-1 WT plaques and putative g*34* mutants. C. Results of PCR with the inner set of primers annotated “II”, amplifying the 5.4 kbp product. Lanes are labeled as in panel B.

4.3.4 Lytic killing by engineered mycobacteriophage

Efficacy of killing by the phiT45-1 mutant was assessed by killing assay, which has been described previously (Dedrick, Guerrero-Bustamante et al. 2019). Briefly, cell culture and phage lysate are serially diluted, combined, and allowed to incubate for 24 and 48 hours. Mixtures are spotted onto naked plates, at both time points, and cell growth after phage killing is assessed after five days.

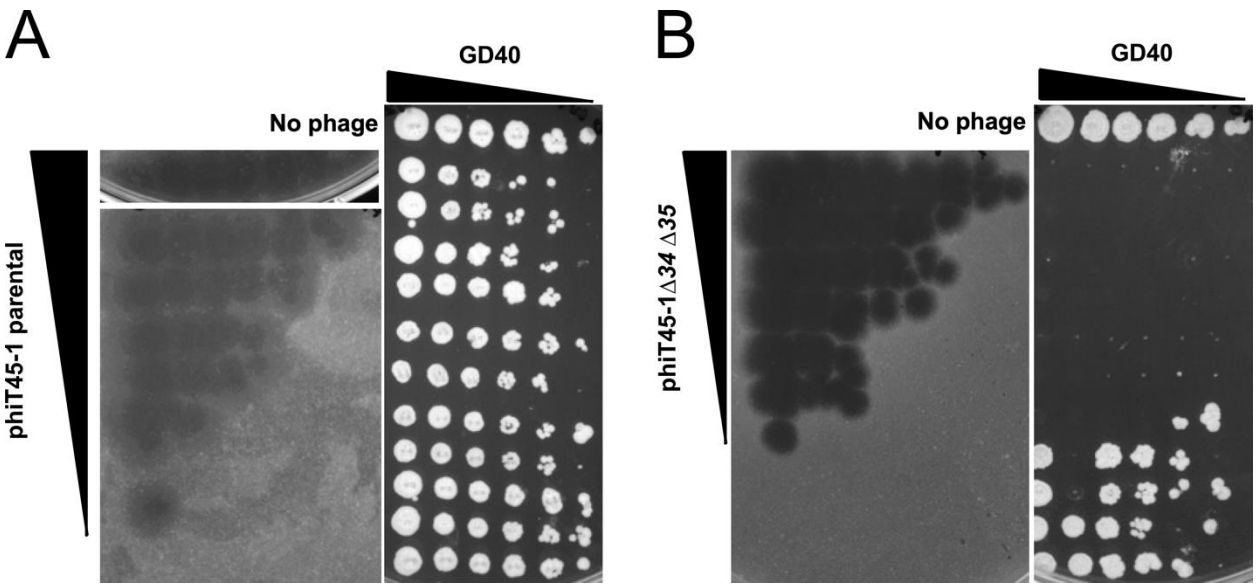

Figure 20 Lytic killing of clinically isolated NTM by phiT45-1 CRISPR mutant

Killing assay performed with parental phiT45-1 (panel A) and phiT45-1_Δ*34* CRISPR mutant (panel B). A. on the left is the parental phiT45-1 diluted and spotted onto a top agar overlay of GD40. On the right is the result of the diluted parental phiT45-1 incubated with a dilution of GD40 cells for 24 hours. B. On the left are the results of

spotting a dilution of a lysate of mixed populations of phiT45-1 CRISPR mutants. On the right are the results of incubating the diluted phiT45-1 CRISPR mutants lysate with GD40 for 24 hrs.

4.4 Chapter 4 Summary

Spontaneously induced prophages from clinically isolated NTM strains can be isolated in their phage form when a susceptible host is available. The nature of the LPSIPs means they are temperate, with apparent variation in levels of lysogeny and plaque turbidity when infecting different hosts. Understandably, these LPSIPs from clinical isolates do not infect the non-pathogenic *M. smegmatis* mc^2155, which can complicate downstream analyses and engineering. However, it may be possible to isolate LPSIPs with expanded host ranges, just as *M. smegmatis* and *M. avium* phages have been isolated with host ranges inclusive of *M. tuberculosis* and *M. smegmatis* respectively. At this time, it is impossible to use established methods of genomic engineering (BRED, CRISPY-BRED, BRIP, CRISPY BRIP), as the recombineering system has not been adapted in MAB or MAC complex strains. Genome editing using the *Sth* CRISPR-Cas9 system can be employed in cases of phages with a host range that excludes *M. smegmatis* mc^2155, as was described here for phiT45-1. It should be noted that in phiT45-1, the integrase (*34*) and repressor (*35*) are adjacent and transcribed in the same direction, and so a CRISPR deletion of ~1 kbp was beneficial for inactivating the integrase and the N-terminus of the repressor, and a similar method may not be appropriate in cases where the integrase and repressor are not adjacent.

5.0 Discussion and Conclusions

The scope of this work is broad and considers phage-host dynamics of NTM belonging to two complexes that can demonstrate vastly differing phenotypes. In this chapter, I give suggestions for future work with these strains. It is important to note that it is not recommended to continue as one scientist researching both complexes simultaneously. If one is particularly organized and rigorous with their data collection, still it would be difficult to gain a deep understanding of these strains and their responses to phage infection. This chapter begins with comments on strain morphotyping, which is particularly important as the findings of Dedrick and Smith et al in 2021 support that strain morphotype can be an indicator for strain susceptibility to phage infection. The following section discusses implications of the prophage analyses described here and next steps, particularly regarding the incomplete prophages identified from the strain WGS, and thoughts on the apparent lack of lytically expressed prophiT45-2 when compared to the twin prophage prophiT46-3. The third section discusses the possible methods of isolating the LPSIPs that were detected by PCR but have not been propagated. This is followed by thoughts on the susceptibility screens performed here and how future efforts can seek environmentally isolated phages that infect clinically isolated NTM and suggestions for how future efforts can have a more complete data set. The last of these sections comments on enzybiotics, namely therapeutic application of phage lysins, and thoughts on future investigations into phage-antibiotic synergy against clinically isolated NTM. This discussion will take into account the observations made in both complexes and possibilities for future directions with these strains. Final thoughts will be outlined in conclusions.

5.1 Discussion

5.1.1 Morphotyping and rescreens

Many of the MAB strains described here display a different morphotype than the one received from the collaborating lab. These strains have been sequenced and verified to be the declared strain, but have demonstrated a conversion from smooth to rough, and in some cases, a conversion from rough to smooth. Previous work from the lab indicates the strain morphotype is a significant indicator of susceptibility to phage infection and killing (Dedrick, Smith et al. 2021), and a thorough susceptibility interrogation of these strains would include screens of all morphotypes observed for a strain. Similarly, the MAC strains described here demonstrate mixed morphotypes when grown from frozen glycerol stocks, and attempts have been made to separate the morphotypes observed. One challenge for separating MAC strain morphotypes is the lengthy incubation times necessary for growing MAC streak plates, during which the plate can become desiccated. Measures to combat plate drying should be taken carefully, as agar plates for MAC strains do not include antibiotics, and so a wet paper towel added to a plastic bag holding a streak plate could be a point of contamination. Another potential challenge for working with MAC strains could be the transparent morphotype, which, simply, can be difficult to visualize on a plate without careful inspection. Once MAC strain morphotypes have been separated, they can be rescreened against phages of interest (i.e.: Group IV phages).

5.1.2 Bioinformatic prophage analyses

Of the *M. abscessus* strains described here, 75% have at least one integrated prophage. Three of the closely related subspecies *abscessus* strains (T36, T38, T48) have identical tandem insertions of a Subcluster HN2 phage and a Subcluster HB3 phage. Three strains that are genomically similar, T35, T44, T52, do not have this tandem prophage. The prophages use integration-dependent immunity systems. The virion forms of the constituent prophages – prophiT36-2a and prophiT36-2b – are detectable in the culture supernatants for all three strains and the entire prophage. The predicted *attP* for the entire tandem prophage prophiT36-2 is detectable in the culture and not the supernatant, suggesting the recombination event between the two different repressors occurs but is not packaged into the capsid.

All but one prophage were detected in virion form, suggesting the mosaicism of the phage genomes does not disallow the prophage from producing virion particles. An example of this can be seen in prophiT36-1, which is identical to prophiT38-1 and prophiT48-1, but has a 45 kbp insertion composed of a duplication of 22.5 kbp. The additional 45 kbp is predicted to make the genome too large to be packaged, but the predicted *attP* of phiT36-1 was detectable by PCR. The similar case of prophiGD20-1 was described previously, wherein the virion form was detected without an insertion. The presence of a Rec-E/T system in genes *15* and *16* of prophiT36-1 supports this prophage undergoes a recombination event removing the 45 kbp insertion before packaging into the capsid, making the genome the appropriate size for capsid packaging

These prophages are not closely related to phages isolated on *M. smegmatis* mc^2155, however, prophages that belong to Clusters A and M appear to be organized similar to *M. smegmatis* mc^2155 phages that belong to Clusters A and Cluster M, respectively. Prophages that

grouped to Cluster A, prophiT46-3, prophiT49-3, and prophiBWHA-1, encode a stoperator system like those seen in Subcluster A4 phages. What, if any, contribution the stoperator system has to phage infection susceptibility of the strains T46, T49, and BWH-A is unclear. The Subcluster M5 prophage prophiT49-2 is similar to Cluster M phages in that it is roughly 80,000 kbp in length, encodes for a serine integrase, and the *attP* is relatively far from the integrase. Prophage prophiT49-2 also encodes for a large set of tRNA genes, which is characteristic of Cluster M phages. Dissimilar to phages in Cluster M and other phages isolated on *M. smegmatis* mc^2155, prophiT49-2 encodes for a polymorphic toxin-immunity cassette, which are common in prophage genomes.

All the prophages are full length; because these analyses were performed on WGS data, it is possible some prophages have gone undetected between the sequencing contigs. These prophages are intact phage genomes that demonstrate substantial variation and exchange of polymorphic toxin-immunity loci within the clusters. The phage forms of these prophages are detectable by amplification of the predicted *attP* sites.

Prophage sequences from the MAB strains in this work have been extracted for all intact prophages that have been identified from WGS. In two cases, the complete prophage sequences were not identified: prophiT45-1 and prophiBWHC-1. In the case of prophiT45-1, isolation and sequencing of the phage form phiT45-1 allows one to infer the integrated prophage sequence, but one cannot rule out that it is possible the prophage sequence may include a mobile element in the sequence that has fallen between the WGS contigs. Revisiting the T45 WGS and attempting to find the end of the prophage in another contig, or re-sequencing strain T45 could confirm the predicted prophage sequence. A similar method could be performed for the prophiBWHC-1 prophage, for which the phage form was not isolated. Strain BWH-C demonstrates broad

insusceptibility to the phages screened here, and understanding whether the prophage has a polymorphic toxin-immunity cassette could inform the genomic bases for how this strain behaves when challenged with phage. Prophage-like elements have been identified in all the MAB strains, and it is possible these tiles in the mosaic that is MAB bacterial genomes could contribute to strain susceptibility to phage infection. Identification of these prophage-like elements in the MAB genomes, and determining which, if any, prophage-like elements are found more often than others, could inform future complementation experiments in strains that are lacking the prophage-like element.

The MAC strains described here have not been assessed for prophage content, as the majority have not been sequenced. One strain (UCSD1) has been sequenced (WGS) and no prophages were discovered. Bioinformatic analysis on tens of thousands of *M. tuberculosis* genomes suggest intact prophages may be rare in this species of mycobacteria, and it is possible this characteristic is shared by the slowly growing MAC complex genomes, but one cannot be certain without strain sequencing and assessment for prophage content. The variation in strain morphotype can make it difficult to determine if a strain has been grown to a sufficient OD_{600} to allow for enough genetic material to yield reliable WGS, as some morphotypes are literally transparent, but it is possible this can be circumvented by ensuring to inoculate strains for sequencing in technical duplicate, combining the pellets, and resuspending in the minimum volume necessary for DNA extraction.

5.1.3 Isolation of LPSIPs for which predicted *attP* were detected

As described in Chapter 2 (2.2.5), PCR detection of predicted *attP* sites suggests most prophages spontaneously induce to form phage particles. Isolation of these phage forms depends

on separating the induced phage from the host cells, and mixing the induced phage and a susceptible strain, and this was done with supernatant spotting assays. The lack of plaquing observed in the supernatant spotting assays performed with MAC complex strains supports the possibility that MAC complex prophages may be rare, as has been seen in Mtb genomes (Gauthier, Abad et al. 2022). It is possible prophages in strains belonging to the MAC complex are not spontaneously induced, or strains belonging to the MAC complex do not have intact and active phage genomes integrated into their chromosomes.

Supernatant spotting assays described here resulted in two phages isolated from two strains (T45 and T46). One form, phiT45-1, was isolated on overlays of two different MAB complex cultures (BWH-C and ATCC19977), yet forms less turbid plaques on clinical strains GD40, GD41, and GD245, highlighting the host range of LPSIPs may not include the strains described here but may include other strains available. It is possible screening supernatant from these MAB complex strains - and perhaps supernatant from the MAC complex strains - on GD### strains of interest could isolate phage forms of other prophages with detectable *attP* sites. This can be performed *en masse*, with supernatant pinning onto GD### lawns. It is better to prepare batches of the filter sterilized supernatants, transfer aliquots into a 96-well plate, and pin from the 96-well plate than it is to transfer culture aliquots to the 96-well plate, centrifuge the plate, and attempt to spot the supernatant onto the bacterial lawns. Cells are more likely to contaminate the supernatant in the latter method, while the former method will ensure only culture supernatant is transferred to the lawn. The other LPSIP isolated, phiT46-1, forms particularly turbid plaques on all strains screened so far, including the isolation strain BWH-C. Engineering the lytic phiT45-1 derivative was performed with active CRISPR-Cas9 nuclease. Future efforts to engineer an obligately lytic phiT46-1 using CRISPR-Cas9 should be conscious

of the two genes separating the integrase (*36*) and repressor (*39*) and the change in transcription directionality (rightward and leftward respectively). Performing the deletions in two steps may be necessary, if seeking to maintain genes *37* and *38*, (HHPRED predicts *37* to be a nucleotidyltransferase and *38* has an unknown function) or co-transforming the CRISPR-Cas9 plasmid and a substrate with a *36 – 39* deletion. In the latter experiment, it would be necessary to be sure that the phenotype is not attributed to deleting the nearby genes *37 38* or from polar effects of this deletion. Engineering phages for therapeutic purposes should consider the stability of the phage capsid as well. The densely packed DNA contributes to the internal pressure of the capsid, and genome truncations upwards of ~ 1 kbp can disrupt this equilibrium, resulting in unstable phage lysates with concentrations that decrease faster than expected when stored.

The only prophage that was not detected in phage form was prophiT45-2, yet the *attP* of the identical prophage prophiT46-3 was detected. I will describe two potential explanations for this difference in phenotypes. The first explanation is based on the prophage sequence undergoes modification subsequent to excision, it is possible the predicted sequences upstream and downstream of the *attP* are different than can be inferred from the integrated prophage sequence. Either or both primers could be attempting to anneal to a sequence that has been lost in a truncation, or an insertion that leads to a product larger than the predicted ~ 400 bp product from these primers. A second possibility is the prophage forms a more stable lysogen in T45 than it does in T46 and so prophiT45-2 is not readily induced whereas prophiT46-3 is readily induced. If this were the case, there are many documented methods of prophage induction, including applying mutagens such as mitomycin C, or by applying reactive oxygen species (ROS) inducers such as hydrogen peroxide (H_2O_2). Oxidative stress activates the host SOS response, that will destabilize the lysogenic state (through encouraging repressor cleavage in lambdoid lysogens).

These methods could be applied to induce a particularly stable prophage, but given the readily detectable *attP* sequences of other prophages described here, and published evidence for transposition events (Dedrick, Aull et al. 2021), perhaps it is more likely the phage form *attP* adjacent sequence is different from what can be predicted with the prophiT45-2 genome. This could be further investigated with long-form PCR, amplifying a product larger than the 426 and 451 bp products attempted to be amplified with the primers used here. Increasing the distance of the primers spanning the *attP* site to upwards of 250 bp on each side of the site may produce a band that subsequently can be sequenced.

5.1.4 Phage susceptibility screening

The MAB complex strains demonstrate broad variation in susceptibility to infection by the phages screened here, and this is to be expected as previous reports have described the same. Most of the strains in this collection grow in the smooth morphotype, however morphotype descriptions sent with the strains, in some cases, are different than the morphotypes seen here. If rough morphotype colonies can be amplified from smooth colonies, and it would be of interest to compare the susceptibility of the rough variants to the broad insusceptibility of the smooth variants. Three of the MAB complex strains described here are rough, and all three are susceptible to the Subcluster AB1 phage Muddy. Killing and survival assays to confirm strain susceptibilities observed in lysate spotting assays should be performed for strains of interest, and this may present challenges when assaying MAC complex strains. Strains that demonstrate one of the transparent morphotypes may be difficult to quantify when looking for a reduction in colony counts, and the long incubation times also can make quantifying growth difficult.

Susceptibility screens in MAC complex strains suggest MAC strains are broadly insusceptible to phage infection. This taken into consideration with the diverse morphotypes seen in comparison to MAB strains, invites the question of whether the susceptibility of MAC complex strains similarly is determined by these morphotypes. The phage screening after morphotype separation would elucidate any connections between MAC strain morphotype and susceptibility to phage infection, but it is possible the plaque assay method may not be the best for determining MAC complex phage susceptibility. During screens described here, it became evident not all MAC strains readily form confluent bacterial lawns when grown in a top-agar, and while this can be ameliorated by increasing the ratio of culture to agar, methods to encourage a confluent lawn were not successful across all strains. Further, the extended incubation times for MAC growth make it possible that any contaminants will grow faster than the MAC strain, obscuring results that have been incubating for weeks at a time. One method of detecting *M. avium* subsp. *paratuberculosis* susceptibility to phage infection has been described wherein real time qPCR of *IS900* is applied to mixtures of 10^9 pfus of phage and serially diluted cells (Harman-McKenna and De Buck 2023), and a positive qPCR result indicated strain susceptibility to phage infection. One concern with using this method would be deciphering lysis caused by phage infection versus lysis induced by other means (i.e.: lysis from without). The KWP phenotype (Figure 13) was observed in many of the strains when challenged with phage, and while *IS900* qPCR indicates cell lysis, a “positive qPCR” result should first be assessed with NTM-phage mixtures for which apparent genetic lysis have been observed in lysate spot titer assays (e.g.: UCSD1 and UCSD3 with Isca and Muddy; UCSD1 with BPs; 8424 and Breezona; and UCSD16 with Group IV phages).

5.1.5 Enzybiotics and Antibiotic-Phage Synergy

Phage lysin has been applied therapeutically as an enzybiotic and has been shown to significantly decrease the pulmonary load of *M. abscessus* (Hurst-Hess, Walz et al. 2023). Work toward understanding whether lysins have the same effect on log phase NTM as it does on stationary phase NTM was explored briefly, and results suggested lysin killing was more efficient on stationary phase cells than log phase cells (unpublished). There is a possibility this difference in phenotypes is of origins other than stationary phase cells being more susceptible to lysin treatment, as the protocol attempts to normalize the colony counts by diluting an aliquot of each culture to the same absorbance (OD_{600}). The number of dead and dying cells in a stationary phase culture is higher than those in a log phase culture, but a spectrophotometer does not differentiate between live and dead cells in the path of the light, just that there is something changing the absorbance. This could mean the number of cells that are being treated with lysin in each condition is lower in the stationary phase culture and the reduction in colony counts observed for the stationary phase culture may be low for reasons other than increased susceptibility to lysin activity.

Applications of phage therapy in cases of NTM mycobacteriosis have been in tandem with the patient's antibiotic regimen. One could imagine the potential for phage-antibiotic synergy may be better understood with a perspective that includes NTM strain response to antibiotics, phage, and a cocktail of phage and antibiotics. Determining the MIC of antibiotics for each strain for common antibiotics that are applied in cases of NTM mycobacteriosis – a macrolide (clarithromycin or azithromycin), β-lactam (cefoxitin or imipenem), an aminoglycoside (amikacin), and the combination rifampin and ethambutol. It is well established that MAB strains can demonstrate robust resistance to antibiotic treatment, and recently the same

has been observed for MAC strains. Strain sequencing and genome comparisons of genes known to induce resistance (e.g.: *rrl*, *erm*(41)), and understanding if these genes change after escape from phage infection can elucidate the dynamics of host response to phage infection in the context of antibiotic treatment.

5.2 Conclusions

NTM demonstrate broad insusceptibility to phage infection, with few exceptions. Most MAB complex NTM genomes contain prophages that are released spontaneously, forming LPSIPs. These LPSIPs can be isolated and propagated when a susceptible strain is available. Genomic engineering LPSIPs to be obligately lytic is possible with CRISPR-Cas9 editing, and using the inactive form would ensure the observed phenotypes are not from off-target editing. It is possible the slowly growing MAC complex strains do not encode intact, active prophages in their genomes as often as has been described in MAB complex strains, but this needs to be confirmed with broad bioinformatic analyses. Phages with expanded host range can be isolated from parental phage for which reduced EOP phenotypes were observed in lysate spotting assays, and this includes phages that were originally isolated on *M. avium*. Understanding how NTM respond to phage in the presence of antibiotics can elucidate phage-host interactions in clinical settings, as well as how NTM respond to phage lysin in the presence of antibiotics. The path forward in phage susceptibility screens with MAC complex strains would benefit from exploiting molecular reporters for products of phage infection, in the form of reporter phage constructs encoding mCherry fused to lytic promoter, detecting *IS90#* with real time qPCR, or other methods.

5.3 Summation

The data described here informs future endeavors into phage therapy. Western medicine is in need of detailed and organized clinical trials, not because the theory of phage therapy is unsound but so Western medicine can acclimate to the post-antibiotic era more successfully. There is much to be done in MAC complex research, and this work aimed to give insights into what phage-host dynamics are of interest in this data set, and easing potential frustrations when working with MAC complex strains. Finally, this work increased the repertoire of therapeutically useful phages, by generating a lytic mutant of a prophage spontaneously induced from a clinically isolated NTM.

Appendix A Phenotypes Observed

Appendix A.1 Infection phenotypes

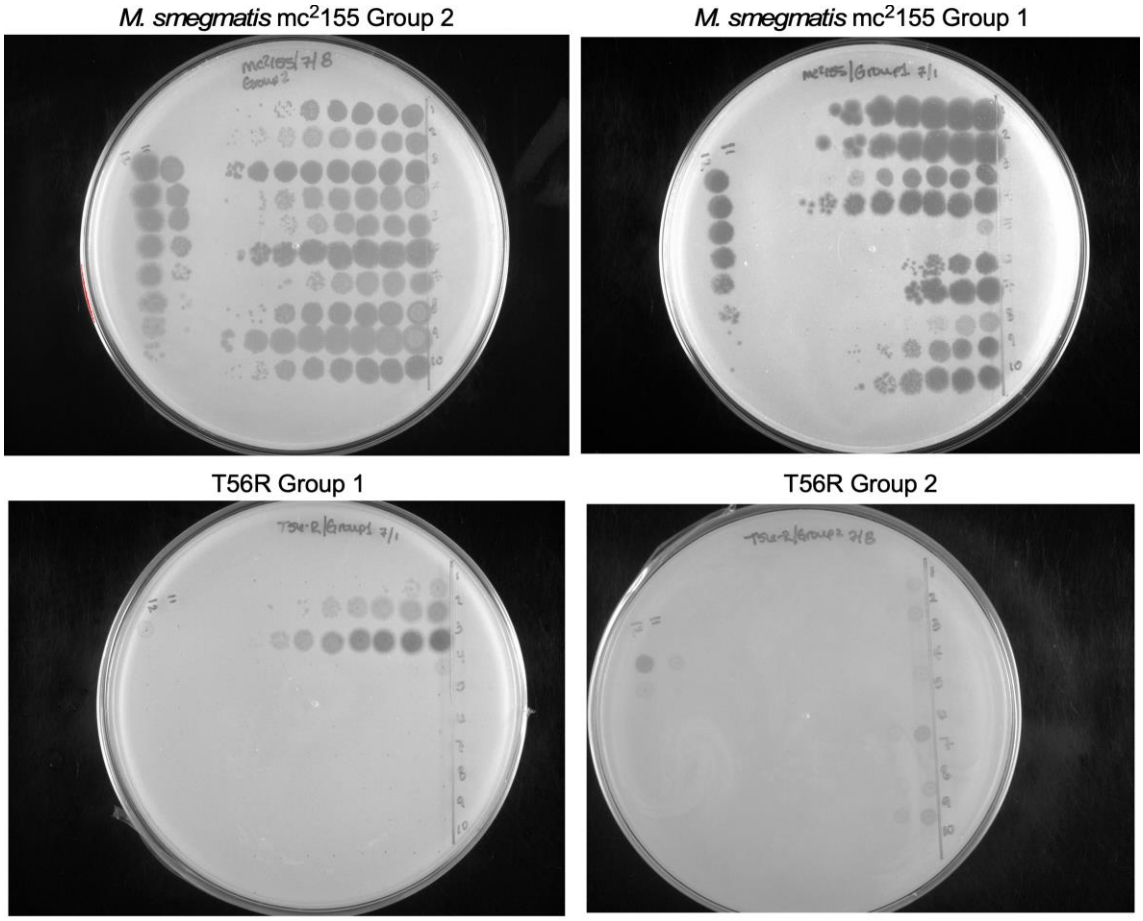

Group 1 Phages (Cluster)
1. Elmo_HRM (A3)
2. Isca (A3)
3. Muddy (AB1)
4. BPs_HRM10_HTHΔ*33*
5. Pinnie (G2)
6. AdephagiaΔ*41*Δ*43*
7. ZoeJΔ45 (K2)
8. Keshu (K3)
9. ShedlockHolmes (K3)
10. Wintermute (K4)
11. TM4 (K2)

Group 2 Phages (Cluster)
1. MkaliMitinis3 (L2)
2. Faith1 (L2)
3. BigCheese (L2)
4. Wilder (L2)
5. Archie (L2)
6. Breezona (L2)
7. Kahlid (L2)
8. Gardann (L2)
9. JAWS (K1)
10. Whirlwind (L3)
11. Angelica (K1)
12. Turbido (A21)

Figure 21 Raw plates from Figure 13

Plates from which the infection phenotypes presented in Figure 13 were compiled.

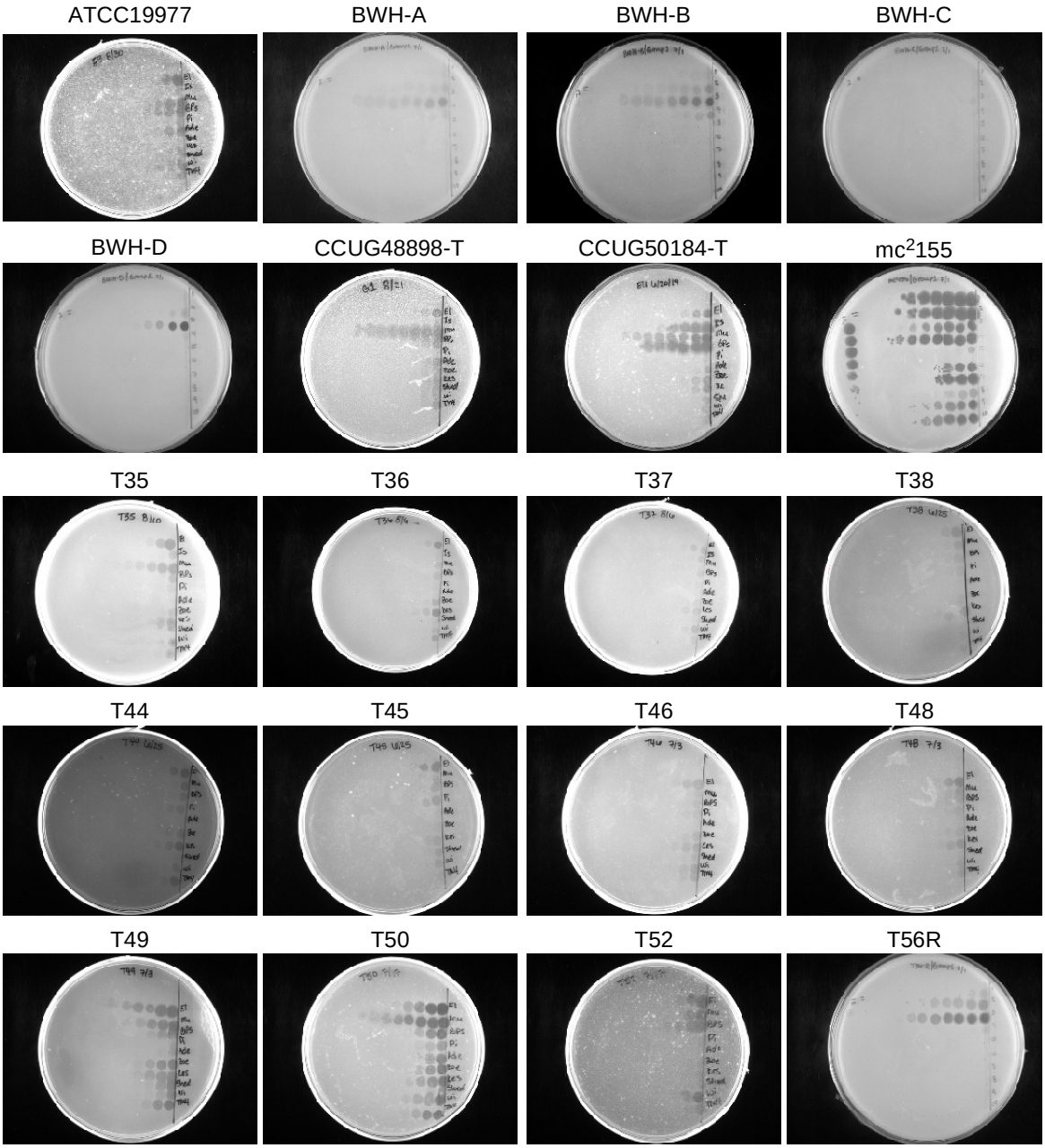

Group I Bacteriophages (cluster)

1. Elmo HRM (A3)
2. Isca (A3)
3. Muddy (AB1)
4. BPs_HRM10_HTH∆*33* (G1)
5. Pinnie (G2)
6. Adephagia∆ (K1)
7. ZoeJ∆*43-45* (K2)
8. Keshu (K3)
9. ShedlockHolmes (K3)
10. Wintermute (K4)
11. TM4∆ (K2)
12. data not included

Figure 22 MAB challenges with Group I bacteriophages

Raw results of MAB challenges with bacteriophages in Group 1. Phages in the group are listed at the bottom with clusters in parentheses. The strain challanged on each plate is noted aboce the respective plate.

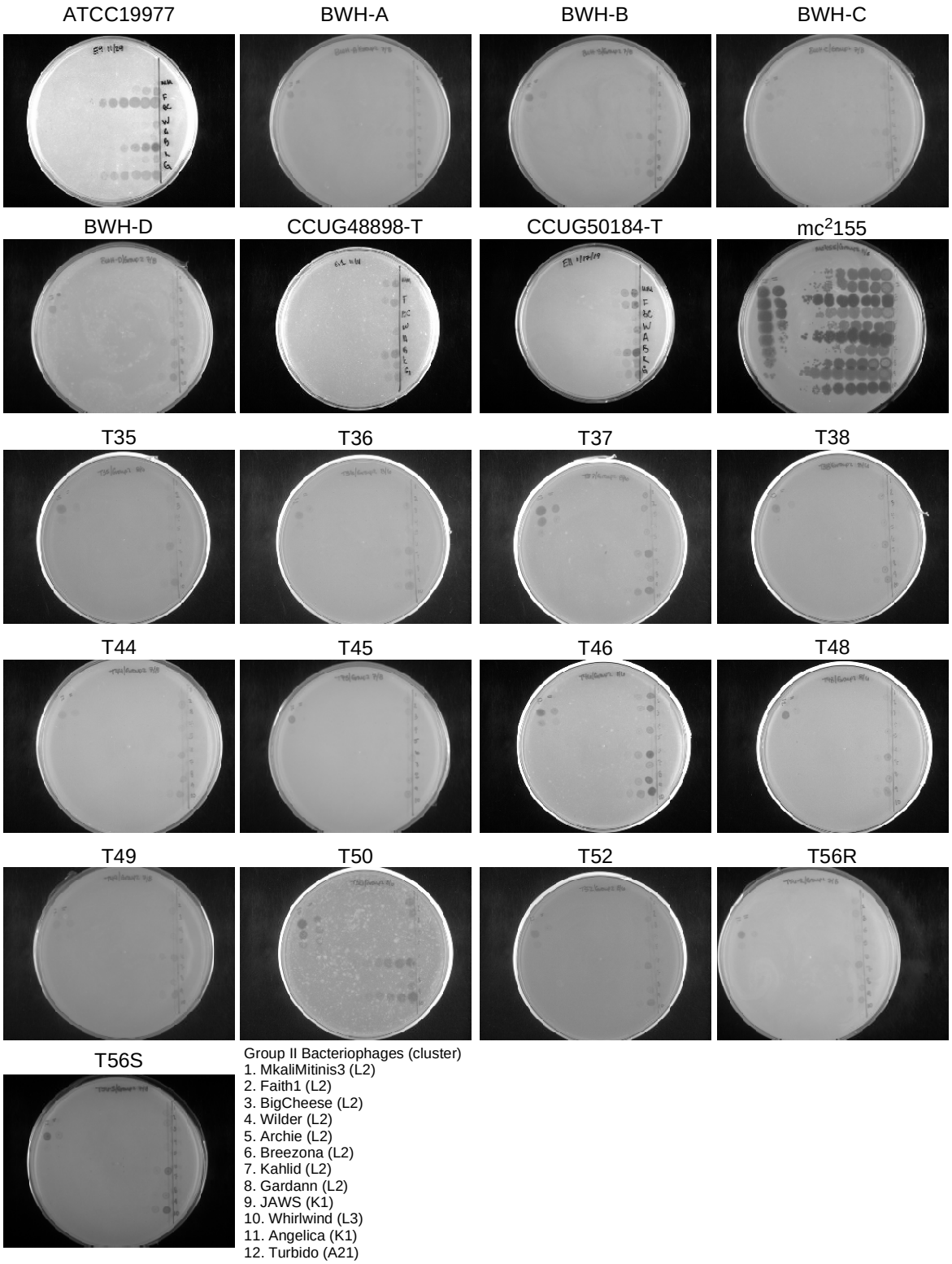

Figure 23 MAB challenges with Group 2 bacteriophages

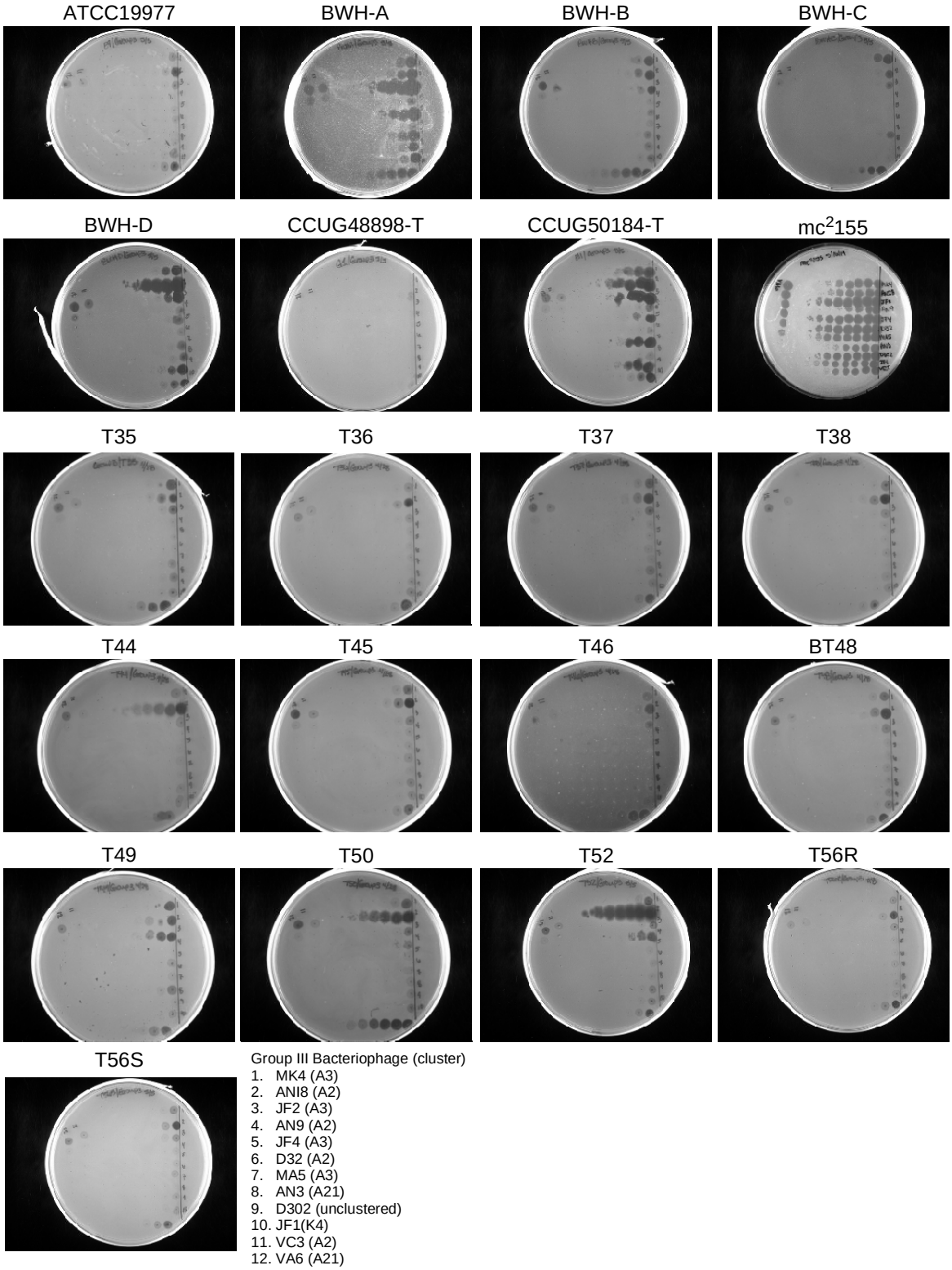

Figure 24 MAB challenges with Group 3 bacteriophages

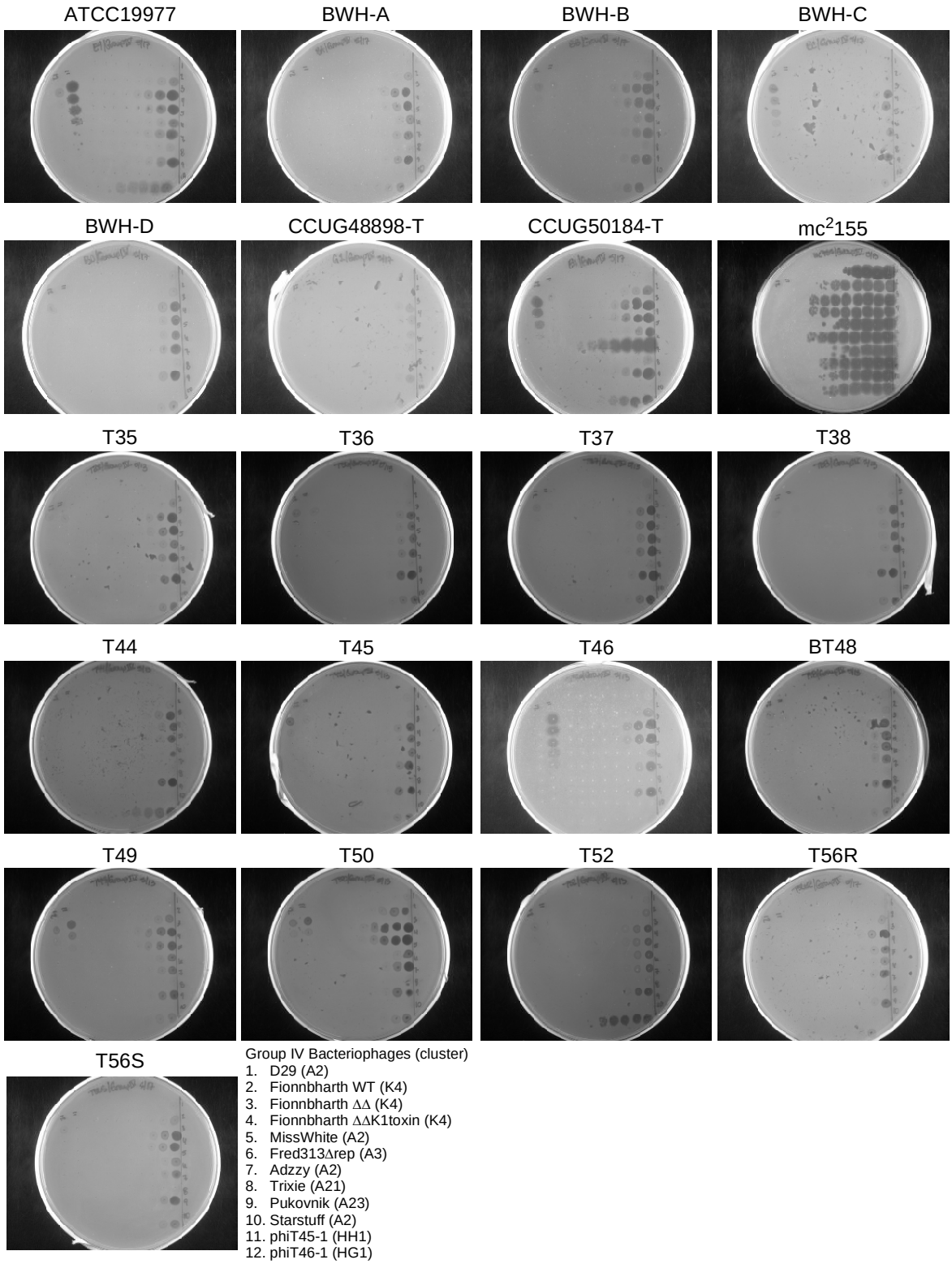

Figure 25 MAB challenges with Group 4 bacteriophages

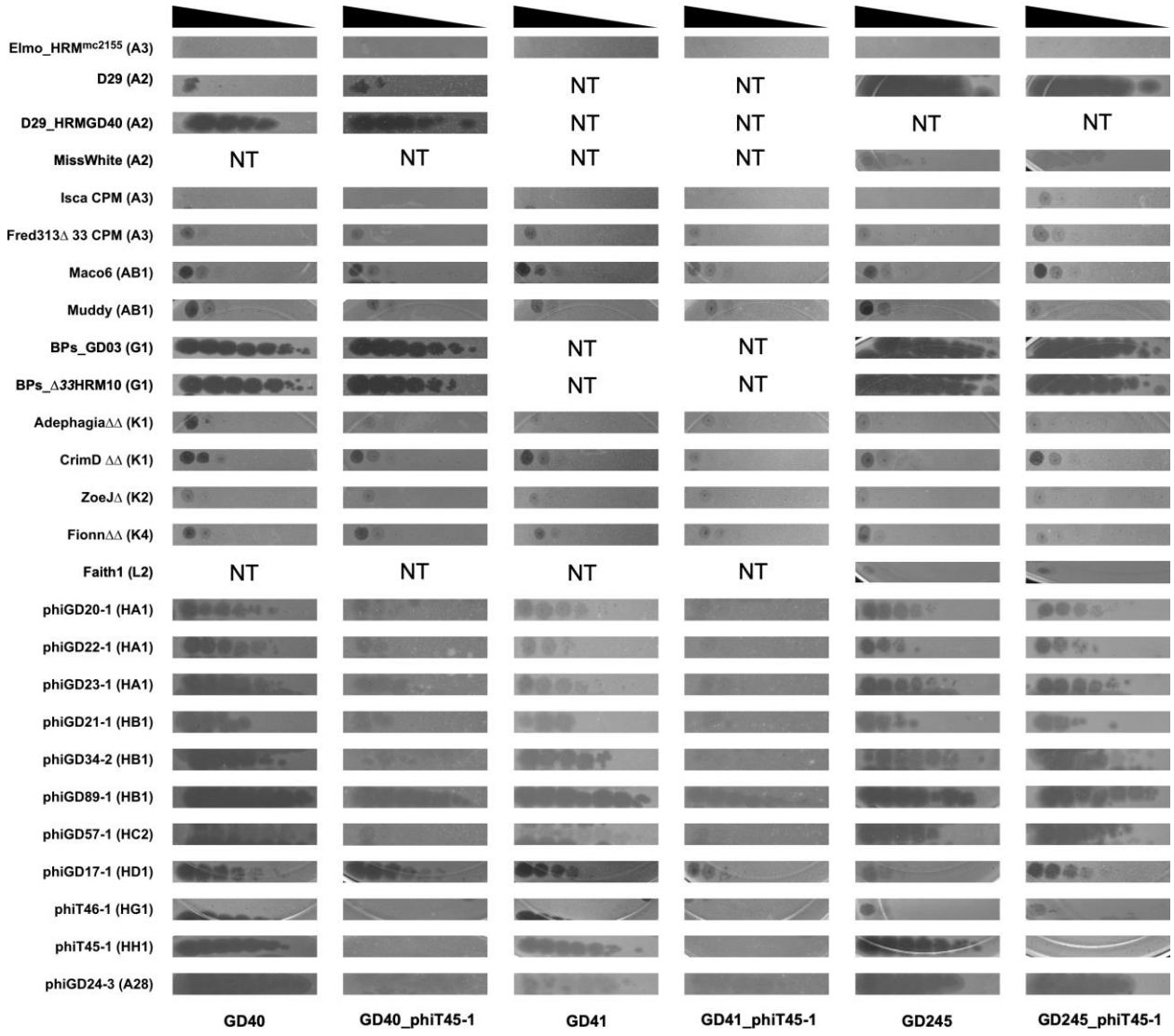

Figure 26 Susceptibility Phenotypes of phiT45-1 Lysogens

Down the left side are the phages screened against phiT45-1 lysogens of clinically isolated strains GD40, GD41, and GD245. Strains are labeled across the bottom. The black triangles along the top indicate ten-fold serial dilutions of the phage lysate. The notation "NT" indicates the phage-host combination was not tested.

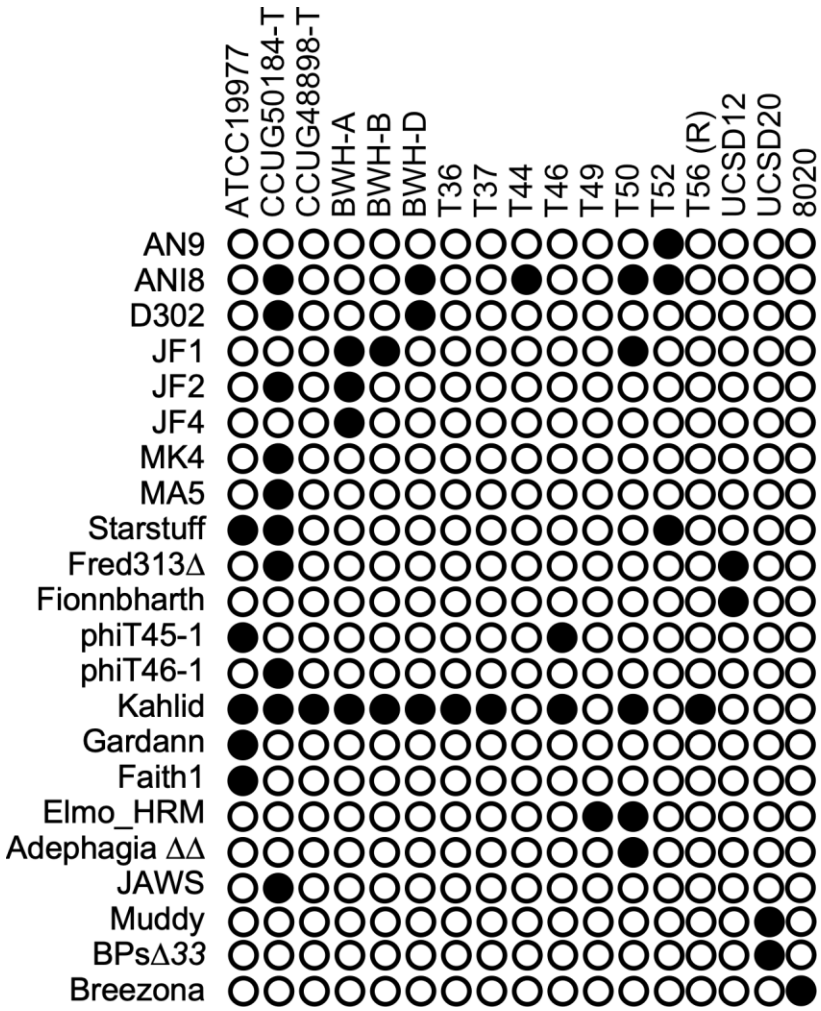

Figure 27 Reduced Infection Phenotypes

Phage and strain combinations that yielded the reduced infection phenotype. Reduced infection phenotype supports that an HRM can be isolated with multiple passages through the host. Phages are listed down the left side, while strains are listed across the top. A darkened circle indicates the reduced infection phenotype was observed; an empty circle indicates there is no infection observed.

Appendix A.2 MAC Colony Morphotypes

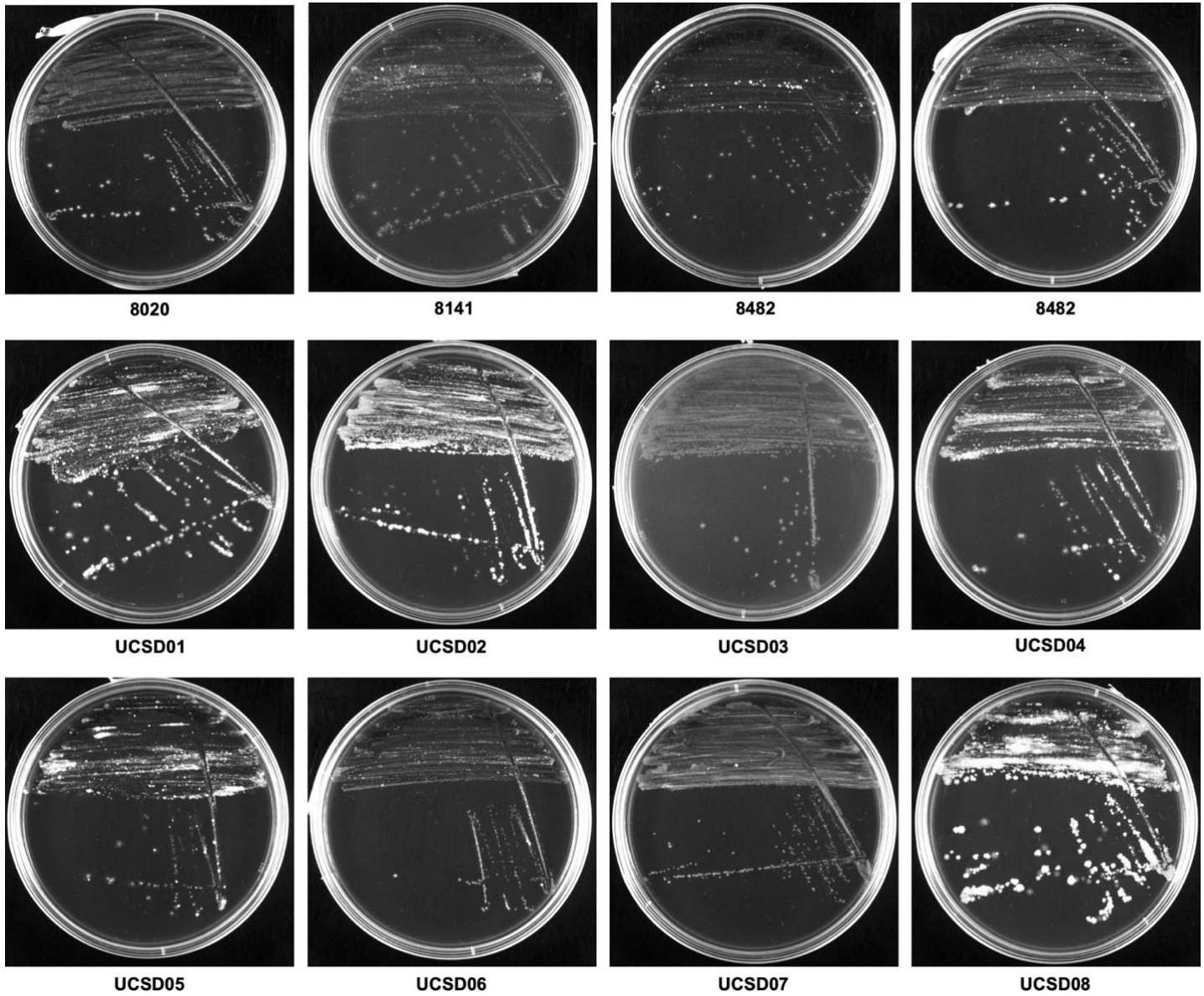

Figure 28 MAC T-streak Plates

Streak plates of MAC strains demonstrating the variation in colony morphotypes. Strain designations are below respective streak-plates. Streaks were prepared from glycerol freezer stocks (-80ºC), and grown on naked 7H10/OADC plates, no antibiotics. Some strains appear to demonstrate two morphotypes (UCSD02, UCSD08) while others form more homogenous colonies (UCSD06).

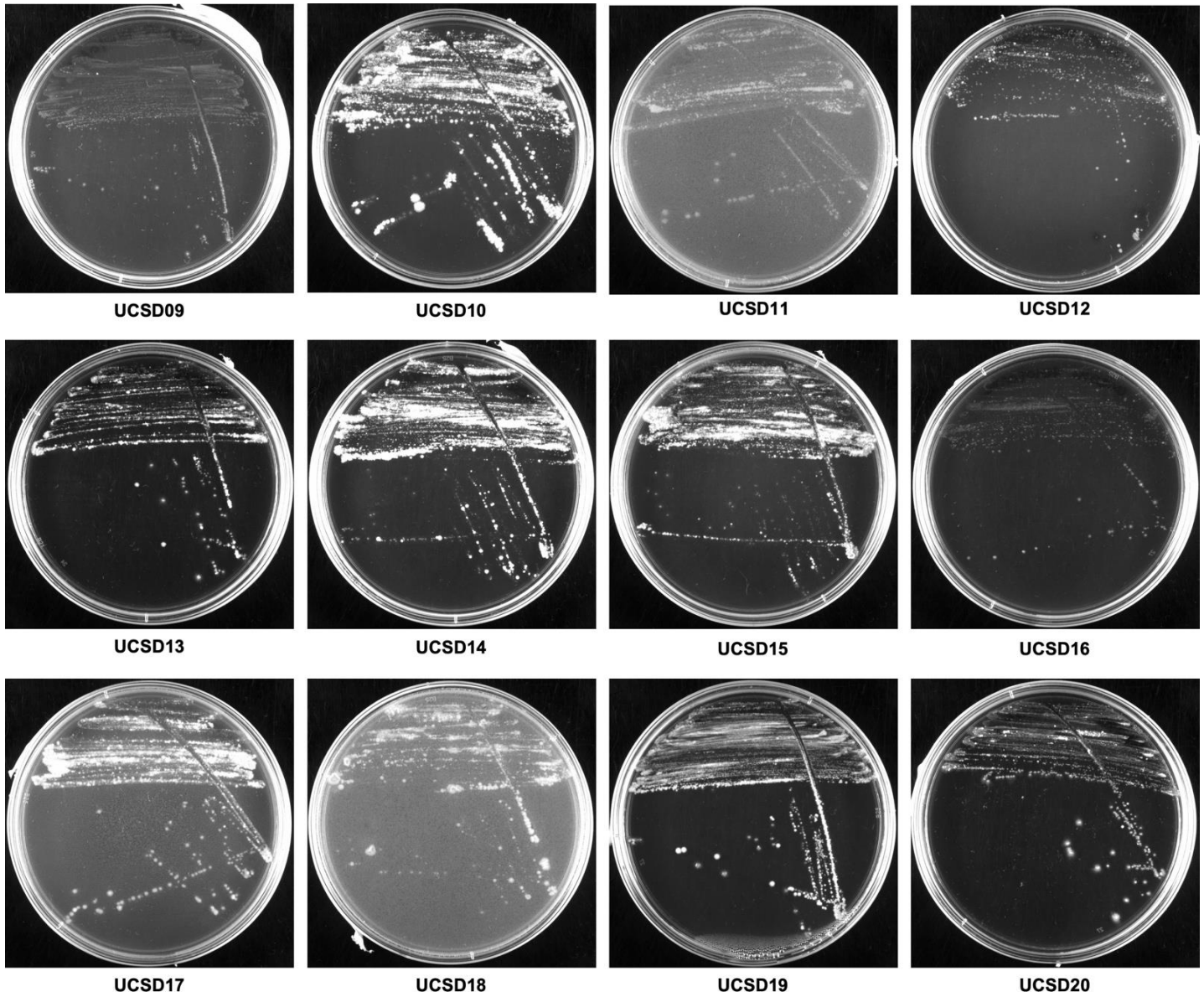

Figure 29 MAC T-streak Plates Continued

Streak plates prepared as descrbed in Figure 23. As in Figure 23, some strains demonstrate two colony morphotypes (UCSD14, UCSD15) while others form more homogenous colonies (UCSD17).

Appendix B Detecting tandem prophage phage virions in identical prophages

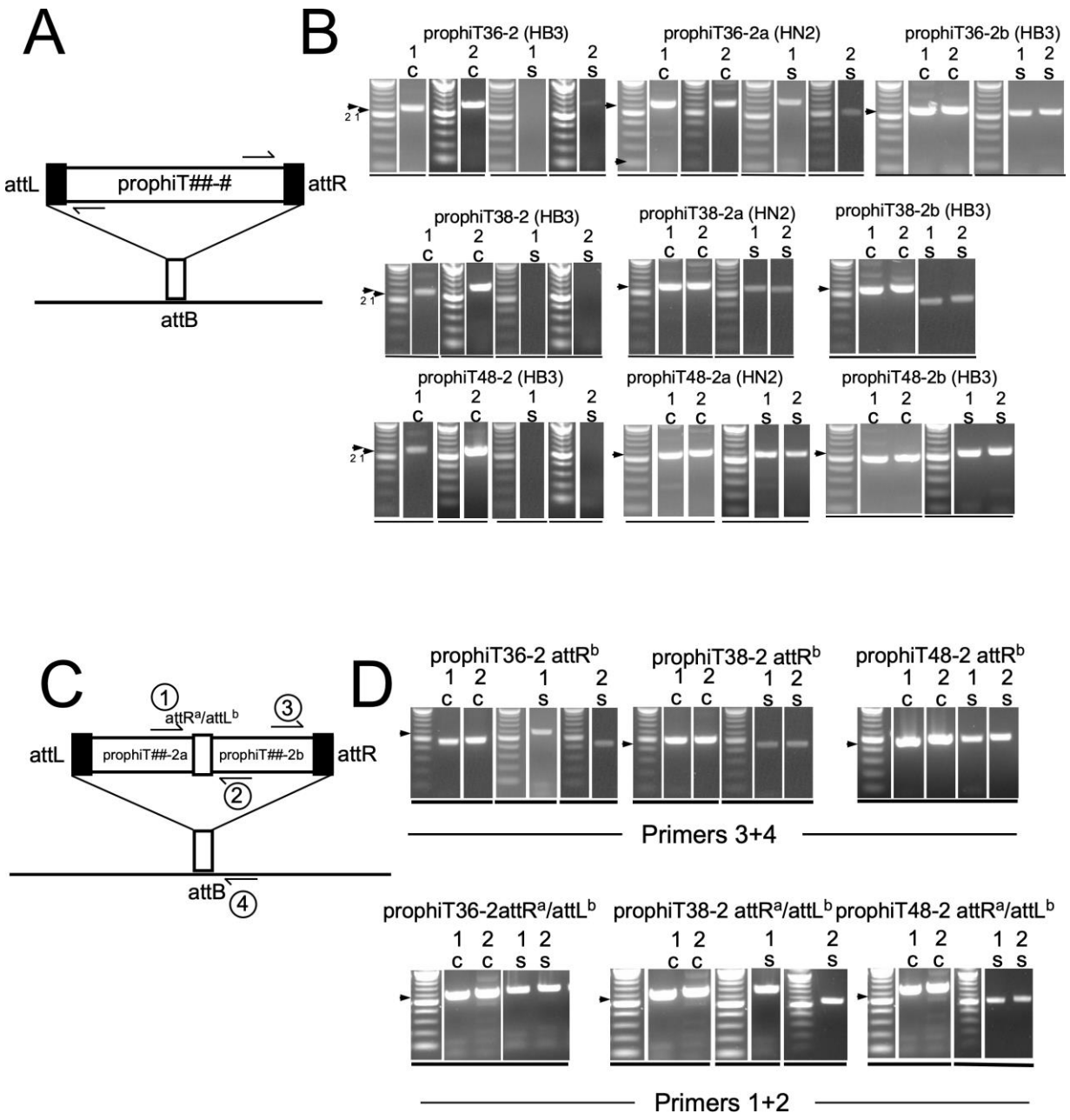

Appendix B Figure 1. Detection of tandem prophage phage virions by PCR.

Panels are annotated as described in the previous figure (Figure 12)**.**

Appendix C Prophage Genome Maps

This appendix contains genome organizations for the prophages not pictured in the main text.

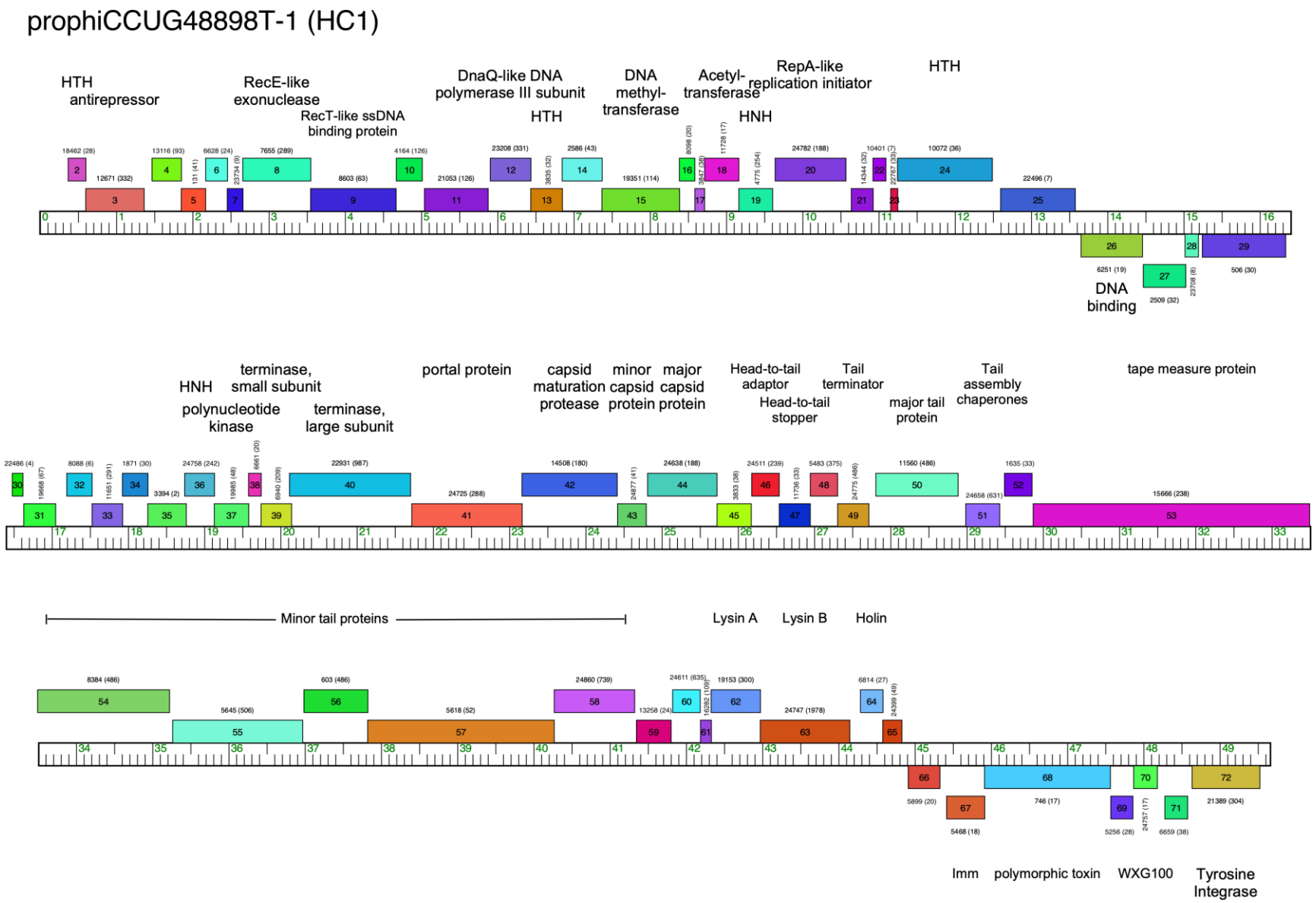

Figure 30 Map of the prophiCCUG48898T-1 genome.

The horizontal ruler represents the nucleotide sequence of the phage genome, with each tick mark indicating 1 kb. Predicted genes are denoted as colored boxes on top of and under the ruler, corresponding to rightwards and leftwards transcription, respectively. Gene colors coordinate with phamily assignments using Phamerator (Cresawn et al., 2011) and database Actino_Mab_4036. Phamily designations and number of phamily members in parenthesis are above the genes. Orphams with no close relatives in this dataset are denoted as white boxes. Predicted gene functions are annotated.

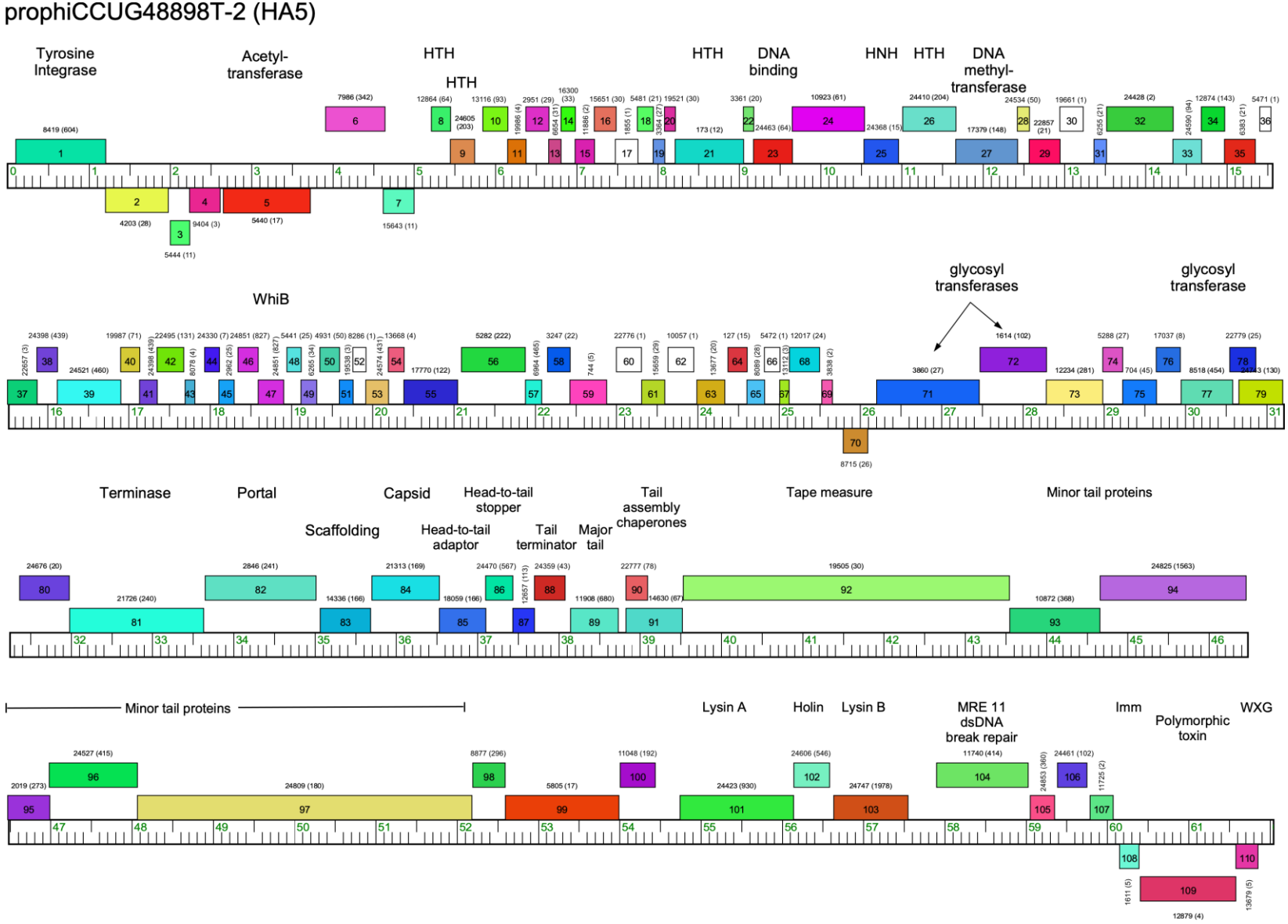

Figure 31 Map of the prophiCCUG48898T-2 genome.

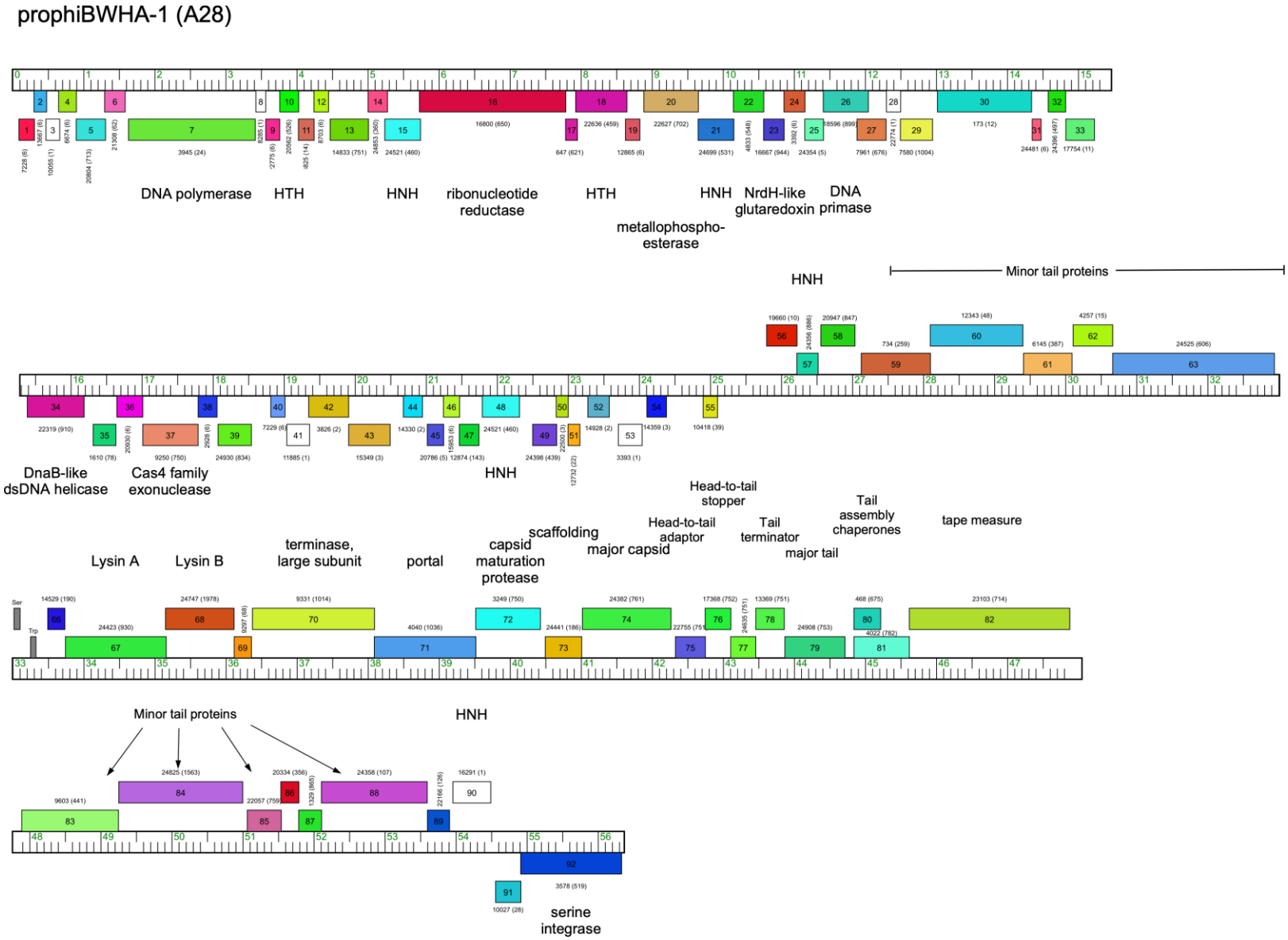

Figure 32 Map of the prophiBWHA-1 genome.

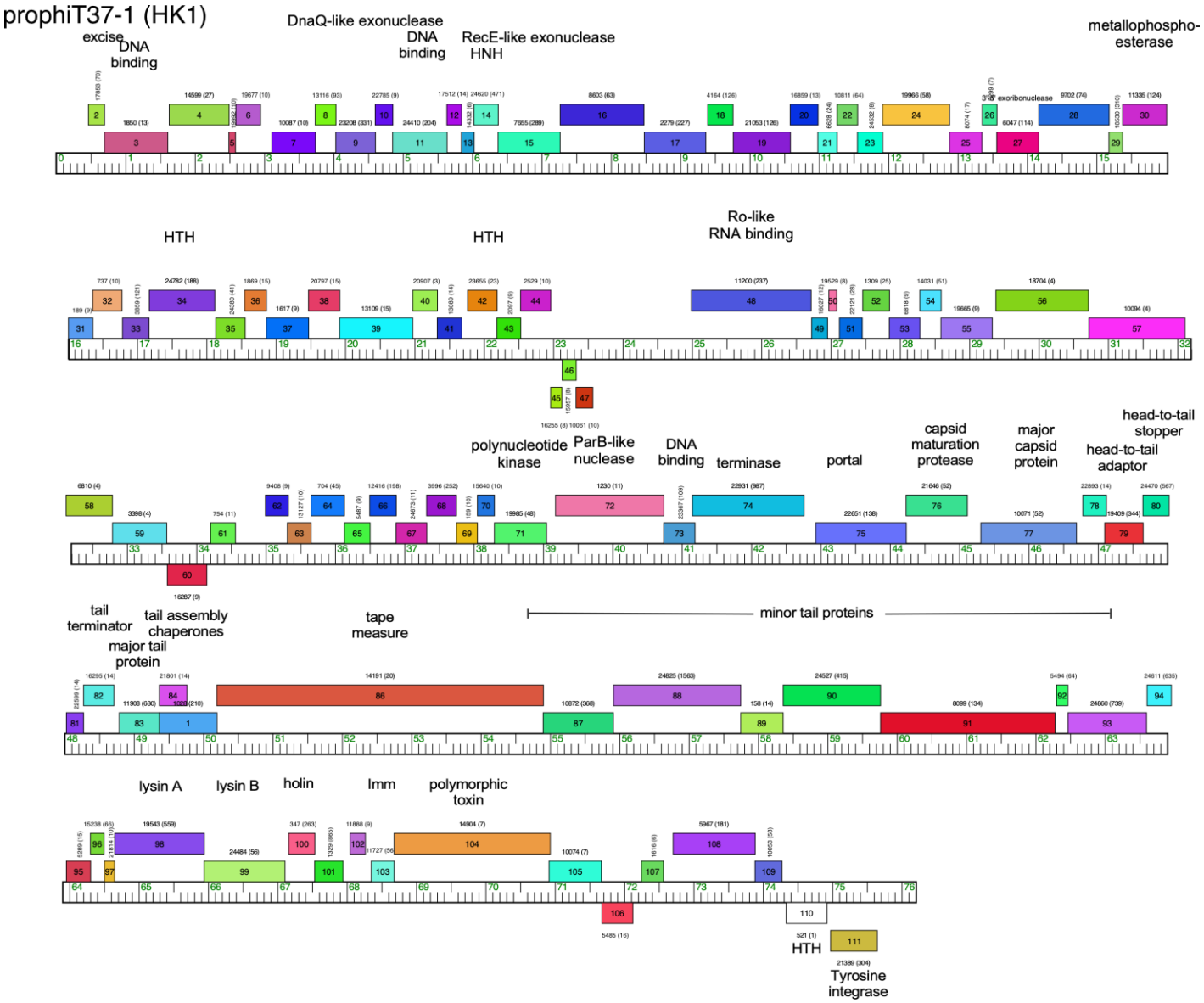

Figure 33 Map of the prophiT37-1 genome.

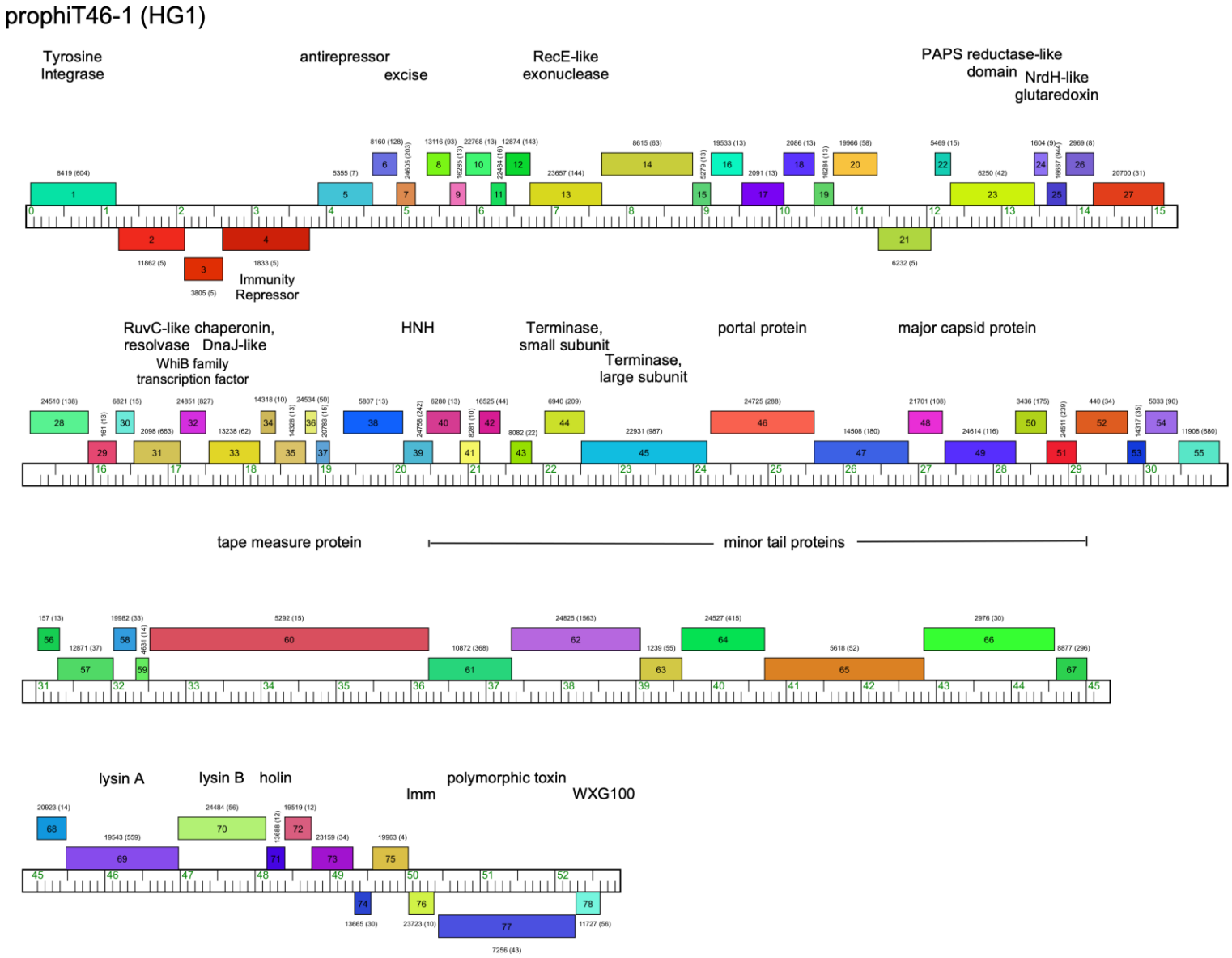

Figure 34 Map of the prophiT46-1 genome.

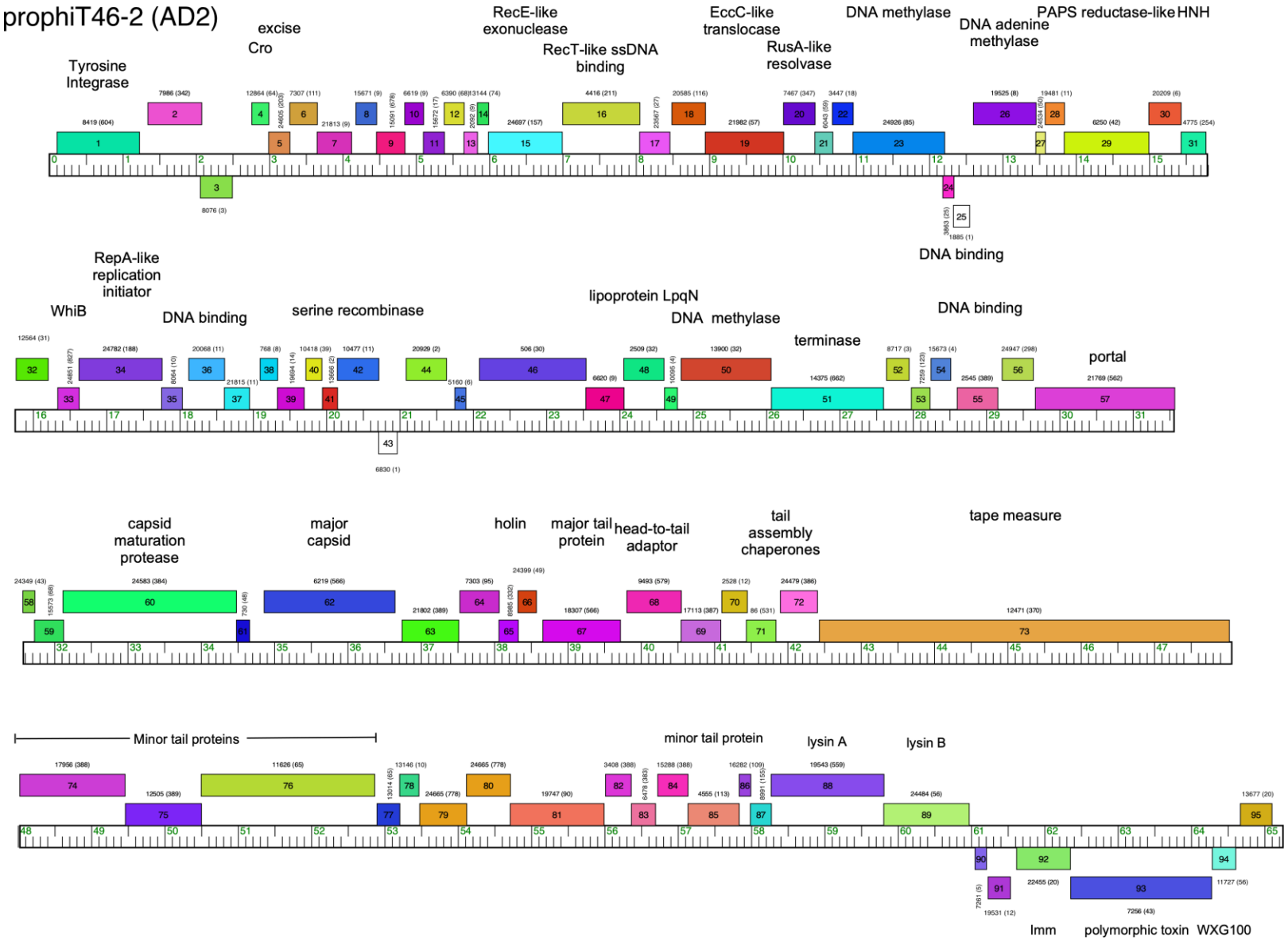

Figure 35 Map of the prophiT46-2 genome.

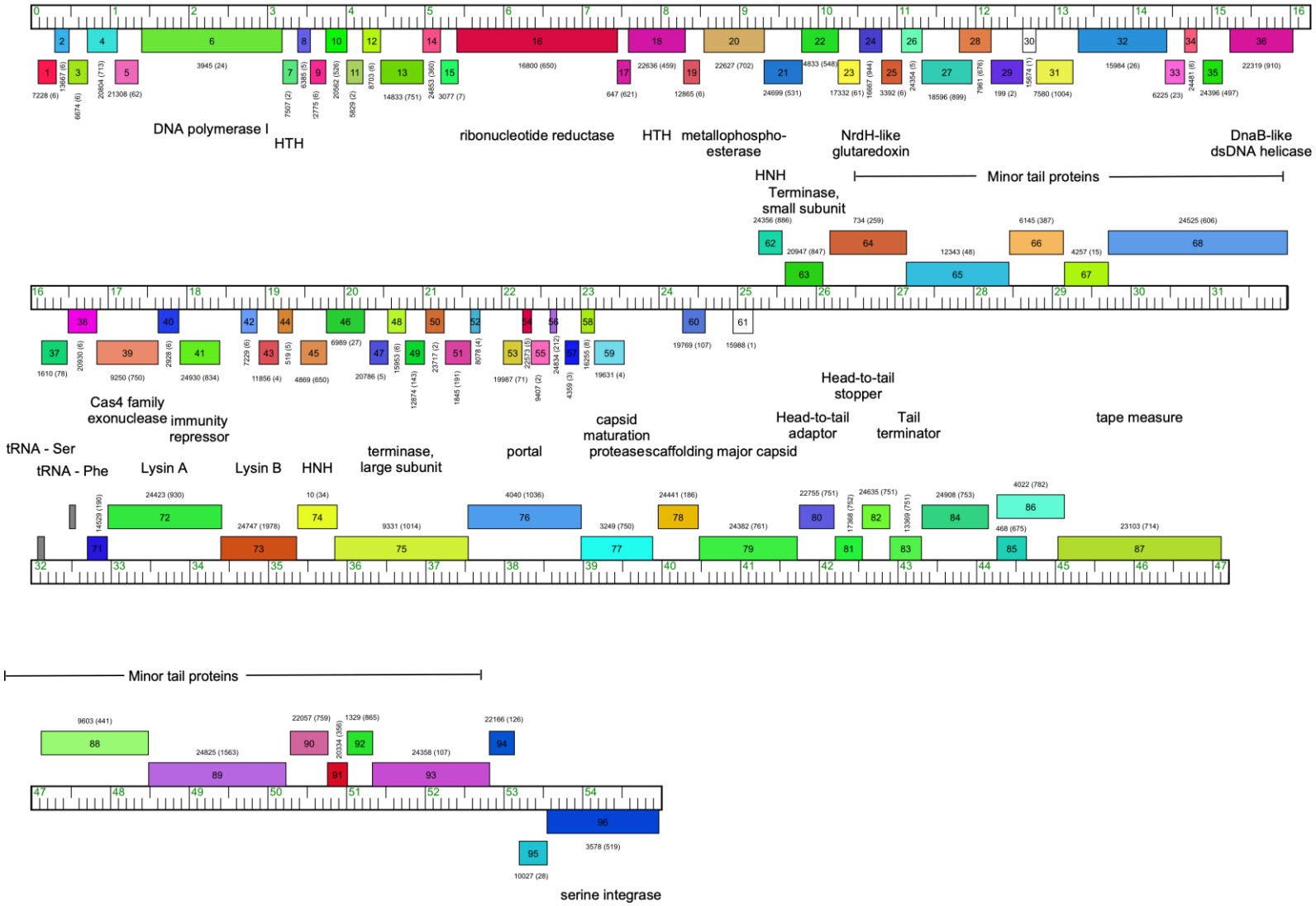

Figure 36 Map of the prophiT46-3 genome.

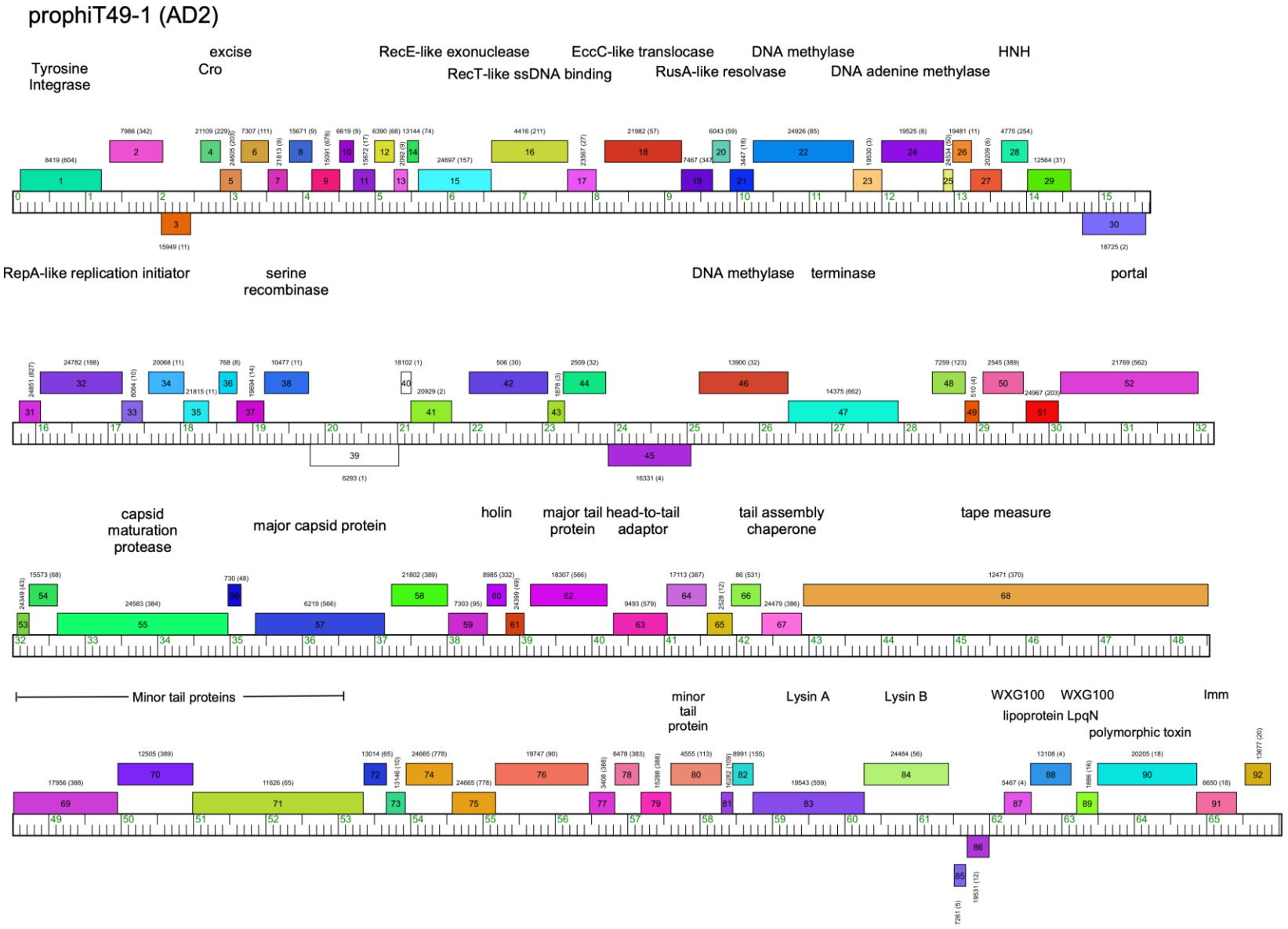

Figure 37 Map of the prophiT49-1 genome.

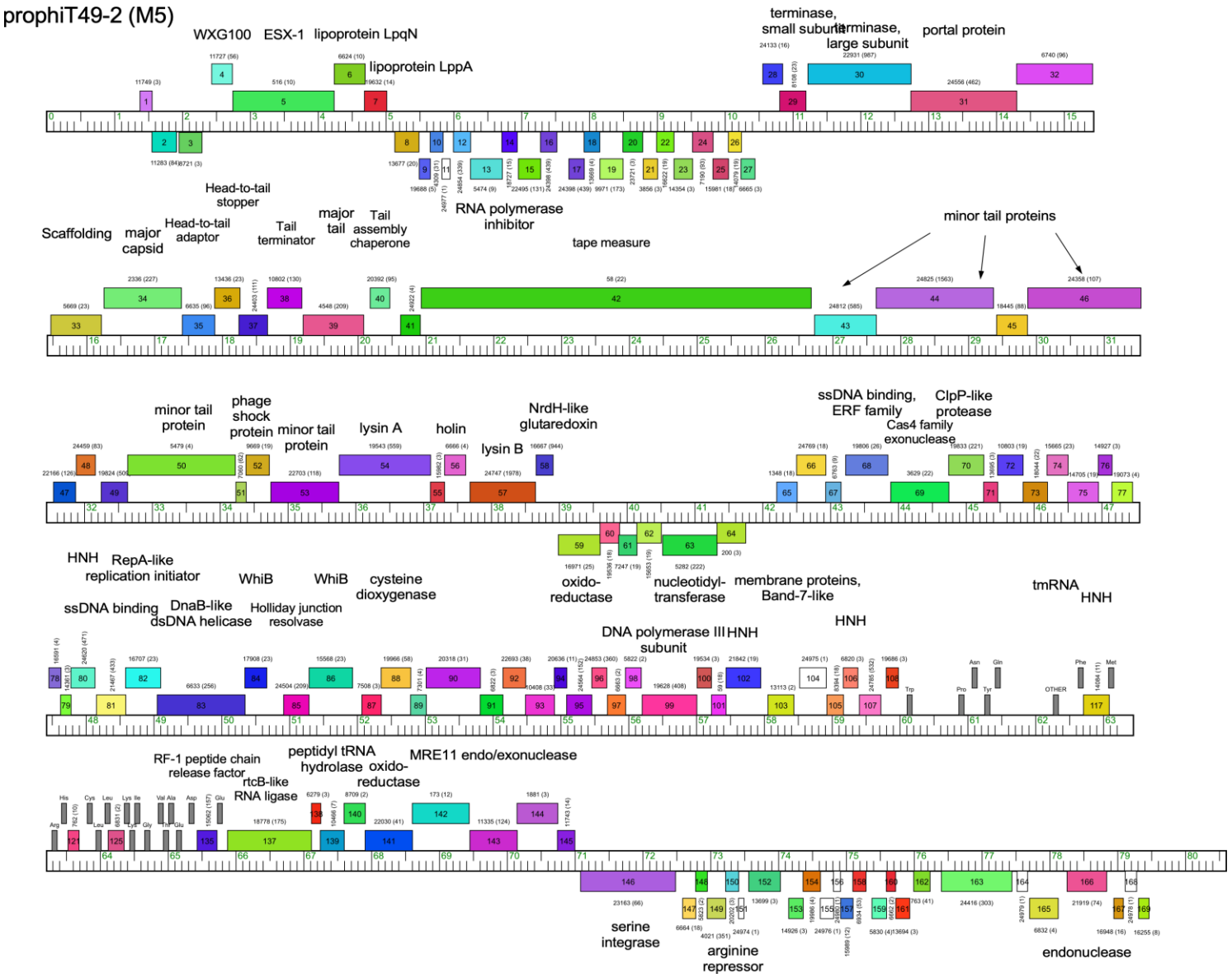

Figure 38 Map of the prophiT49-2 genome.

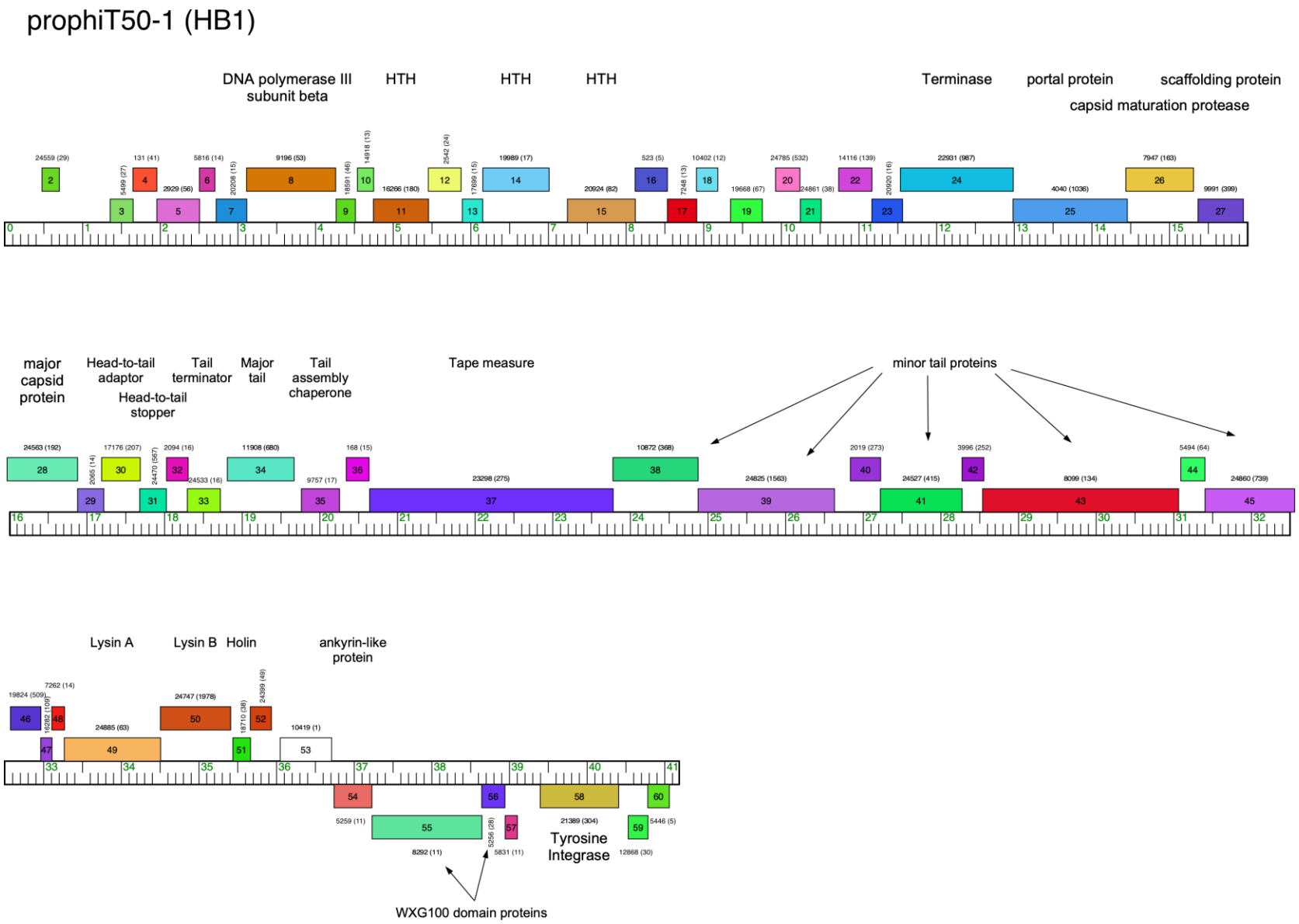

Figure 39 Map of the prophiT50-1 genome.

Appendix D *M. abscessus* Sequencing Supplemental.

Table 4 Genomic sequencing of *M. abscessus*

Strain[1]	Length (bp)[2]	Contigs[3]	Coverage[4]	Status[5]	Accession #[6]
T35	5248033	67	51	WGS	SRR19357812
T36	5075015	1	53	Complete	SRR19357811
T37	5337129	67	72	WGS	SRR19357810
T38	4990610	27	59	WGS	JAQLTU000000000
T44	4869593	30	93	WGS	JAQLTT000000000
T45	5371068	69	33	WGS	SRR19357825
T46	5335090	54	131	WGS	JAQLTS000000000
T48	4990171	34	149	WGS	JAQLTR000000000
T49	5092962	37	123	WGS	JAQLTQ000000000
T50	5295651	67	55	WGS	SRR19357822
T52	4826919	105	36	WGS	JAQLTP000000000
T56S	5227337	72	133	WGS	JAQLTO000000000
T56R	5227737	85	50	WGS	JAQLTN000000000
BWH-A	4977099	43	70	WGS	JAQLTM000000000
BWH-B	4995327	49	77	WGS	SRR19357831
BWH-C	5088980	44	127	WGS	JAQLTL000000000

BWH-D	5117974	15	209	WGS	JAQLTG000000000
CCUG50184-T	5053525	24	150	WGS	PRJNA281565
CCUG48898-T	4969787	25	N/A	WGS	SRR315577

[1]Clinically isolated strains were given a designation based on their location of origin; strains received from Taiwan begin with "T". An "S" or "R" suffix denotes smooth and rough colony morphotypes, respectively. Strains with "BWH" were isolated from Brigham and Women's Hospital, Boston, Massachussetts. Strains from the Culture Collection University of Gothenburgh archives are indicated by "CCUG".

[2]The length of strain T36 presented here is of the complete genome; all others present the sum of all the contig lengths.

[3]Number of contigs greater than 100 bp, generated following assembly with Unicycler v 0.4.8.

[4]WGS coverage

[5]Whole genome shotgun sequencing performed with Illumina Miseq; complete genome sequencing performed with Illumina HiSeq and Oxford Nanopore.

[6]Accession numbers under which the strain sequences can be found. Genome accession numbers that are available are shown; in other cases the Sequence Read Archive (SRA) number is provided.

Table 5 attB characteristics and coordinates in M. abscessus type strain ATCC19977

Cluster	Core Sequences	Int	attB	attB	ATCC19977 coordinates
HA	GGGTTCGAAACCCTCCGCGCCCACCAA	Int-Y	attB-20	tRNA-Val (Mab_t5029)	1739377
HB	GTAATGAATAGGTCGGGGGTTCGATTCCCCCGGGCAGCTC	Int-Y	attB-2	tRNA-Thr (t5010)	490925
	GTAATGAATAGGTCCGGGGTTGGCTTCCCCTGGATTGTCA				
	GTAATGAATAGGTCAGGGGTTCGATTCCCCTGGGTGGCTC				
HC	TACTCGTGAGTAAGAACT	Int-Y	attB-13	Mab_3947	3995698
HG	CGGGTTCAATTCCCGGCAGCTCCAC	Int-Y	attB-11	tmRNA	3513406
M	GGGCT	Int-S	attB-17	Mab_3265c	3302860
A	AAGTCGTA	Int-S	attB-7	Mab_2445	2502029
	AC		attB-21	Mab_1851	18493335
HK	CAGAAGGTTAGGGGTTCGAATCCCTTCGGGCGCACCA**T**	Int-Y	attB-1	tRNA-Arg (Mab_t5006)	233517
	CAGAAGGTTGGGGGTTCGAATCCCTTCGGGCGCACCA**C**				
AD	AGGGGTTCGAGTCCCCTTAGCTCCAC	Int-Y	attB-10	tRNA-Ala (Mab_5041c)	3491832
	AGGGGTTCGAGTCCCCTTAGCTCCAC**AATA**				
	AGGGGTTCGAGTCCCCTTAGCTCCAC**CATA**				

Bibliography

Abad, L., C. H. Gauthier, I. Florian, D. Jacobs-Sera and G. F. Hatfull (2023). "The heterogenous and diverse population of prophages in Mycobacterium genomes." mSystems **8**(5): e0044623.

Abdallah, A. M., J. Bestebroer, N. D. Savage, K. de Punder, M. van Zon, L. Wilson, C. J. Korbee, A. M. van der Sar, T. H. Ottenhoff, N. N. van der Wel, W. Bitter and P. J. Peters (2011). "Mycobacterial secretion systems ESX-1 and ESX-5 play distinct roles in host cell death and inflammasome activation." J Immunol **187**(9): 4744-4753.

Abedon, S. T. (2011). "Lysis from without." Bacteriophage **1**(1): 46-49.

Abedon, S. T., S. J. Kuhl, B. G. Blasdel and E. M. Kutter (2011). "Phage treatment of human infections." Bacteriophage **1**(2): 66-85.

Ackermann, H. W. (1998). "Tailed bacteriophages: the order caudovirales." Adv Virus Res **51**: 135-201.

Altschul, S. F., W. Gish, W. Miller, E. W. Myers and D. J. Lipman (1990). "Basic local alignment search tool." J Mol Biol **215**(3): 403-410.

Amarh, E. D., R. M. Dedrick, R. A. Garlena, D. A. Russell, C. H. Gauthier, H. G. Aull, L. Abad, D. Jacobs-Sera, C. Akusobi, E. J. Rubin and G. F. Hatfull (2023). "Unusual prophages in Mycobacterium abscessus genomes and strain variations in phage susceptibilities." PLoS One **18**(2): e0281769.

Amarh, E. D., R. M. Dedrick, R. A. Garlena, D. A. Russell, D. Jacobs-Sera and G. F. Hatfull (2021). "Genome Sequence of Mycobacterium abscessus Phage phiT46-1." Microbiol Resour Announc **10**(2).

Amarh, E. D., C. H. Gauthier, R. M. Dedrick, R. A. Garlena, D. A. Russell, D. Jacobs-Sera, K. M. Zack and G. F. Hatfull (2021). "Genome Sequence of Mycobacterium abscessus Phage phiT45-1." Microbiol Resour Announc **10**(10).

Aminov, R. I. (2010). "A brief history of the antibiotic era: lessons learned and challenges for the future." Front Microbiol **1**: 134.

Arndt, D., A. Marcu, Y. Liang and D. S. Wishart (2019). "PHAST, PHASTER and PHASTEST: Tools for finding prophage in bacterial genomes." Brief Bioinform **20**(4): 1560-1567.

Bacon, J., L. J. Alderwick, J. A. Allnutt, E. Gabasova, R. Watson, K. A. Hatch, S. O. Clark, R. E. Jeeves, A. Marriott, E. Rayner, H. Tolley, G. Pearson, G. Hall, G. S. Besra, L. Wernisch, A. Williams and P. D. Marsh (2014). "Non-replicating Mycobacterium tuberculosis elicits a reduced infectivity profile with corresponding modifications to the cell wall and extracellular matrix." PLoS One **9**(2): e87329.

Baird, T. and S. Bell (2023). "Cystic Fibrosis-Related Nontuberculous Mycobacterial Pulmonary Disease." Clin Chest Med **44**(4): 847-860.

Baker, A. W., S. S. Lewis, B. D. Alexander, L. F. Chen, R. J. Wallace, Jr., B. A. Brown-Elliott, P. J. Isaacs, L. C. Pickett, C. B. Patel, P. K. Smith, J. M. Reynolds, J. Engel, C. R. Wolfe, C. A. Milano, J. N. Schroder, R. D. Davis, M. G. Hartwig, J. E. Stout, N. Strittholt, E. K. Maziarz, J. H. Saullo, K. C. Hazen, R. J. Walczak, Jr., R. Vasireddy, S. Vasireddy, C. M. McKnight, D. J. Anderson and D. J. Sexton (2017). "Two-Phase Hospital-Associated Outbreak of Mycobacterium abscessus: Investigation and Mitigation." Clin Infect Dis **64**(7): 902-911.

Bansal-Mutalik, R. and H. Nikaido (2014). "Mycobacterial outer membrane is a lipid bilayer and the inner membrane is unusually rich in diacyl phosphatidylinositol dimannosides." Proc Natl Acad Sci U S A **111**(13): 4958-4963.

Bar-Oz, M., M. Meir and D. Barkan (2022). "Virulence-Associated Secretion in Mycobacterium abscessus." Front Immunol **13**: 938895.

Barczak, A. K., R. Avraham, S. Singh, S. S. Luo, W. R. Zhang, M. A. Bray, A. E. Hinman, M. Thompson, R. M. Nietupski, A. Golas, P. Montgomery, M. Fitzgerald, R. S. Smith, D. W. White, A. D. Tischler, A. E. Carpenter and D. T. Hung (2017). "Systematic, multiparametric analysis of Mycobacterium tuberculosis intracellular infection offers insight into coordinated virulence." PLoS Pathog **13**(5): e1006363.

Bartholomew, J. W. and T. Mittwer (1952). "The Gram stain." Bacteriol Rev **16**(1): 1-29.

Betts, J. C., P. T. Lukey, L. C. Robb, R. A. McAdam and K. Duncan (2002). "Evaluation of a nutrient starvation model of Mycobacterium tuberculosis persistence by gene and protein expression profiling." Mol Microbiol **43**(3): 717-731.

Boutte, C. C., C. E. Baer, K. Papavinasasundaram, W. Liu, M. R. Chase, X. Meniche, S. M. Fortune, C. M. Sassetti, T. R. Ioerger and E. J. Rubin (2016). "A cytoplasmic peptidoglycan amidase homologue controls mycobacterial cell wall synthesis." Elife **5**.

Brambilla, C., M. Llorens-Fons, E. Julian, E. Noguera-Ortega, C. Tomas-Martinez, M. Perez-Trujillo, T. F. Byrd, F. Alcaide and M. Luquin (2016). "Mycobacteria Clumping Increase Their Capacity to Damage Macrophages." Front Microbiol **7**: 1562.

Brennan, P. J., M. Heifets and B. P. Ullom (1982). "Thin-layer chromatography of lipid antigens as a means of identifying nontuberculous mycobacteria." J Clin Microbiol **15**(3): 447-455.

Broussard, G. W. and G. F. Hatfull (2013). "Evolution of genetic switch complexity." Bacteriophage **3**(1): e24186.

Broussard, G. W., L. M. Oldfield, V. M. Villanueva, B. L. Lunt, E. E. Shine and G. F. Hatfull (2013). "Integration-dependent bacteriophage immunity provides insights into the evolution of genetic switches." Mol Cell **49**(2): 237-248.

Brown, K. L., G. J. Sarkis, C. Wadsworth and G. F. Hatfull (1997). "Transcriptional silencing by the mycobacteriophage L5 repressor." EMBO J **16**(19): 5914-5921.

Casjens, S. R. and R. W. Hendrix (2015). "Bacteriophage lambda: Early pioneer and still relevant." Virology **479-480**: 310-330.

Chan, B. K., M. Sistrom, J. E. Wertz, K. E. Kortright, D. Narayan and P. E. Turner (2016). "Phage selection restores antibiotic sensitivity in MDR Pseudomonas aeruginosa." Sci Rep **6**: 26717.

Chan, B. K., P. E. Turner, S. Kim, H. R. Mojibian, J. A. Elefteriades and D. Narayan (2018). "Phage treatment of an aortic graft infected with Pseudomonas aeruginosa." Evol Med Public Health **2018**(1): 60-66.

Chiaradia, L., C. Lefebvre, J. Parra, J. Marcoux, O. Burlet-Schiltz, G. Etienne, M. Tropis and M. Daffe (2017). "Dissecting the mycobacterial cell envelope and defining the composition of the native mycomembrane." Sci Rep **7**(1): 12807.

Consortium, C. R., G. P. the, C. Allix-Beguec, I. Arandjelovic, L. Bi, P. Beckert, M. Bonnet, P. Bradley, A. M. Cabibbe, I. Cancino-Munoz, M. J. Caulfield, A. Chaiprasert, D. M. Cirillo, D. A. Clifton, I. Comas, D. W. Crook, M. R. De Filippo, H. de Neeling, R. Diel, F. A. Drobniewski, K. Faksri, M. R. Farhat, J. Fleming, P. Fowler, T. A. Fowler, Q. Gao, J. Gardy, D. Gascoyne-Binzi, A. L. Gibertoni-Cruz, A. Gil-Brusola, T. Golubchik, X. Gonzalo, L. Grandjean, G. He, J. L. Guthrie, S. Hoosdally, M. Hunt, Z. Iqbal, N. Ismail, J. Johnston, F. M. Khanzada, C. C. Khor, T. A. Kohl, C. Kong, S. Lipworth, Q. Liu, G. Maphalala, E. Martinez, V. Mathys, M. Merker, P.

Miotto, N. Mistry, D. A. J. Moore, M. Murray, S. Niemann, S. V. Omar, R. T. Ong, T. E. A. Peto, J. E. Posey, T. Prammananan, A. Pym, C. Rodrigues, M. Rodrigues, T. Rodwell, G. M. Rossolini, E. Sanchez Padilla, M. Schito, X. Shen, J. Shendure, V. Sintchenko, A. Sloutsky, E. G. Smith, M. Snyder, K. Soetaert, A. M. Starks, P. Supply, P. Suriyapol, S. Tahseen, P. Tang, Y. Y. Teo, T. N. T. Thuong, G. Thwaites, E. Tortoli, D. van Soolingen, A. S. Walker, T. M. Walker, M. Wilcox, D. J. Wilson, D. Wyllie, Y. Yang, H. Zhang, Y. Zhao and B. Zhu (2018). "Prediction of Susceptibility to First-Line Tuberculosis Drugs by DNA Sequencing." N Engl J Med **379**(15): 1403-1415.

Cortes, M. G., Y. Lin, L. Zeng and G. Balazsi (2021). "From Bench to Keyboard and Back Again: A Brief History of Lambda Phage Modeling." Annu Rev Biophys **50**: 117-134.

Cresawn, S. G., M. Bogel, N. Day, D. Jacobs-Sera, R. W. Hendrix and G. F. Hatfull (2011). "Phamerator: a bioinformatic tool for comparative bacteriophage genomics." BMC Bioinformatics **12**: 395.

D'Hérelle, F. (1917). "Sur un microbe invisible antagoniste des bacilles dysentériques." C.R. Acad. Sci. Paris **165**: 373-375.

da Silva, J. L., M. Piuri, G. Broussard, L. J. Marinelli, G. M. Bastos, R. D. Hirata, G. F. Hatfull and M. H. Hirata (2013). "Application of BRED technology to construct recombinant D29 reporter phage expressing EGFP." FEMS Microbiol Lett **344**(2): 166-172.

Daley, C. L., J. M. Iaccarino, C. Lange, E. Cambau, R. J. Wallace, Jr., C. Andrejak, E. C. Bottger, J. Brozek, D. E. Griffith, L. Guglielmetti, G. A. Huitt, S. L. Knight, P. Leitman, T. K. Marras, K. N. Olivier, M. Santin, J. E. Stout, E. Tortoli, J. van Ingen, D. Wagner and K. L. Winthrop (2020). "Treatment of Nontuberculous Mycobacterial Pulmonary Disease: An Official ATS/ERS/ESCMID/IDSA Clinical Practice Guideline." Clin Infect Dis **71**(4): e1-e36.

Dedrick, R. M., H. G. Aull, D. Jacobs-Sera, R. A. Garlena, D. A. Russell, B. E. Smith, V. Mahalingam, L. Abad, C. H. Gauthier and G. F. Hatfull (2021). "The Prophage and Plasmid Mobilome as a Likely Driver of Mycobacterium abscessus Diversity." mBio **12**(2).

Dedrick, R. M., C. A. Guerrero-Bustamante, R. A. Garlena, D. A. Russell, K. Ford, K. Harris, K. C. Gilmour, J. Soothill, D. Jacobs-Sera, R. T. Schooley, G. F. Hatfull and H. Spencer (2019). "Engineered bacteriophages for treatment of a patient with a disseminated drug-resistant Mycobacterium abscessus." Nat Med **25**(5): 730-733.

Dedrick, R. M., T. N. Mavrich, W. L. Ng and G. F. Hatfull (2017). "Expression and evolutionary patterns of mycobacteriophage D29 and its temperate close relatives." BMC Microbiol **17**(1): 225.

Dedrick, R. M., B. E. Smith, M. Cristinziano, K. G. Freeman, D. Jacobs-Sera, Y. Belessis, A. Whitney Brown, K. A. Cohen, R. M. Davidson, D. van Duin, A. Gainey, C. B. Garcia, C. R. Robert George, G. Haidar, W. Ip, J. Iredell, A. Khatami, J. S. Little, K. Malmivaara, B. J. McMullan, D. E. Michalik, A. Moscatelli, J. A. Nick, M. G. Tupayachi Ortiz, H. M. Polenakovik, P. D. Robinson, M. Skurnik, D. A. Solomon, J. Soothill, H. Spencer, P. Wark, A. Worth, R. T. Schooley, C. A. Benson and G. F. Hatfull (2023). "Phage Therapy of Mycobacterium Infections: Compassionate Use of Phages in 20 Patients With Drug-Resistant Mycobacterial Disease." Clin Infect Dis **76**(1): 103-112.

Dedrick, R. M., B. E. Smith, R. A. Garlena, D. A. Russell, H. G. Aull, V. Mahalingam, A. M. Divens, C. A. Guerrero-Bustamante, K. M. Zack, L. Abad, C. H. Gauthier, D. Jacobs-Sera and G. F. Hatfull (2021). "Mycobacterium abscessus Strain Morphotype Determines Phage Susceptibility, the Repertoire of Therapeutically Useful Phages, and Phage Resistance." mBio **12**(2).

Delcher, A. L., K. A. Bratke, E. C. Powers and S. L. Salzberg (2007). "Identifying bacterial genes and endosymbiont DNA with Glimmer." Bioinformatics **23**(6): 673-679.

Falkinham, J. O., 3rd (2015). "Environmental sources of nontuberculous mycobacteria." Clin Chest Med **36**(1): 35-41.

Falkinham, J. O., 3rd (2021). "Ecology of Nontuberculous Mycobacteria." Microorganisms **9**(11).

Gauthier, C. H., L. Abad, A. K. Venbakkam, J. Malnak, D. A. Russell and G. F. Hatfull (2022). "DEPhT: a novel approach for efficient prophage discovery and precise extraction." Nucleic Acids Res **50**(13): e75.

Gauthier, C. H., S. G. Cresawn and G. F. Hatfull (2022). "PhaMMseqs: a new pipeline for constructing phage gene phamilies using MMseqs2." G3 (Bethesda) **12**(11).

Gauthier, C. H. and G. F. Hatfull (2023). "PhamClust: a phage genome clustering tool using proteomic equivalence." mSystems **8**(5): e0044323.

Griffith, D. E., T. Aksamit, B. A. Brown-Elliott, A. Catanzaro, C. Daley, F. Gordin, S. M. Holland, R. Horsburgh, G. Huitt, M. F. Iademarco, M. Iseman, K. Olivier, S. Ruoss, C. F. von Reyn, R. J. Wallace, Jr., K. Winthrop, A. T. S. M. D. Subcommittee, S. American Thoracic and A. Infectious Disease Society of (2007). "An official ATS/IDSA statement: diagnosis, treatment, and prevention of nontuberculous mycobacterial diseases." Am J Respir Crit Care Med **175**(4): 367-416.

Griffith, D. E., B. A. Brown-Elliott, J. L. Benwill and R. J. Wallace, Jr. (2015). "Mycobacterium abscessus. "Pleased to meet you, hope you guess my name..."." Ann Am Thorac Soc **12**(3): 436-439.

Grindley, N. D., K. L. Whiteson and P. A. Rice (2006). "Mechanisms of site-specific recombination." Annu Rev Biochem **75**: 567-605.

Grose, J. H. and S. R. Casjens (2014). "Understanding the enormous diversity of bacteriophages: the tailed phages that infect the bacterial family Enterobacteriaceae." Virology **468-470**: 421-443.

Guerin, M. E., J. Kordulakova, P. M. Alzari, P. J. Brennan and M. Jackson (2010). "Molecular basis of phosphatidyl-myo-inositol mannoside biosynthesis and regulation in mycobacteria." J Biol Chem **285**(44): 33577-33583.

Guo, J., B. Bolduc, A. A. Zayed, A. Varsani, G. Dominguez-Huerta, T. O. Delmont, A. A. Pratama, M. C. Gazitua, D. Vik, M. B. Sullivan and S. Roux (2021). "VirSorter2: a multi-classifier, expert-guided approach to detect diverse DNA and RNA viruses." Microbiome **9**(1): 37.

Gupta, R. S., B. Lo and J. Son (2018). "Phylogenomics and Comparative Genomic Studies Robustly Support Division of the Genus Mycobacterium into an Emended Genus Mycobacterium and Four Novel Genera." Front Microbiol **9**: 67.

Hanauer, D. I., M. J. Graham, P. Sea, L. Betancur, A. Bobrownicki, S. G. Cresawn, R. A. Garlena, D. Jacobs-Sera, N. Kaufmann, W. H. Pope, D. A. Russell, W. R. Jacobs, Jr., V. Sivanathan, D. J. Asai and G. F. Hatfull (2017). "An inclusive Research Education Community (iREC): Impact of the SEA-PHAGES program on research outcomes and student learning." Proc Natl Acad Sci U S A **114**(51): 13531-13536.

Harding, C. V. and W. H. Boom (2010). "Regulation of antigen presentation by Mycobacterium tuberculosis: a role for Toll-like receptors." Nat Rev Microbiol **8**(4): 296-307.

Harman-McKenna, V. K. and J. De Buck (2023). "Effective Isolation and Characterization of Mycobacteriophages with the Ability to Lyse Mycobacterium avium subsp. paratuberculosis." Viruses **16**(1).

Hatfull, G. F. (2012). "The secret lives of mycobacteriophages." Adv Virus Res **82**: 179-288.

Hatfull, G. F. (2018). "Mycobacteriophages." Microbiol Spectr **6**(5).

Hatfull, G. F., D. Jacobs-Sera, J. G. Lawrence, W. H. Pope, D. A. Russell, C. C. Ko, R. J. Weber, M. C. Patel, K. L. Germane, R. H. Edgar, N. N. Hoyte, C. A. Bowman, A. T. Tantoco, E. C. Paladin, M. S. Myers, A. L. Smith, M. S. Grace, T. T. Pham, M. B. O'Brien, A. M. Vogelsberger, A. J. Hryckowian, J. L. Wynalek, H. Donis-Keller, M. W. Bogel, C. L. Peebles, S. G. Cresawn and R. W. Hendrix (2010). "Comparative genomic analysis of 60 Mycobacteriophage genomes: genome clustering, gene acquisition, and gene size." J Mol Biol **397**(1): 119-143.

Hatfull, G. F. and G. J. Sarkis (1993). "DNA sequence, structure and gene expression of mycobacteriophage L5: a phage system for mycobacterial genetics." Mol Microbiol **7**(3): 395-405.

Hendrix, R. W., M. C. Smith, R. N. Burns, M. E. Ford and G. F. Hatfull (1999). "Evolutionary relationships among diverse bacteriophages and prophages: all the world's a phage." Proc Natl Acad Sci U S A **96**(5): 2192-2197.

Hilborn, E. D., T. C. Covert, M. A. Yakrus, S. I. Harris, S. F. Donnelly, E. W. Rice, S. Toney, S. A. Bailey and G. N. Stelma, Jr. (2006). "Persistence of nontuberculous mycobacteria in a drinking water system after addition of filtration treatment." Appl Environ Microbiol **72**(9): 5864-5869.

Honda, J. R., R. Virdi and E. D. Chan (2018). "Global Environmental Nontuberculous Mycobacteria and Their Contemporaneous Man-Made and Natural Niches." Front Microbiol **9**: 2029.

Hubalek, Z. (2003). "Emerging human infectious diseases: anthroponoses, zoonoses, and sapronoses." Emerg Infect Dis **9**(3): 403-404.

Hurst-Hess, K., A. Walz, Y. Yang, H. McGuirk, M. Gonzalez-Juarrero, G. F. Hatfull, P. Ghosh and A. K. Ojha (2023). "Intrapulmonary Treatment with Mycobacteriophage LysB Rapidly Reduces Mycobacterium abscessus Burden." Antimicrob Agents Chemother **67**(6): e0016223.

Jacobs-Sera, D., L. J. Marinelli, C. Bowman, G. W. Broussard, C. Guerrero Bustamante, M. M. Boyle, Z. O. Petrova, R. M. Dedrick, W. H. Pope, G. Science Education Alliance Phage Hunters Advancing, P. Evolutionary Science Sea-Phages, R. L. Modlin, R. W. Hendrix and G. F. Hatfull (2012). "On the nature of mycobacteriophage diversity and host preference." Virology **434**(2): 187-201.

Jarlier, V. and H. Nikaido (1990). "Permeability barrier to hydrophilic solutes in Mycobacterium chelonei." J Bacteriol **172**(3): 1418-1423.

Johansen, M. D., J. L. Herrmann and L. Kremer (2020). "Non-tuberculous mycobacteria and the rise of Mycobacterium abscessus." Nat Rev Microbiol **18**(7): 392-407.

Johansen, M. D., H. P. Spaink, S. H. Oehlers and L. Kremer (2023). "Modeling nontuberculous mycobacterial infections in zebrafish." Trends Microbiol.

Jordan, T. C., S. H. Burnett, S. Carson, S. M. Caruso, K. Clase, R. J. DeJong, J. J. Dennehy, D. R. Denver, D. Dunbar, S. C. Elgin, A. M. Findley, C. R. Gissendanner, U. P. Golebiewska, N. Guild, G. A. Hartzog, W. H. Grillo, G. P. Hollowell, L. E. Hughes, A. Johnson, R. A. King, L. O. Lewis, W. Li, F. Rosenzweig, M. R. Rubin, M. S. Saha, J. Sandoz, C. D. Shaffer, B. Taylor,

L. Temple, E. Vazquez, V. C. Ware, L. P. Barker, K. W. Bradley, D. Jacobs-Sera, W. H. Pope, D. A. Russell, S. G. Cresawn, D. Lopatto, C. P. Bailey and G. F. Hatfull (2014). "A broadly implementable research course in phage discovery and genomics for first-year undergraduate students." mBio **5**(1): e01051-01013.

Kaczmarkowska, A., A. Didkowska, E. Kwiecien, I. Stefanska, M. Rzewuska and K. Anusz (2022). "The Mycobacterium avium complex - an underestimated threat to humans and animals." Ann Agric Environ Med **29**(1): 22-27.

Kansal, R. G., R. Gomez-Flores and R. T. Mehta (1998). "Change in colony morphology influences the virulence as well as the biochemical properties of the Mycobacterium avium complex." Microb Pathog **25**(4): 203-214.

Kaur, P., M. Rausch, B. Malakar, U. Watson, N. P. Damle, Y. Chawla, S. Srinivasan, K. Sharma, T. Schneider, G. D. Jhingan, D. Saini, D. Mohanty, F. Grein and V. K. Nandicoori (2019). "LipidII interaction with specific residues of Mycobacterium tuberculosis PknB extracytoplasmic domain governs its optimal activation." Nat Commun **10**(1): 1231.

Kazda, J., I. Pavlik, J. O. Falkinham Iii and K. Hruska (2009). The Ecology of Mycobacteria: Impact on Animal's and Human's Health.

Kim, K. J., S. H. Oh, D. Jeon and C. L. Chang (2023). "Isolation and Antimicrobial Susceptibility of Nontuberculous Mycobacteria in a Tertiary Hospital in Korea, 2016 to 2020." Tuberc Respir Dis (Seoul) **86**(1): 47-56.

Kim, Y. S., C. S. Yang, L. T. Nguyen, J. K. Kim, H. S. Jin, J. H. Choe, S. Y. Kim, H. M. Lee, M. Jung, J. M. Kim, M. H. Kim, E. K. Jo and J. C. Jang (2017). "Mycobacterium abscessus ESX-3 plays an important role in host inflammatory and pathological responses during infection." Microbes Infect **19**(1): 5-17.

Koleske, B. N., W. R. Jacobs, Jr. and W. R. Bishai (2023). "The Mycobacterium tuberculosis genome at 25 years: lessons and lingering questions." J Clin Invest **133**(19).

Kutter, E., D. De Vos, G. Gvasalia, Z. Alavidze, L. Gogokhia, S. Kuhl and S. T. Abedon (2010). "Phage therapy in clinical practice: treatment of human infections." Curr Pharm Biotechnol **11**(1): 69-86.

Kutter, E. M., S. J. Kuhl and S. T. Abedon (2015). "Re-establishing a place for phage therapy in western medicine." Future Microbiol **10**(5): 685-688.

Laencina, L., V. Dubois, V. Le Moigne, A. Viljoen, L. Majlessi, J. Pritchard, A. Bernut, L. Piel, A. L. Roux, J. L. Gaillard, B. Lombard, D. Loew, E. J. Rubin, R. Brosch, L. Kremer, J. L. Herrmann and F. Girard-Misguich (2018). "Identification of genes required for Mycobacterium abscessus growth in vivo with a prominent role of the ESX-4 locus." Proc Natl Acad Sci U S A **115**(5): E1002-E1011.

Landy, A. (2015). "The lambda Integrase Site-specific Recombination Pathway." Microbiol Spectr **3**(2): MDNA3-0051-2014.

Laslett, D. and B. Canback (2004). "ARAGORN, a program to detect tRNA genes and tmRNA genes in nucleotide sequences." Nucleic Acids Res **32**(1): 11-16.

Lederberg, E. M. (1950). "Lysogenicity in Escherichia coli strain K-12." Microbial Genetics Bulletin **33**(1): 5-8.

Lee, M. R., W. H. Sheng, C. C. Hung, C. J. Yu, L. N. Lee and P. R. Hsueh (2015). "Mycobacterium abscessus Complex Infections in Humans." Emerg Infect Dis **21**(9): 1638-1646.

Lewis, J. A. and G. F. Hatfull (2003). "Control of directionality in L5 integrase-mediated site-specific recombination." J Mol Biol **326**(3): 805-821.

Lunt, B. L. and G. F. Hatfull (2016). "Brujita Integrase: A Simple, Arm-Less, Directionless, and Promiscuous Tyrosine Integrase System." J Mol Biol **428**(11): 2289-2306.

Luthra, S., A. Rominski and P. Sander (2018). "The Role of Antibiotic-Target-Modifying and Antibiotic-Modifying Enzymes in Mycobacterium abscessus Drug Resistance." Front Microbiol **9**: 2179.

Maiga, M., S. Siddiqui, S. Diallo, B. Diarra, B. Traore, Y. R. Shea, A. M. Zelazny, B. P. Dembele, D. Goita, H. Kassambara, A. S. Hammond, M. A. Polis and A. Tounkara (2012). "Failure to recognize nontuberculous mycobacteria leads to misdiagnosis of chronic pulmonary tuberculosis." PLoS One **7**(5): e36902.

Mamadou Daffé, H. M. (2019). "Unraveling the Structure of the Mycobacterial Envelope."

Marinelli, L. J., M. Piuri, Z. Swigonova, A. Balachandran, L. M. Oldfield, J. C. van Kessel and G. F. Hatfull (2008). "BRED: a simple and powerful tool for constructing mutant and recombinant bacteriophage genomes." PLoS One **3**(12): e3957.

Marrakchi, H., M. A. Laneelle and M. Daffe (2014). "Mycolic acids: structures, biosynthesis, and beyond." Chem Biol **21**(1): 67-85.

Mavrich, T. N. and G. F. Hatfull (2017). "Bacteriophage evolution differs by host, lifestyle and genome." Nat Microbiol **2**(9): 17112.

Mavrich, T. N. and G. F. Hatfull (2019). "Evolution of Superinfection Immunity in Cluster A Mycobacteriophages." mBio **10**(3).

Mendum, T. A., B. Z. Chilima and P. R. Hirsch (2000). "The PCR amplification of non-tuberculous mycobacterial 16S rRNA sequences from soil." FEMS Microbiol Lett **185**(2): 189-192.

Meroueh, S. O., K. Z. Bencze, D. Hesek, M. Lee, J. F. Fisher, T. L. Stemmler and S. Mobashery (2006). "Three-dimensional structure of the bacterial cell wall peptidoglycan." Proc Natl Acad Sci U S A **103**(12): 4404-4409.

Mignard, S. and J. P. Flandrois (2008). "A seven-gene, multilocus, genus-wide approach to the phylogeny of mycobacteria using supertrees." Int J Syst Evol Microbiol **58**(Pt 6): 1432-1441.

Naka, T., N. Nakata, S. Maeda, R. Yamamoto, M. Doe, S. Mizuno, M. Niki, K. Kobayashi, H. Ogura, M. Makino and N. Fujiwara (2011). "Structure and host recognition of serotype 13 glycopeptidolipid from Mycobacterium intracellulare." J Bacteriol **193**(20): 5766-5774.

Nataraj, V., C. Varela, A. Javid, A. Singh, G. S. Besra and A. Bhatt (2015). "Mycolic acids: deciphering and targeting the Achilles' heel of the tubercle bacillus." Mol Microbiol **98**(1): 7-16.

Nessar, R., E. Cambau, J. M. Reyrat, A. Murray and B. Gicquel (2012). "Mycobacterium abscessus: a new antibiotic nightmare." J Antimicrob Chemother **67**(4): 810-818.

Nigou, J., T. Vasselon, A. Ray, P. Constant, M. Gilleron, G. S. Besra, I. Sutcliffe, G. Tiraby and G. Puzo (2008). "Mannan chain length controls lipoglycans signaling via and binding to TLR2." J Immunol **180**(10): 6696-6702.

Parmar, S. and E. I. Tocheva (2023). "The cell envelope of Mycobacterium abscessus and its role in pathogenesis." PLoS Pathog **19**(5): e1011318.

Patin, E. C., A. C. Geffken, S. Willcocks, C. Leschczyk, A. Haas, F. Nimmerjahn, R. Lang, T. H. Ward and U. E. Schaible (2017). "Trehalose dimycolate interferes with FcgammaR-mediated phagosome maturation through Mincle, SHP-1 and FcgammaRIIB signalling." PLoS One **12**(4): e0174973.

Pavlik, I., V. Ulmann and J. O. Falkinham, 3rd (2022). "Nontuberculous Mycobacteria: Ecology and Impact on Animal and Human Health." Microorganisms **10**(8): 1516.

Pedulla, M. L., M. E. Ford, J. M. Houtz, T. Karthikeyan, C. Wadsworth, J. A. Lewis, D. Jacobs-Sera, J. Falbo, J. Gross, N. R. Pannunzio, W. Brucker, V. Kumar, J. Kandasamy, L. Keenan, S. Bardarov, J. Kriakov, J. G. Lawrence, W. R. Jacobs, Jr., R. W. Hendrix and G. F. Hatfull (2003). "Origins of highly mosaic mycobacteriophage genomes." Cell **113**(2): 171-182.

Pedulla, M. L., M. H. Lee, D. C. Lever and G. F. Hatfull (1996). "A novel host factor for integration of mycobacteriophage L5." Proceedings of the National Academy of Sciences of the United States of America **93**(26): 15411-15416.

Ptashne, M., A. Jeffrey, A. D. Johnson, R. Maurer, B. J. Meyer, C. O. Pabo, T. M. Roberts and R. T. Sauer (1980). "How the lambda repressor and cro work." Cell **19**(1): 1-11.

Publications, s. (2007). "On an invisible microbe antagonistic toward dysenteric bacilli: brief note by Mr. F. D'Herelle, presented by Mr. Roux." Research in Microbiology **158**(7): 553-554.

Rajagopal, M. and S. Walker (2017). "Envelope Structures of Gram-Positive Bacteria." Curr Top Microbiol Immunol **404**: 1-44.

Rath, P., O. Saurel, G. Czaplicki, M. Tropis, M. Daffe, A. Ghazi, P. Demange and A. Milon (2013). "Cord factor (trehalose 6,6'-dimycolate) forms fully stable and non-permeable lipid bilayers required for a functional outer membrane." Biochim Biophys Acta **1828**(9): 2173-2181.

Ratnatunga CN, L. V., Kupz A (2019). "The rise of non-tuberculosis mycobacterial lung disease."

Reich, J. M. and R. E. Johnson (1992). "Mycobacterium avium complex pulmonary disease presenting as an isolated lingular or middle lobe pattern. The Lady Windermere syndrome." Chest **101**(6): 1605-1609.

Reznikov, M. and J. H. Leggo (1972). "Modification of Schaefer's procedure for serotyping of organisms of the Mycobacterium avium-M. intracellulare-M. scrofulaceum complex." Appl Microbiol **23**(4): 819-823.

Rock, J. M., F. F. Hopkins, A. Chavez, M. Diallo, M. R. Chase, E. R. Gerrick, J. R. Pritchard, G. M. Church, E. J. Rubin, C. M. Sassetti, D. Schnappinger and S. M. Fortune (2017). "Programmable transcriptional repression in mycobacteria using an orthogonal CRISPR interference platform." Nat Microbiol **2**: 16274.

Ruis, C., J. M. Bryant, S. C. Bell, R. Thomson, R. M. Davidson, N. A. Hasan, J. van Ingen, M. Strong, R. A. Floto and J. Parkhill (2021). "Dissemination of Mycobacterium abscessus via global transmission networks." Nat Microbiol **6**(10): 1279-1288.

Russell, D. A. and G. F. Hatfull (2017). "PhagesDB: the actinobacteriophage database." Bioinformatics **33**(5): 784-786.

Sanger, F., A. R. Coulson, G. F. Hong, D. F. Hill and G. B. Petersen (1982). "Nucleotide sequence of bacteriophage lambda DNA." J Mol Biol **162**(4): 729-773.

Santacroce, L., R. Del Prete, I. A. Charitos and L. Bottalico (2021). "Mycobacterium leprae: A historical study on the origins of leprosy and its social stigma." Infez Med **29**(4): 623-632.

Sarathy, J., V. Dartois, T. Dick and M. Gengenbacher (2013). "Reduced drug uptake in phenotypically resistant nutrient-starved nonreplicating Mycobacterium tuberculosis." Antimicrob Agents Chemother **57**(4): 1648-1653.

Schooley, R. T., B. Biswas, J. J. Gill, A. Hernandez-Morales, J. Lancaster, L. Lessor, J. J. Barr, S. L. Reed, F. Rohwer, S. Benler, A. M. Segall, R. Taplitz, D. M. Smith, K. Kerr, M. Kumaraswamy, V. Nizet, L. Lin, M. D. McCauley, S. A. Strathdee, C. A. Benson, R. K. Pope, B. M. Leroux, A. C. Picel, A. J. Mateczun, K. E. Cilwa, J. M. Regeimbal, L. A. Estrella, D. M.

Wolfe, M. S. Henry, J. Quinones, S. Salka, K. A. Bishop-Lilly, R. Young and T. Hamilton (2017). "Development and Use of Personalized Bacteriophage-Based Therapeutic Cocktails To Treat a Patient with a Disseminated Resistant Acinetobacter baumannii Infection." Antimicrob Agents Chemother **61**(10).

Schorey, J. S. and L. Sweet (2008). "The mycobacterial glycopeptidolipids: structure, function, and their role in pathogenesis." Glycobiology **18**(11): 832-841.

Schreiber, P. W., S. P. Kuster, B. Hasse, C. Bayard, C. Ruegg, P. Kohler, P. M. Keller, G. V. Bloemberg, F. Maisano, D. Bettex, M. Halbe, R. Sommerstein and H. Sax (2016). "Reemergence of Mycobacterium chimaera in Heater-Cooler Units despite Intensified Cleaning and Disinfection Protocol." Emerg Infect Dis **22**(10): 1830-1833.

Silhavy, T. J., D. Kahne and S. Walker (2010). "The bacterial cell envelope." Cold Spring Harb Perspect Biol **2**(5): a000414.

Soding, J., A. Biegert and A. N. Lupas (2005). "The HHpred interactive server for protein homology detection and structure prediction." Nucleic Acids Res **33**(Web Server issue): W244-248.

Sun, X., T. Zhang, H. Sun and X. Sun (2022). "Disseminated nontuberculous mycobacterial infection with cryptic immunodeficiency mimicking malignancy: a case report." BMC Pulm Med **22**(1): 452.

Torrelles, J. B., D. Chatterjee, J. G. Lonca, J. M. Manterola, V. R. Ausina and P. J. Brennan (2000). "Serovars of Mycobacterium avium complex isolated from AIDS and non-AIDS patients in Spain." J Appl Microbiol **88**(2): 266-279.

Torrens, J. K., P. Dawkins, S. P. Conway and E. Moya (1998). "Non-tuberculous mycobacteria in cystic fibrosis." Thorax **53**(3): 182-185.

Tortoli, E., B. A. Brown-Elliott, J. D. Chalmers, D. M. Cirillo, C. L. Daley, S. Emler, R. A. Floto, M. J. Garcia, W. Hoefsloot, W. J. Koh, C. Lange, M. Loebinger, F. P. Maurer, K. Morimoto, S. Niemann, E. Richter, C. Y. Turenne, R. Vasireddy, S. Vasireddy, D. Wagner, R. J. Wallace, Jr., N. Wengenack and J. van Ingen (2019). "Same meat, different gravy: ignore the new names of mycobacteria." Eur Respir J **54**(1).

Tortoli, E., T. Fedrizzi, C. J. Meehan, A. Trovato, A. Grottola, E. Giacobazzi, G. F. Serpini, S. Tagliazucchi, A. Fabio, C. Bettua, R. Bertorelli, F. Frascaro, V. De Sanctis, M. Pecorari, O. Jousson, N. Segata and D. M. Cirillo (2017). "The new phylogeny of the genus Mycobacterium: The old and the news." Infect Genet Evol **56**: 19-25.

Tortoli, E., C. J. Meehan, A. Grottola, G. Fregni Serpini, A. Fabio, A. Trovato, M. Pecorari and D. M. Cirillo (2019). "Genome-based taxonomic revision detects a number of synonymous taxa in the genus Mycobacterium." Infect Genet Evol **75**: 103983.

Tsang, A. Y., J. C. Denner, P. J. Brennan and J. K. McClatchy (1992). "Clinical and epidemiological importance of typing of Mycobacterium avium complex isolates." J Clin Microbiol **30**(2): 479-484.

Turenne, C. Y., R. Wallace, Jr. and M. A. Behr (2007). "Mycobacterium avium in the postgenomic era." Clin Microbiol Rev **20**(2): 205-229.

Twort, F. W. (1915). "AN INVESTIGATION ON THE NATURE OF ULTRA-MICROSCOPIC VIRUSES." The Lancet **186**(4814): 1241-1243.

Tzou, C. L., M. A. Dirac, A. L. Becker, N. K. Beck, K. M. Weigel, J. S. Meschke and G. A. Cangelosi (2020). "Association between Mycobacterium avium Complex Pulmonary Disease and Mycobacteria in Home Water and Soil." Ann Am Thorac Soc **17**(1): 57-62.

van Ingen, J., C. Y. Turenne, E. Tortoli, R. J. Wallace, Jr. and B. A. Brown-Elliott (2018). "A definition of the Mycobacterium avium complex for taxonomical and clinical purposes, a review." Int J Syst Evol Microbiol **68**(11): 3666-3677.

van Kessel, J. C. and G. F. Hatfull (2007). "Recombineering in Mycobacterium tuberculosis." Nat Methods **4**(2): 147-152.

van Kessel, J. C., L. J. Marinelli and G. F. Hatfull (2008). "Recombineering mycobacteria and their phages." Nat Rev Microbiol **6**(11): 851-857.

van Tonder, A. J., H. C. Ellis, C. P. Churchward, K. Kumar, N. Ramadan, S. Benson, J. Parkhill, M. F. Moffatt, M. R. Loebinger and W. O. C. Cookson (2023). "Mycobacterium avium complex genomics and transmission in a London hospital." Eur Respir J **61**(4).

Vilcheze, C., V. Molle, S. Carrere-Kremer, J. Leiba, L. Mourey, S. Shenai, G. Baronian, J. Tufariello, T. Hartman, R. Veyron-Churlet, X. Trivelli, S. Tiwari, B. Weinrick, D. Alland, Y. Guerardel, W. R. Jacobs, Jr. and L. Kremer (2014). "Phosphorylation of KasB regulates virulence and acid-fastness in Mycobacterium tuberculosis." PLoS Pathog **10**(5): e1004115.

Wetzel, K. S., C. A. Guerrero-Bustamante, R. M. Dedrick, C. C. Ko, K. G. Freeman, H. G. Aull, A. M. Divens, J. M. Rock, K. M. Zack and G. F. Hatfull (2021). "CRISPY-BRED and CRISPY-BRIP: efficient bacteriophage engineering." Sci Rep **11**(1): 6796.

Wright, E. L., S. Zywno-van Ginkel, N. Rastogi and W. W. Barrow (1996). "Monoclonal infection involving Mycobacterium avium presenting with three distinct colony morphotypes." J Clin Microbiol **34**(10): 2475-2478.

Zhang, D., R. F. de Souza, V. Anantharaman, L. M. Iyer and L. Aravind (2012). "Polymorphic toxin systems: Comprehensive characterization of trafficking modes, processing, mechanisms of action, immunity and ecology using comparative genomics." Biol Direct **7**: 18.

Zhang, M., P. Wang, C. Li, O. Segev, J. Wang, X. Wang, L. Yue, X. Jiang, Y. Sheng, A. Levy, C. Jiang and F. Chen (2023). "Comparative genomic analysis reveals differential genomic characteristics and featured genes between rapid- and slow-growing non-tuberculous mycobacteria." Front Microbiol **14**: 1243371.